Port Hamiltonian Modelling of an Integrated Mechanical Ventilator-Human Respiratory System

Milka M. C.I Madahana (0304755j)

A thesis submitted to the Faculty of Engineering and the Built Environment, at the University of the Witwatersrand, Johannesburg, in fulfilment of the requirements for the degree of Doctor of Philosophy.

February 2024

Port Hamiltonian Modelling of an Integrated Mechanical Ventilator-Human Respiratory System,

Author:
Milka M. C.I Madahana (0304755j)

Supervisor:
Dr. Otis T. C. Nyandoro

Institution:
University of the Witwatersrand, Johannesburg, South Africa

CONTENTS

LIST OF FIGURES

LIST OF TABLES

ABSTRACT

Mechanical ventilation is a life-saving treatment for critically ill patients who are struggling to breathe independently due to injury or disease. Globally, large numbers of individuals have always required mechanical ventilation per year. In this research work, a comprehensive integrated Mechanical ventilator human respiratory system which is a complex dynamical system is modelled using the Port Hamiltonian approach. The Port Hamiltonian framework provides a powerful tool for the analysis, modelling, and control of such systems. The objectives of this research work are separated into four main outcomes: The first objective is formulation of the human respiratory system using a Port Hamiltonian based approach. In this formulation, the first abstraction is a nominal Port Hamiltonian mechanical ventilator human respiratory system model. The second level of abstraction formulates a comprehensive integrated Port Hamiltonian model of the human respiratory system which includes the alveoli. The third abstraction is the Multi-physics and Multi-scale Port Hamiltonian model of the human respiratory system, which is integrated with the mechanical ventilator. The second objective is the formulation of a comprehensive Port-Hamiltonian model of a mixed finite/infinite dimensional electro-hydro-mechanical model of the mechanical ventilator. The third objective is the presentation of a multi-physics Port Hamiltonian generalized model of a Mechanical Ventilator-Human respiratory system with Naiver stokes for the fluid flow in the mechanical ventilator respiratory system model. The generalized formulation leads to a new class of algebraic constraints in the modelling of the mechanical ventilator respiratory system. The main result presented is a novel interconnected Dirac structure of the fluid/electrically coupled system. Finally, two novel applications of the mechanical ventilator human respiratory system model are presented. Simulations for this research work are conducted using the Matlab platform and the respiratory system model results and the mechanical ventilator results are compared to results in existing literature and are found to be comparable. This work can be developed further in future to include robust controllers in the Port Hamiltonian framework for improved mechanical ventilator patient dynamics.

STATEMENT OF AUTHORSHIP

I declare that this thesis is my own, unaided work, except where otherwise acknowledged. It is being submitted for the degree of Doctor of Philosophy in the University of the Witwatersrand, Johannesburg. It has not been submitted before for any degree or examination at any other university.

Signed on this 23rd day of February 2024

Milka M. C.I Madahana (0304755J).

ACKNOWLEDGMENTS

I would like to express exceeding gratitude to my heavenly Father, God Almighty for granting me life, health, and the finishing grace. I would also like to thank the following people:

- Dr. Otis. T. C. Nyandoro, my supervisor, for the guidance that led to the completion of this research project.
- Prof. M. A. van Wyk, the head of the Systems and Control research group, for providing useful insights and affirmations.
- Prof. Brian Wigdorowitz, for insightful discussions on model generalization that motivated me to pursue my doctoral studies in the modeling of the respiratory system using the Port Hamiltonian Approach.
- Prof. Olutayo Oyerinde, believing in me and encouraging me to the completion of my research work.
- Prof. Muzi Maseko, Faculty of Health Science, School of Physiology, Head of the Research Group, Human Nutrition Research Laboratory, for permitting me to use the laboratory under his research group for experimental validation
- Prof. Katijah Khoza-Shangase, for believing in me, for research collaborations and for encouraging me to be the best.
- Dr. Tinashe. Chingozha, For the provision of mentorship and research discussions
- Dr. John. E.D Ekoru, for the mentorship, all the research collaborations, research discussions and for motivating me to always give my best.
- All my research collaborators, colleagues, friends and family that have contributed to the completion of my doctoral work, I am so thankful for your contribution.

PUBLICATIONS

The following are the author's list of publications:

1. Madahana, Milka & Nyandoro, Otis & Ekoru, John. (2020). Intelligent comprehensive Occupational health monitoring system for mine workers. IFAC-PapersOnLine. Volume 53, Issue 2, 2020, pp 16494-16499
2. M. Madahana, E. John and N. Otis, 'Compositional and geometric unifying approach for modeling the mechanical ventilator-human respiratory system', Applied Sciences,2023. doi: UnderReview.
3. M. Madahana, E. John and N. Otis, 'Formulation of a comprehensive intergrated model of the human respiratory system via the porthamiltonian approach', Applied Sciences, 2023. doi: UnderReview.
4. M. Madahana, E. John and N. Otis, 'A mixed finite/infinite dimensional porthamiltonian model of a mechanical ventilator', Applied Sciences, 2023. doi: UnderReview.
5. M. Madahana, E. John and N. Otis, 'Formulation of a generalized multiphysics porthamiltonian model of the mechanical ventilator human respiratory system', Applied Sciences, 2023. doi: UnderReview.
6. Madahana, Milka & Ekoru, John & Nyandoro, Otis. (2020). Energy based model of the human Ear canal and tympanic membrane for sound transmission. IFAC-PapersOnLine. Volume 53, Issue 2, pp 16406-16411
7. Madahana, Milka & Nyandoro, & Otis Ekoru, John. (2020). A Human Inner Ear Model for assessment of Noise Induced Hearing Loss via energy methods. IFAC-PapersOnLine. Volume 53, Issue 2, 2020, pp 16424-16429
8. Madahana, Milka & Ngwako, Mohlalakoma & Nyandoro, Otis & Ekoru, John. (2021) Modelling of the human middle ear via the Port Hamiltonian approach, The 2021 International Automatic Control Conference, IEEE Xplore
9. Madahana, Milka & Nyandoro, & Otis Ekoru, John. (2017) Sliding mode controller for a feedback accelerometer with a distributed Mass, IFAC-PapersOnLine, Volume 50, Issue 2, 2017, Pages 295-300
10. Madahana, Milka & Nyandoro, Otis & Ekoru, John. (2019) Smart noise policy monitoring and feedback control system for mining application, IFAC - Journal Papers online IFAC-PapersOnLine, Volume 52, Issue 14, 2019, Pages 177-182.

11. Madahana, Milka & Ekoru, John &, Mashinini,Thabang& Nyandoro, Otis. (2019) Noise level policy advising system, IFAC-PapersOnLine, Volume 52, Issue 14, 2019, Pages 249-254.

12. Madahana, Milka & Ekoru, John &, Mashinini,Thabang& Nyandoro, Otis. (2019)Mine workers threshold shift estimation via optimization algorithms for deep recurrent neural networks, IFAC-PapersOnLine, Volume 52, Issue 14, 2019, Pages 117-122.

13. Madahana, M. C. I., Nyandoro, O. T. and Moroe, M. F., Engineering noise control for mines: Lessons from the world, South African Journal of Communication Disorders. Volume 67, Issue 2, 2020, pp 1 – 5, 684.

14. Madahana, Milka& Khoza-Shangase, Katijah & Moroe, Nomfundo & Ekoru, John & Nyandoro, otis.(2022), Application of machine learning approaches to analyse student success for contact learning and emergency remote teaching and learning during the COVID-19 era in speech–language pathology and audiology. South African Journal of Communication Disorders. Volume 69, Issue 2,pp 13.

15. Madahana, Milka& Khoza-Shangase, Katijah & Moroe, Nomfundo & Ekoru, John & Mayombo, Daniel & Nyandoro, otis.(2022), A proposed artificial intelligence-based real-time speech-to-text to sign language translator for South African official languages for the COVID-19 era and beyond: In pursuit of solutions for the hearing impaired. South African Journal of Communication Disorders. Volume 69, Issue 2,pp 11.

16. Madahana, Milka& Khoza-Shangase, Katijah & Moroe, Nomfundo & Ekoru, John & Nyandoro, otis.(2022), Application of machine learning approaches to analyse student success for contact learning and emergency remote teaching and learning during the COVID-19 era in speech–language pathology and audiology. South African Journal of Communication Disorders. Volume 69, Issue 2,pp 13.

17. Madahana, M.C.I and Ekoru, J. E.D,. A Comparative Study of the Application of Machine Learning Techniques to Analysis and Prediction of the Market Prices for Precious Group Metals. 41st APCOM International conference, South Dakota, USA

18. Madahana, M.C.I and Ekoru, J. E.D, Comparative Data Analysis Using Machine Learning Based Approach for Estimation of Particulate Matter Concentration in the Mines and the Vicinities. 41st APCOM International conference, South Dakota, USA

19. J.E.D. Ekoru, M. Ngwako, M.C.I. Madahana and O.T.C. Nyandoro. 'Singular optimal control of UAV/UGV Rendezvous Problem', IFAC-PapersOnLine,

20. J.E.D. Ekoru, M. Ngwako, M.C.I. Madahana and O.T.C. Nyandoro. 'Optimal Control for Maximum payload for transport of UAV with suspended payload', IEEE, "Under Review"

21. J.E.D. Ekoru, M. Ngwako, M.C.I. Madahana and O.T.C. Nyandoro. 'Time optimal control of a Hybrid UAV-Suspended load transport system', IEEE, "Under Review"
22. Ngwako, Mohlalakoma & Nyandoro, O.T.C. & Van Coller, John & Madahana, Milka. (2019). A Condition for Singular Optimal Control Formulation for a Tandem Pair of Gravity Fed Linear DC Machine Powered Mine Locomotive. IFAC-PapersOnLine. 52. 201-206. 10.1016/j.ifacol.2019.09.188.
23. Ngwako, Mohlalakoma & Nyandoro, O.T.C. & Van Coller, John & Madahana, Milka. (2019). Modeling and Control of an Autonomous Linear DC Machine Powered Mine Locomotive. IFAC-PapersOnLine. 52. 195-200. 10.1016/j.ifacol.2019.09.187.
24. Ngwako, Mohlalakoma & Madahana, Milka & Nyandoro, Otis & Ekoru, John. (2023). Full state feedback linearization for a haulage trolley system: a novel differentiable manifold approach,IFAC-PapersOnLine.
25. Moroe, Nomfundo & Khoza-Shangase, Katijah & Madahana, Milka & Nyandoro, otis. (2019) A proposed preliminary model for monitoring hearing conservation programmes in the mining sector in South Africa, Journal of the Southern African Institute of Mining and Metallurgy, Volume119, Issue 7, pp 671
26. Moroe, Nomfundo & Shangase, Katijah & Madahana Milka & Nyandoro, Otis.(2020) Feedback-based noise management matrix in action, South African Journal of Communication Disorders, Volume 67, Issue 2, 2,p. 1 – 9.
27. Nagdee, Nabeelah & Sebothoma, Ben & Madahana, Milka & Khoza-Shangase, Katijah & Moroe, Nomfundo (2022) Simulations as a mode of clinical training in healthcare professions: A scoping review to guide planning in speech-language pathology and audiology during the COVID-19 pandemic, Volume 69, Issue 2, 2,p. 13.
28. Khoza-Shangase, Katijah & Moroe, Nomfundo & Ntlhakana, Liepollo & Petrocchi-Bartal, Luisa & Musiba, Zumbi & Madahana, Milka & Nyandoro Otis .(2022), Occupational noise induced hearing loss.

0.1 WORK DISTRIBUTION FOR KEY PUBLICATIONS

This section provides work distribution for the publications that have directly been extracted from this research work:

For the following publications: 1, 2, 3, 4, 5, 6, 7 ,8, the work distribution provided below applies: Where M.C.I.M refers to Milka Cynthia Ijunga Madahana.

- Conceptualization, M.C.I.M.;
- methodology, M.C.I.M.;
- software, M.C.I.M.;
- validation, M.C.I.M.,J.E.D.E.;and O.T.C.N.

- formal analysis, M.C.I.M.;
- investigation, M.C.I.M.;
- data curation, M.C.I.M.;
- writing—original draft preparation, M.C.I.M.;
- writing—review and editing, J.E.D.E.;
- visualization, M.C.I.M.;
- supervision, O.T.C.N.;

DEDICATION

To my loving parents John and Pauline Madahana

ACRONYMS

MHRA short = MHRA, long = The Medicines and Healthcare Products Regulatory Agency

ODEs short = ODEs, long = Ordinary Differential Equations

PDEs short = PDEs, long = Partial Differential Equations

MV short = MV, long = Mechanical Ventilators

PH short = PH, long = Port Hamiltonian

ICU short = ICU, long = Intensive Care Unit

PEEP short = PEEP, long = Positive End Expiratory Pressure

BIPAP short = BIPAP, long = Bi-Level Positive Airway Pressure

UARS short = UARS, long = Upper Airway Resistance Syndrome

CFD short = CFD, long = Computational Fluid Dynamics

LTS short = LTS, long = laryngoTracheal Stenosis

COPD short = COPD, long = Chronic Obstructive Pulmonary Disease

RLC short = RLC, long = Resistor Inductor Capacitor

FSI short = FSI, long = Fluid-structure Interaction

CDF short = CDF, long = Computational Fluid Dynamics

LTI short = LTI, long = Linear Time Invariant

ILC short = ILC , long = Iterative Learning Control

1

INTRODUCTION

1.1 INTRODUCTION

Mechanical ventilation is an approach used to assist patients who need support to breathe sufficiently [1]. These patients are usually admitted to the Intensive Care Unit (ICU) on a mechanical ventilator (MV), which is a machine that is commonly used to assist patients who are partially or unable to breathe without assistance for various reasons, for instance, illnesses or surgical procedures [2]. Control Engineering plays a fundamental role in the precise and safe provision of gas to the patient [3]. Maintaining human life requires the efficient inspiration of air and the dissemination of oxygen to all cells in the human body. The distribution is achieved by the heart and the blood vessels, whereas the lungs act as the essential interface between the human being and the atmosphere. The lungs facilitate the exchange of carbon dioxide and oxygen in the human body [3]. When a healthy lung is injured or infected by diseases, the respiratory mechanics become overburdened or strained and the muscles in charge of breathing struggle to maintain the efficiency of gaseous exchange. With extended efforts, the muscles atrophy and they cease to function. This results in an urgent need for partial or entire breathing support to be effected. A ventilator is therefore used to facilitate the breathing process through precise control of the gas flow, mechanical ventilator gas composition, pressure and volume. [3].

1.2 BACKGROUND

1.2.1 *The human respiratory system anatomy*

The respiratory system is made up of a network of organs and tissues in the human body which are involved in the breathing process. The human respiratory system is made up of the nose and nasal cavity, sinuses, mouth, throat(pharynx), windpipe (trachea), diaphragm, lungs, bronchial tubes (bronchi), bronchioles, air sacs, and capillaries as shown in figure 1.1, [4], [5].

1.2.2 *The human mechanism of breathing*

The main goal of breathing is to supply oxygen to the alveoli and to remove carbon dioxide. Respiration physiology can be described by air moving in and out of the lungs. The

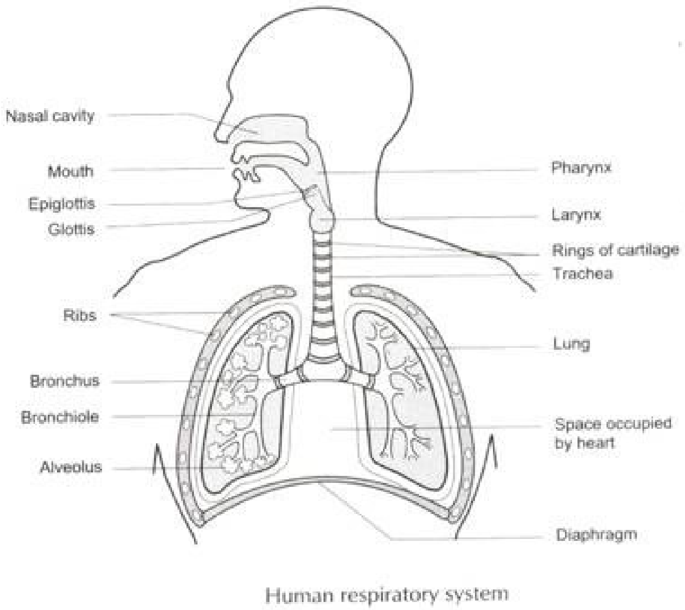

Figure 1.1: The human respiratory system, [4], [5].

intercostal muscles and the diaphragm are involved in the breathing process [4], [5]. Inspiration occurs when there is a contraction of the external intercostal muscle and a relaxation of the internal intercostal muscles. The ribs are pulled upward due to the contraction of the external intercostal muscles and as a result, there is an increase in the thoracic cavity size. As the diaphragm contracts and further lowers, there is an increase in the size of the thoracic cavity [4], [5]. Due to the increase in the size of the thorax, the lungs expand, and the inside air pressure is reduced, thus the pressure is equalized and atmospheric air moves to the lungs. There are several events that take place in order for expiration to occur. The external intercostal muscles relax, and the diaphragm is pushed upwards at the same time the internal intercostal muscle contracts resulting in the ribs being pulled inwards. As a result of this series of events, the lungs are compressed and their pressure increases, forcing air to move out [4], [5].

1.2.3 *Mechanical ventilation development*

A ventilator is a machine that is used to facilitate life support via precise control of airflow, pressure, volume, and gas composition [3]. In 1927, the iron lung which used negative pressure ventilation was introduced. In iron lung ventilation, the patient's entire body below the head was encapsulated in a rigid compartment [3]. In the compartment below, cyclical pressure reduction resulted in air pressure decreasing, this caused the lungs to expand and the gas was able to enter the airway. As much as the iron lung played a critical role in saving lives, it was extremely difficult to continue with other treatments on the patient while they were in the iron lung. For example, conducting X-rays or performing surgery. The iron lung was replaced by positive pressure ventilation in which the gas under

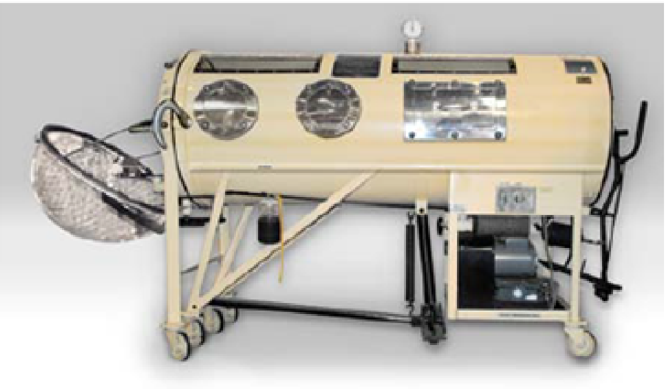

Figure 1.2: Iron lung ventilator, [6].

Figure 1.3: The Positive Pressure Ventilator, [3].

pressure is introduced through the patient's airway [3]. Figure 1.2 and Figure 1.3 show the iron lung ventilator and the positive pressure ventilator.

1.2.4 *Operating principles of the intensive care unit mechanical ventilators*

The MV block diagram of for an Intensive Care Unit (ICU) is shown in figure 1.4. The gas inlet connection (0) allows the entry of air and oxygen into the MV. The air and the oxygen flow through a parallel path in the first section of the ventilator. The air then flows through an impurity removal filter (1). A check valve (2) is employed to stop any flow in the reverse direction. The pressure-reducing valve (3) acts as the entry point for the oxygen and the air, The pressure of the two gases that flow from the wall of the outlet supplies is reduced by the two pressure-reducing valves. The desired pressure value downstream is measured by the pressure sensors (4). The desired pressure is approximately 500 mbar gauge and it can be adjusted using a control signal or manually. The air (5) and the oxygen (6) metering valves are typically directional proportional valves, [2]. To obtain the desired mixture of the gas with the chosen percentage of oxygen, the valves can be precisely adjusted using the control signal transmitted to the solenoids. In some instances, high proportional valves can be applied to remove the necessity for the pressure-reducing valves [2]. The gas mixture then enters a tank (7) which facilitates the unifying of the air and the oxygen and also the pressure variations are smoothed. Some models of the MVs have a tank with a capacity of 5.8 L and the pressure is sustained in the ranges of 200 to 350 mbar gauge. This large volume has the merit of being able to provide high peak flows when needed according to the manufacturer [2].

The role of the tank pressure relief valve (8) is to ensure that there is no uncontrolled pressure upsurge in the tank in cases when a fault occurs. It operates in such a way that when the pre-set maximum value has been achieved, the gas is automatically discharged into a room by the automatic opening of the valve. An oxygen sensor (9) is used to monitor oxygen concentration in the tank. The output voltage that is proportional to the concentration of oxygen generated is applied in regulating the opening degree of the inlet metering valves (5) and (6). If there is an abnormal increase in levels of oxygen concentration, then an alarm is used as an indicator. To protect the patient and the inspiratory valve against the possibility of encountering contaminated particles from the gas, a filter (10) is employed. Current MVs have an accurate proportional inspiratory valve (11) that permits precise control of the patient's inspiratory gas. Some manufacturers have models for instance Galileo, [2], whose inspiratory valve is equipped with a differential pressure sensor coupled with a position sensor. The pressure difference across the orifice in the inspiratory valve is measured by the position sensor. The flow of gas through this valve can therefore be calculated. For some ventilator models for example automatic resuscitators and small ventilators used during the transportation of a patient, the inspiratory valve is a fixed orifice flow resistor that allows for a steady flow of gas. For some ventilators used on infants for example the Bourns BP-200 and infant Flow SIPAPA device by care fusion, the inspiratory valve is normally manually adjusted [2]. To avoid an upsurge in uncontrolled pressure downstream of the patient, which might result in the damaging of the patient's lungs, a pressure relief valve (12) is included in the circuit. When a maximum pre-set pressure is reached which is also known as the cracking pressure, the gas is discharged into the external environment via the automatic opening of the valve. If the system malfunctions, then a further safety valve (13) is on standby and it usually opens when there is a fault thus allowing the patient to breathe. During a normal uninterrupted operation, valves 12 and 13 are closed. The pressure sensor (14) is used to measure pressure. The control of the temperature and humidity of the gas inspired by the patient is conducted through a humidification device and a heat exchanger (15). To measure and monitor the patient-inspired and expired gas flow, a strategically positioned flow sensor (16) placed in close proximity to the mouth of the

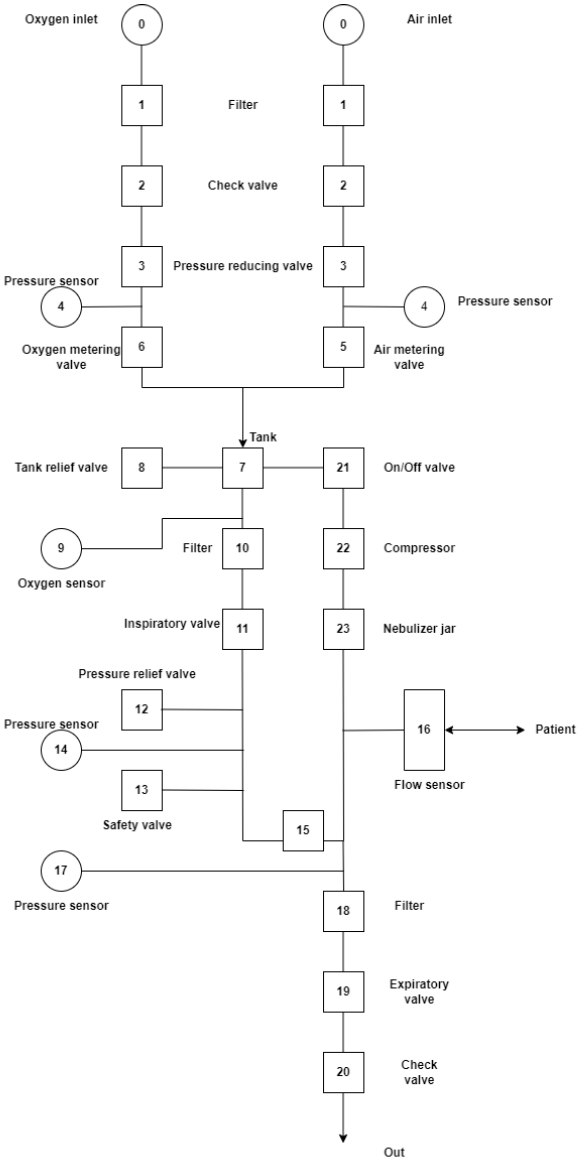

Figure 1.4: ICU mechanical ventilator block diagram, [2].

patient is employed. The other parts of the circuit are a pressure sensor (17), an optional additional filter (18), an expiratory valve (19) and a check valve (20). Dräger Infinity V500 and the Galileo, [2] models, have the expiratory valve which is a proportional directional valve. This valve is used to regulate the minimum pressure in the patient circuit and to control the flow of expiratory gases from the patient to the surroundings. The reverse flow is avoided in the expiratory circuit when the check valve (20) is employed. [2], research shows that for Galileo, the directional on/off valve (21) opens when an additional function is activated. There is an increase in the pressure of the gas tank by the compressor (22) to approximately 900 mbar which is translated into the nebulizer jar (23) [2]. There are several control strategies for the system. Some of the control strategies used for critical patients are Volume Controlled Ventilation (VCV) and Pressure Controlled Ventilation (PCV).

The VCV is a type of ventilation where the predetermined volume of gas also known as tidal volume is supplied to the patient [7]. To meet the desired goal, the inspiratory valve (11) is opened and the patient-inspired flow rate is measured using a flow sensor (16).

After the desired tidal volume has been achieved and the patient's lungs are filled, the inspiratory valve is closed and the expiratory valve (19) opens thus permitting the patient to expire. During this process, the Positive End Expiratory Pressure (PEEP) is sustained higher than the preset values thus preventing the lungs from collapsing. The other strategy used namely PCV applies pressure in which the ventilator adjusts the inspiratory flow and keeps the maximum airway pressure at the set level during inspiration [7]. For patients who can breathe on their own, the MVs have a spontaneous breathing support mode which is known as the Bi-Level Positive Airway Pressure (BIPAP). It is a ventilation mode that is noninvasive and provides various levels of pressure for the patient. When the patient is allowed to spontaneously breathe and the machine supports the patient's breathing, that mode of ventilation operation is known as the synchronized intermittent Mandatory Ventilation-Pressure Controlled (SIMV -PC) [7]. The Medicines and Healthcare Products Regulatory Agency (MHRA) provides the criteria to be satisfied for the operating parameters of a mechanical ventilator as [7]:

- The plateau pressure, must not exceed 34.32 mbar (35 cmH2O) gauge [7].
- The fail-safe valve of the MV must open at 78.45 mbar (80 cmH2O) gauge [7].
- The Positive end-expiratory pressure (PEEP) must be greater than 4.903 mbar (5 cmH2O) gauge, adjustable in at least 4.903 mbar (5 cmH2O) increments [7].

1.3 IDENTIFIED GAPS IN THE LITERATURE

Considering the comprehensive literature review conducted in Chapter 2 of this work, to the best knowledge of the author:

- There are currently no detailed Port Hamiltonian models of the mechanical ventilator subsystem integrated with a human respiratory system
- There are currently no comprehensive or integrated or Port Hamiltonian modelling frameworks for the mechanical ventilator- Human respiratory system.
- There is currently no generalized multi-physics Port Hamiltonian modelling frameworks of the mechanical Ventilator-Human respiratory system.
- There are currently no applications of Port Hamiltonian models of the mechanical ventilator human respiratory system for investigation of the influence of airway secretion on airflow dynamics for mechanical ventilation and for applications in Smart dual occupational health monitoring systems for mine workers

1.4 PROBLEM CONTEXTUALIZATION

MVs are one of the basic elements of the Intensive Care Unit (ICU). Globally, large numbers of Individuals have always required mechanical ventilation per year [1]. The Covid 19 pandemic elevated the significance of the MVs which have played a significant role in sustaining critically ill patients due to Covid 19, who could not breathe on their own. The pandemic drew the attention of the world to the shortage of ventilators globally. It was extremely difficult for hospitals to meet the demand of the required number of ventilators at very short notice. Some manufacturers changed their entire production line to offer their resources to assist in the production of ventilators, for instance, General Motors, Ford, Nissan, Formula One, and Tesla [2]. Considering the past and the current need for ventilator machines, it is important that efficient MVs machines be researched, modelled, designed and implemented. To test and improve the accuracy and efficacy of MVs in the delivery of air or medicines to patients, it is imperative that integrated models of MV-patient dynamics have to be developed

1.5 RESEARCH RATIONALE AND MOTIVATION

Currently, there are no energy-based models of MV-patient systems that can be used in systems that have dissipation of energy from the ports. Complex dynamical systems can be modelled and controlled in the Port Hamiltonian framework because the framework provides a powerful tool for the analysis, modelling and control of such systems. The key attributes of the Port Hamiltonian(pH) framework is: firstly, it is established on the multi-domain bond-graph modelling method which connects various physical elements via ports. The interconnection in Port Hamiltonian is such that there is power conservation. Secondly, there is a significance on the energy variables as well as the total energy stored which is also known as the Hamiltonian as the foundation for multi-physics system modelling. The Port Hamiltonian approach provides the basis for understanding the energy transfer in the various physical domains that govern the respiratory system. Sampled data can be obtained when the Port Hamiltonian structure is exploited and preserved in discretization. This research work applies the Port Hamiltonian systems approach to model the MV-human respiratory system. The resulting model explicitly shows the energy storage, energy dissipation and the interconnection underlying the system. The obtained Port Hamiltonian model has numerous applications for instance, it may be applied in the design of various medical devices and respiratory disease diagnostics and treatment

1.6 RELATED FIELDS

The Port Hamiltonian approach has previously been applied to other systems. Some of the authors that have presented the application of the Port Hamiltonian theory as a contribution to the Port Hamiltonian field are and are not limited to: Port Hamiltonian modelling of the human outer ear, [8], middle ear [9] and inner ear [10]. Other researchers have presented research work in the modelling of vocal fold using the Port Hamiltonian approach [11], [12], [13]. Modeling of audio and acoustics systems, [14], [15]. Control and modelling of flexible structures [16].

1.7 PROBLEM STATEMENT

In Intensive Care Units (ICU), mechanical ventilation plays a significant role in the provision of life support functions for patients who are encountering challenges or are incapable of breathing on their own. MVs are the machines employed in this important task. Control Engineering is usually applied and it plays a crucial role in the safe and accurate delivery of gas to the patient. Delivery of gas to a patient may be controlled through the volume or it may be controlled through pressure. In cases where there are unintentional leaks for non-invasive ventilation, accurate and precise target pressure tracking becomes critical in ensuring sufficient support for the patient. In addition, pressure tracking is essential in ensuring an improved MV patient synchrony which prevents false triggers. The high mortality rate is linked to asynchrony between the MV and the patient. Conventionally, Linear time-invariant feedback controllers have been applied in MVs which has produced sub-optimal performance in terms of settling time and overshoot. A controller system in mechanical ventilation is expected to ensure robust performance over a wider spectrum of patients ranging from adults to infants. Current research is showing improved performance in pressure tracking. However, there is a need to develop better target tracking pressure such that the specification criteria are satisfied. In order for better robust controllers to be designed, implemented and tested on the MV-human lung system, there is a need for alternative models using better approaches that would easily permit the use of robust controllers to be developed. Research, modelling, designing and controlling of integrated mechanical-ventilator systems is essential in ensuring that varying types of controllers are applied to the system thus ensuring the efficient and accurate tracking of target pressure. Considering the past, current and future need for better models of mechanical ventilator lung systems:

The problem statement can therefore be summarized as follows:

- **The Port Hamiltonian approach has not been used in the modelling of the mechanical ventilator system in an integrated Mechanical Ventilator respiratory system**
- **A comprehensive integrated Port Hamiltonian model of the Mechanical Ventilator Human Lung system has not been developed**
- **There currently are no existing applications of mechanical ventilator Human respiratory system in the Port Hamiltonian framework**

1.8 RESEARCH QUESTIONS

1. Can a Mechanical Ventilator human respiratory system be modelled using the Port Hamiltonian framework

2. Can a Mechanical Ventilator human respiratory system be interconnected using the Port Hamiltonian Approach?
3. Are there any applications of a Port Hamiltonian Mechanical Ventilator Lung system?

1.9 RESEARCH OBJECTIVES

Therefore, the research objectives are:

- To provide a comprehensive Port Hamiltonian model of the mechanical ventilator.
- To Comprehensively model and integrate the mechanical ventilator-human respiratory system dynamics using the Port Hamiltonian approach.
- To model and interconnect an electrical and fluid system using the Port Hamiltonian approach
- To provide applications of the developed Port Hamiltonian mechanical ventilator human respiratory system model.

1.10 CONTRIBUTIONS OF THIS THESIS

The main contributions of this research work are:

1.1 Formulation of a detailed novel Port Hamiltonian model of the mechanical ventilator which can be integrated with various Port Hamiltonian models of the human respiratory system.

1.2 Formulation of a comprehensive integrated Port Hamiltonian model of a mechanical ventilator human respiratory system. The Port Hamiltonian models of the Human respiratory system are formulated at three levels of abstraction, each with an increasing level of detail.

  - The first model presents the formulation of an integrated Port Hamiltonian lumped parameter model of the Mechanical Ventilator lung system.
  - The second model is the formulation of a comprehensive Port Hamiltonian model of the Mechanical Ventilator Lung system to include the alveoli using electrical analogies.
  - The third model is a multi-physics and multi-scale Port Hamiltonian model of the human lung in which the mechanical ventilator lung system is modelled as a mechano-hydro-electrical system that includes the alveoli and the diaphragm.

1.3 A generalized multi-physics Port Hamiltonian modelling approach of the mechanical ventilator human respiratory system with Navier stokes for the fluid flow in the mechanical ventilator lung system (distributed parameter system). This contribution

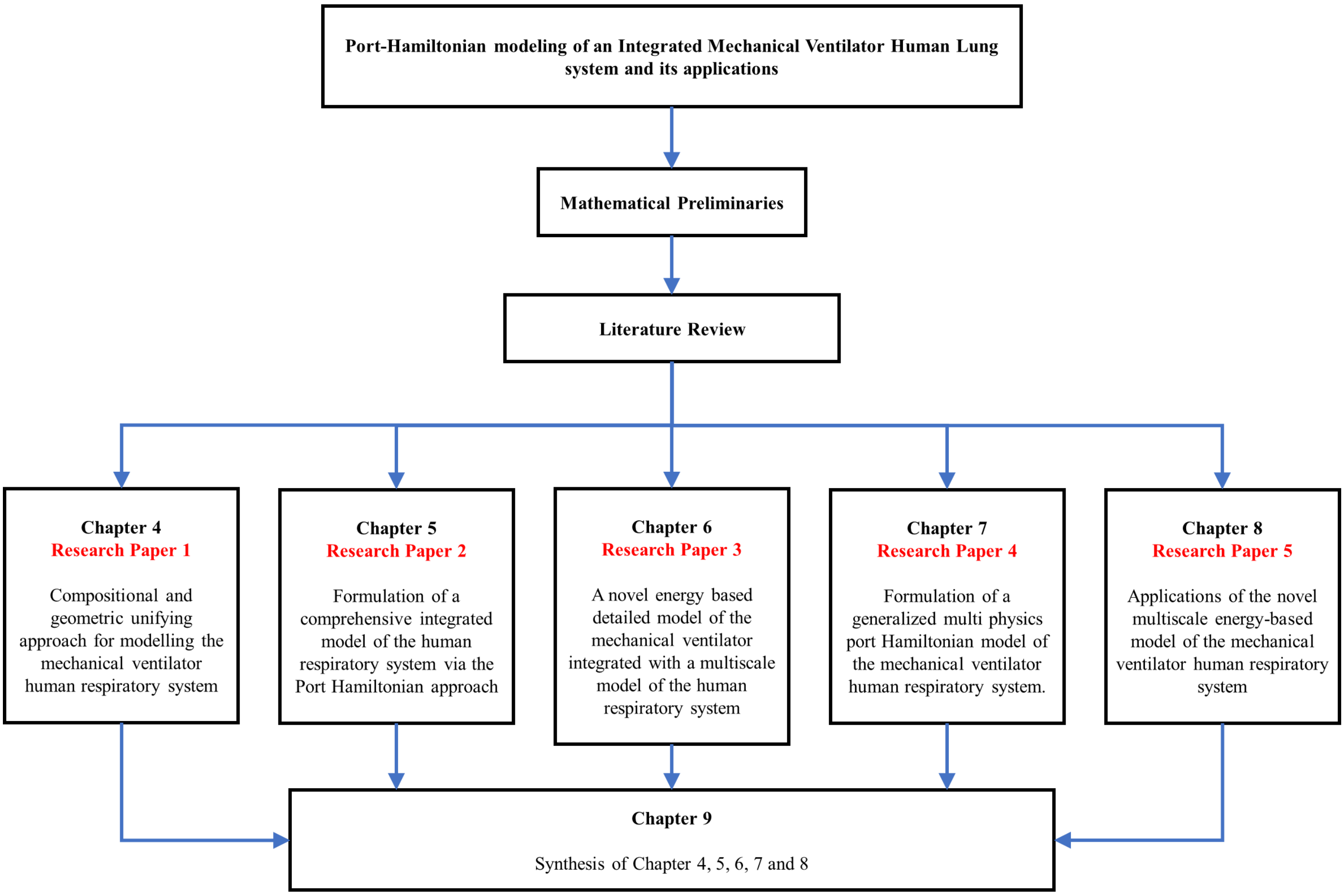

Figure 1.5: Overview of the research method and strategy.

results in a novel Dirac structure that can also be applied in the modelling of fluid power systems.

To demonstrate the applications of the derived theory: two novel applications are presented namely:

- A Port Hamiltonian multi-phase flow Mechanical Ventilator - Human respiratory system for investigation of the impact of respiratory system airway secretion on the dynamics of airflow for a mechanical ventilated respiratory system
- Applications of Port Hamiltonian human respiratory system model in a mine worker's respiratory health monitoring system.

1.11 RESEARCH STRATEGY AND METHODOLOGY

This section provides the strategy and steps that were applied to answer the research question. The methodology was applied in the development of the model. Data collection and ethical clearance issues are also discussed in this chapter.

1.11.1 *Research Approach*

The main objective of this research work is to develop a novel integrated Port Hamiltonian model of the mechanical ventilator human respiratory system. The developed model can be used in various applications for instance the development of higher-order controllers that allow for a better pressure-tracking strategy for the MV lung system. Existing works are used to obtain quantitative data that is used in validating the mechanical ventilator human lung model. To illustrate the applications of the developed model, data is collected from a Platinum mine in South Africa. Qualitative data is used in the discussion, analysis and explanation of results.

1.11.2 *Description of the methodology*

The overall methodology followed in this research work is presented in figure 1.5. and the Port Hamiltonian approach followed in modelling the mechanical ventilator and the respiratory system is shown in figure 1.6.

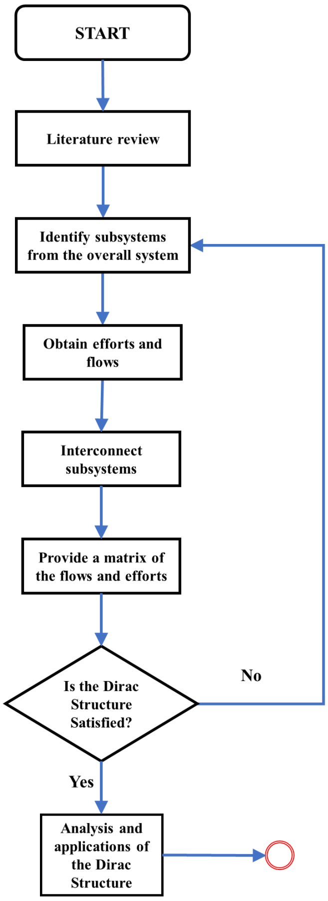

Figure 1.6: Port Hamiltonian modelling of the mechanical ventilator - human respiratory system

1.11.3 *Ethical clearance*

This research work uses respiratory health information collected from a Platinum mine in South Africa. The ethical clearance and permission to use the data sets have been provided. In addition to that, results from an experimental set-up using real human participants are also presented. All ethics and protocols for dealing with human participants were followed. Other data sets used were obtained from publications which are already in the public domain. This research work has an ethical waiver letter, and medical ethical clearance letter and hence the findings of this research work may be published. The certificate is provided in Appendix A.

1.12 SCOPE AND LIMITATIONS OF THIS THESIS

- This research work will only consider the Human respiratory system
- Non-invasive patient ventilation will be considered
- This research work considers a stationary patient and not a patient being transported (On an aeroplane, ambulance, personal vehicle etc)

1.13 THESIS OUTLINE

The remainder of this thesis is organized as follows

Chapter 2

This chapter provides a detailed literature review of the research work under consideration. The modelling of the mechanical ventilator-human respiratory system is considered in this chapter.

Chapter 3

This chapter provides the mathematical preliminaries and notation that is developed/used throughout the remainder of the content presented in the chapters.

Chapter 4

This chapter presents the author's own research work (Research paper 1) submitted in a journal paper titled " Compositional and geometric unifying approach for modelling the mechanical ventilator human respiratory system " [17]

Chapter 5

This chapter presents an extension of Research Paper 1 which is the author's own research work (Research Paper 2) submitted in a journal paper titled. " Formulation of a comprehensive integrated model of the human respiratory system via the Port Hamiltonian approach" [18]

Chapter 6

This chapter presents an extended formulation of the mechanical ventilator aspect of the research work which is the author's own research work (Research paper 3) submitted in a journal paper titled " A mixed finite/infinite dimensional Port Hamiltonian model of a mechanical ventilator " [19]

Chapter 7

This chapter presents a generalized Port Hamiltonian formulation of the mechanical ventilator respiratory system which is the author's own research work (Research paper 4) submitted in a journal paper titled. "Formulation of a generalized Multi physics Port Hamiltonian model of the mechanical ventilator human respiratory system " [20]

Chapter 8

This chapter is a summarized illustration of the applications of the previously developed Port Hamiltonian models which is the author's own research work (Research papers 5 and 6). One publication is already available online. The titles of the research papers are as follows: Research paper 5: "Port Hamiltonian model for investigation of the influence of airway secretion on airflow dynamics for mechanical ventilation". Research paper 6: "Smart dual occupational health monitoring system for mine workers"

Chapter 9

This chapter presents the final synthesis of the presented publications in chapters 4, 5, 6, and 7. In addition to that, this chapter also presents the recommendations and the conclusions of the presented research work.

1.14 CONCLUSION

This chapter has provided a brief introduction to Mechanical ventilators and the human respiratory system. The problem statement, research gaps, objectives, research questions, and contributions have also been discussed. To further comprehend the gaps in the research work being conducted, a comprehensive literature review is provided in the next chapter.

2

LITERATURE REVIEW

2.1 SUMMARY

The section that follows provides the details of the literature review. The literature review approach is presented. Followed by a presentation of literature on the modelling of the mechanical ventilator human respiratory system. Models of the human respiratory system, mechanical ventilators, integrated models, and the applications of integrated mechanical ventilators are also presented.

2.2 INTRODUCTION

This section provides the introduction to the literature review. The contribution and the approach for the literature review is also provided in this section. This chapter resulted in a review publication and hence the contribution of this chapter even though not listed among the formal contributions of this research work still remains an important contribution to researchers who are seeking to gain knowledge in the same field of study.

2.3 SIGNIFICANCE OF THE CHAPTER

The chapter investigates the existing literature on the modelling of the integrated mechanical ventilator human respiratory systems using the Port Hamiltonian framework. The applications of such models if they exist is also researched. The main significance of this chapter is the presentation of a detailed review that investigates the application of the Port Hamiltonian-based approach in the formulation of an integrated Mechanical Ventilator human respiratory system.

2.3.1 *Approach for the literature review*

Adhering to Levac et al.'s [21] methodology, the author of this research decided on a broad research question which formed the focus of this literature review, the specification of MeSH terms/keywords/ phrases and the choice of databases to be searched. The Arksey and O'Malley's [22] framework was adopted. The broad question that guided the literature review is, "Can mechanical ventilator human respiratory system be modelled in the Port Hamiltonian framework?" The exploration of this question was a precursor to the development of a comprehensive integrated Port-Hamiltonian model of the MV-human respiratory system. The search was conducted in December 2020 and a rerun to establish available information was conducted in July 2023 in the following electronic databases: IEEE Xplore, ScienceDirect, Biomed Central, web of Science, Academic Search Complete, Scopus, Medline, PubMed, and ProQuest. It was required that the only studies to be included should have been conducted in English between 1970 and 2023. The search comprised the following terms: Modeling mechanical ventilators, human respiratory system models, Port Hamiltonian models of the respiratory system, integrated mechanical ventilator respiratory system models and applications of Integrated models of the mechanical ventilator human respiratory system.

To begin with, 209 publications were identified for the possibility of being included in this study. In the process of data organization, 40 studies were duplicated and hence they were excluded; therefore, 169 research articles were considered. Out of the 169, 40 were eliminated based on the information provided on the titles and/or abstracts that were found not to satisfy the requirements of the current research work. Subsequently, 129 research articles were evaluated for eligibility, and from these, 40 were excluded as they did not meet the study's inclusion criteria. During the review of the full text, an additional 42 manuscripts were excluded, hence 47 manuscripts were finally included for analysis. This is also illustrated in the Prisma flow diagram in figure 2.1.

2.4 MODELLING OF MECHANICAL VENTILATOR HUMAN RESPIRATORY SYSTEM

There are two aspects to be considered when looking at human respiratory health. Firstly; it's the anatomy of the respiratory system and secondly; it's the transportation of air and particles in the respiratory system and their deposition. For improved respiratory health risk evaluation, there is a need for a better understanding of gaseous air exchange during breathing, when an individual is coughing and sneezing. Current literature has provided an increase in the knowledge and understanding of the anatomy of the human respiratory system. Particle transportation and airflow characterization in the human respiratory system have also been extensively studied hence the knowledge has resulted in significant improvements in the prediction and prevention of respiratory diseases. There are currently various techniques for modelling the anatomy and air transportation of the human respiratory system. For example; the Finite element, provides a good approximation to the dynamics and geometry of the respiratory system. However, they have also been cited to have numerical challenges when acoustic resonances, collisions and fluid mechanics are put into consideration. Finite element models are also computationally costly. Lumped element models provide a good trade-off between simplicity and feature representation. They also reproduce clinical features with good precision and reasonably low computational costs and are usually preferred for studying and investigating pathological and normal functions. Finite element models, Electro-mechanical models, mechanical models and, lumped-element models have been used for both clinical and scientific research stud-

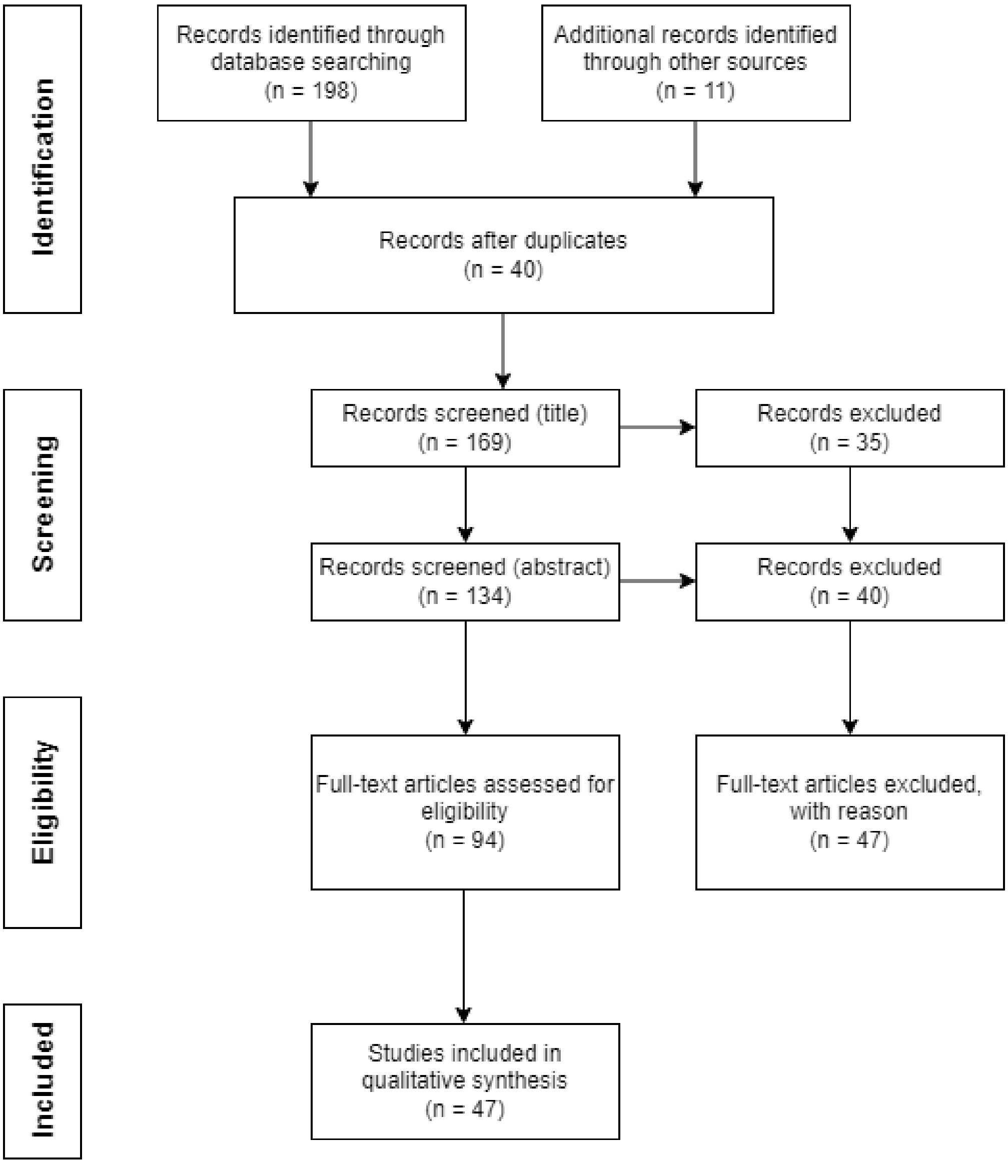

Figure 2.1: A Prisma flow diagram showing a summary statistics of the literature review.

ies. These models have been used to understand the functioning of the respiratory system and to provide diagnosis and treatment for individuals with respiratory diseases.

2.5 MODELING OF THE HUMAN RESPIRATORY SYSTEM

Dynamic models of the human respiratory system are mathematical representations that simulate the mechanics of breathing and gas exchange in the lungs. These models can be used to investigate the behaviour of the respiratory system under different conditions and to predict the effects of various interventions or treatments. There are different types of dynamic models of the respiratory system, ranging from simple lumped-parameter models to more complex distributed-parameter models that simulate the spatial distribution of airflow and gas exchange in the lungs [23]. One of the most commonly used models is the so-called "two-compartment model", which represents the respiratory system as two interconnected compartments: the airway compartment and the lung compartment. In this model, the airway compartment is represented as a series of resistances and capacitances that simulate the resistance and compliance of the airways, while the lung compartment is represented as a series of alveolar sacs that simulate the gas exchange process. More complex models may incorporate additional factors such as lung tissue compliance, airway branching, and the effects of respiratory muscles. These models can be used to study the dynamics of lung diseases such as asthma, chronic obstructive pulmonary disease (COPD), and pulmonary fibrosis, and to evaluate the efficacy of various treatment options [23]. Overall, dynamic models of the respiratory system provide a valuable tool for understanding the mechanics of breathing and gas exchange, and for developing improved treatments for respiratory disorders.

2.5.1 *Mathematical models of the respiratory system*

Sound mathematical formulations of the underlying physics of the respiratory system are very important in understanding the anatomy and physiology of the organ. Classical modelling methodologies which employ a physiological or clinical perspective have been previously used majorly for data fitting of single compartment model parameters for example [24]. Human lungs are usually mathematically viewed to be made up of intricate networks of branching compliant tubes spanning a broad range of scales and flow regimes. The flow may be a highly pulsatile flow or an almost laminar diffusion-dominated process. Flow enters a sponge-like microstructure of lung tissue from the terminal branches of the airway. The lung tissue material behaviour is very non-linear and for efficient gaseous exchange, the topology is optimized with small], embedded blood vessels. Current research developments in the mechanical and mathematical modelling of the lung have mainly focused on studying isolated effects which are difficult to understand and assess in vivo, to advance medical imaging and functional diagnostics and assist in patient-specific treatment planning and optimization. Bates [25] used the system identification approach to provide a mathematical description of the lung mechanics with evolving intricacies in the mathematical formulations. This ranged from single linear compartments to generalized multi-compartmental models. Maury [26] further developed the concept proposed by Bates, [25] and described the lung as a resistive tree. Various levels of description are proposed, which include lumped models with a small number of parameters described by Ordinary Differential Equations (ODEs), up to infinite dimensional models based on Partial Differential Equations (PDEs). The resistive networks and the way they can be used to investigate the dependence of the lung's resistance upon geometrical characteristics are also presented. The analysis of the various models from a theoretical perspective is provided. The approximate solutions techniques provided allow for a good comparison with experimental measurements. Other researchers that propose similar works are Burrowes et al, [27], Tawhai et al, [28], Berger et al [29]. Research has also been conducted by Roth et al, [30], using Navier–Stokes equations for fluid flow from a very mathematical perspective. This research work also provides comprehensive and computationally fully resolved fluid representations of the human respiratory models or parts thereof. The solutions of the three-dimensional Navier-Stokes equations on rigid geometries have also been formulated. Information from medical imaging alongside the fluid domain has been used to formulate real fluid-structure interaction effects [30]. As an approach to replicating real fluid structure impacts, techniques have been developed and published that demonstrate this concept in the fluid domain by application of data from medical imaging information. To quantify particle deposition or drug delivery in the lower and upper airways and for investigation of patterns in the lungs such as jets or vortices, a fully resolved fluid model may be used [20-24]. Such models are very complex and, in most cases, only parts of the human respiratory system are investigated thus eliminating the important impacts on the entire organ. A holistic human respiratory system model requires both a consistent physiological realistic representation of the respiratory mechanics in addition to the purely mechanical or structural aspects because the basic physics of respiratory mechanics is governed by the interaction of the fluid with the anatomy. The normal function of the lung is possible due to the deformation of the associated muscles, airway tree and lung tissue. Indeed, tissue properties have an influence on airflow and the processes that occur during air transportation for instance during gaseous exchange or aerosols transportation.

2.5.2 *Modeling of airflow and particle deposition in the human respiratory system*

Doorly et al [31], Explored the mechanics of airflow in the human nasal airways using both experimental and computational approaches. The authors describe the anatomy of the nasal airways and discuss the factors that influence airflow patterns, such as the geometry of the nasal passages, the nasal cycle, and the presence of nasal septal deviations. The article also presents findings from computational simulations of nasal airflow, including the effects of nasal obstruction on airflow patterns and the role of the nasal valve in regulating airflow resistance. Experimental studies of nasal airflow using techniques such as particle image velocimetry and acoustic rhinometry are also described. The study provides insights into the complex mechanics of nasal airflow and highlights the importance of considering the role of the nasal airways in respiratory function. The findings could have implications for the diagnosis and treatment of respiratory disorders related to nasal obstruction, such as allergies, sinusitis, and sleep apnea.

Bahamman et al, [32], presents an investigation into the effects of nasal dilation, sleep stage, and sleep position on upper airway resistance syndrome (UARS). UARS is a sleep disorder characterized by increased resistance to airflow during sleep, which can lead to symptoms such as snoring, daytime fatigue, and insomnia. The study found that nasal dilation, which is achieved using nasal strips or sprays, can significantly reduce upper airway resistance in individuals with UARS.

Sandeau et al, [33], Describes a computational fluid dynamics (CFD) simulation of the deposition of particles in the oral extrathoracic airway. The researchers constructed a 3D model of the oral extrathoracic airway based on anatomical data from human subjects and used it to simulate the deposition of particles of different sizes and densities under various flow conditions. The study found that particle deposition in the oral extrathoracic airway is strongly influenced by the size and density of the particles, as well as the flow rate and composition of the gas mixture. The researchers observed that helium-oxygen mixtures, which are used clinically to improve oxygenation in patients with respiratory distress, result in lower particle deposition compared to air. The article also discusses the potential applications of these findings for the development of improved respiratory therapies and the design of medical devices.

Ball et al, [34], researched the use of computational fluid dynamics (CFD) to model airflow in an idealized human extra-thoracic airway. The researchers used a high-resolution turbulence model to simulate the airflow through the airway under different flow rates and configurations. The study found that turbulence plays a significant role in airflow dynamics in the extra-thoracic airway. The researchers observed that the degree of turbulence was strongly influenced by the flow rate and the configuration of the airway. The article also discusses the potential applications of these findings for the diagnosis and treatment of respiratory diseases.

Xu et al, [35], Describe the use of computational fluid dynamics (CFD) to model the airflow, heat transfer, and particle deposition in a realistic human upper airway model during oral breathing. The researchers investigated the effects of various factors, such as flow rate, particle size, and breathing cycle, on these parameters. The study found that the flow rate and breathing cycle significantly affect the airflow patterns, heat transfer, and particle deposition in the upper airway. The researchers observed that a higher flow rate resulted in increased turbulence and particle deposition, while a lower flow rate resulted in decreased turbulence and particle deposition. The insights gained from this research could lead to the development of new and more effective treatments for respiratory diseases, as well as improved inhalation devices for delivering those treatments

Sarangapani et al, [36], Discuss the modelling of particle deposition in the extrathoracic airways, which are the nasal passages, mouth-throat, pharynx, and larynx. The research work also reviews the current understanding of the deposition mechanisms and factors affecting particle deposition in these airways, such as particle size, shape, and flow rate. The mathematical model predicts particle deposition in the extrathoracic airways, which considers the anatomical and physiological characteristics of these airways. Overall, the modelling approach presented in the paper has the potential to improve our understanding of particle deposition in the extrathoracic airways and inform the development of interventions to protect and promote respiratory health.

Heena et al, [37], investigates the relationship between the flow field and regional deposition in realistic extra-thoracic airways. The authors used computational fluid dynamics (CFD) simulations to investigate the effects of various parameters, such as flow rate, airway geometry, and particle size, on the deposition of particles in the extra-thoracic airways. The study found that the airway geometry and flow rate significantly affect the flow field and regional deposition in the extra-thoracic airways. The findings of this study have significant implications for improving respiratory health and developing more effective respiratory therapies. The insights gained from this research could lead to the development of new and more effective treatments for respiratory diseases, as well as improved inhalation devices for delivering those treatments.

Johnstone et al, [38], research work investigated the fluid dynamics of airflow in an idealized form of the human extra-thoracic airway. The authors used computational fluid dynamics (CFD) simulations to investigate the effects of various parameters, such as Reynolds number and airway geometry, on the flow characteristics of the air in the extra-thoracic airway. The study found that the geometry of the extra-thoracic airway significantly affects the flow field, with constrictions in the airway, such as the nasal valve, causing increased turbulence and changes in velocity. The researchers observed that the flow field is highly dependent on the Reynolds number, with laminar flow occurring at lower Reynolds numbers and turbulent flow occurring at higher Reynolds numbers. They also found that the flow in the extra-thoracic airway is asymmetrical, with the right nasal passage having a higher flow rate than the left nasal passage. Overall, the findings of this study have significant implications for improving respiratory health and developing more effective respiratory therapies and inhalation devices

[39], research work explored the mechanisms by which the larynx regulates respiratory airflow. The authors discuss the anatomy and physiology of the larynx and its role in the control of respiratory airflow. The study found that the larynx plays a crucial role in the regulation of airflow during respiration, with its primary function being to protect the lower airways from foreign objects and prevent the entry of air into the stomach during swallowing. The authors discuss the complex interactions between the muscles and structures of the larynx during respiration, including the vocal cords, arytenoid cartilages, and epiglottis. The article also discusses the implications of laryngeal dysfunction for respiratory health. Overall, the findings of this study have significant implications for improving respiratory health, developing treatments for laryngeal disorders, and enhancing diagnostic methods for respiratory diseases.

Tevfik et al, [40], research paper investigates the dynamics of spray formation and deposition in a simple throat model. The authors used numerical simulations and experimental measurements to analyze the characteristics of the spray, including droplet size and velocity, and the deposition patterns on the throat walls. The study found that the spray dynamics in the throat model were complex, with significant variations in droplet size and velocity. The authors observed that the deposition patterns were influenced by various factors, including spray velocity, droplet size, and throat geometry. The study's findings could ultimately enhance treatment outcomes for respiratory diseases and other conditions. By developing more effective inhalation devices and drug delivery methods, healthcare providers could improve the effectiveness of treatments and potentially reduce the risk of adverse side effects. The findings of this study have significant implications for improving drug delivery methods and enhancing treatment outcomes for respiratory diseases and other conditions.

[41], Conducted research work to compare the results of numerical simulations using the turbulence model with experimental data on aerosol deposition in the mouth and throat. The main objectives of the study were to evaluate the accuracy of the turbulence

model in predicting aerosol deposition and to identify any limitations of the model. The turbulence model was found to provide a reasonable prediction of the deposition patterns in the mouth and throat. However, there were some discrepancies between the numerical simulations and experimental measurements, particularly in regions with high curvature and rapid changes in flow direction. The study's findings could inform the development of more accurate numerical models for predicting aerosol deposition in the mouth and throat, which could help optimize drug delivery methods.

Jayaraju et al, [42], research work applied numerical simulations to study fluid flow and particle deposition in the human mouth and throat. The authors aimed to evaluate the effectiveness of two different turbulence models; large eddy simulation (LES) and detached eddy simulation (DES), in predicting fluid flow and particle deposition in the mouth and throat. The study's findings could help optimize treatment for respiratory diseases and other conditions by providing insights into the factors that affect particle deposition in the mouth and throat. By understanding how particles deposit in different regions of the respiratory system, researchers can develop more effective treatment strategies and adjust treatment methods as needed.

Allen et al,[43], applied computational simulations to study airflow in an in vitro model of the pediatric upper airways. The authors used a three-dimensional model of a child's airway to investigate the effects of various factors on airflow, including the size of the airway, the shape of the airway, and the position of the tongue. The results of the study showed that the size and shape of the airway have a significant impact on airflow patterns, with narrower airways resulting in increased resistance to airflow. The position of the tongue was also found to have a significant effect on airflow, with a more posteriorly positioned tongue resulting in greater airflow resistance. The study provides valuable insights into the factors that affect airflow in the pediatric upper airways and could help inform the development of more effective treatments for conditions such as obstructive sleep apnoea and other respiratory disorders.

Cheng et al,[44], investigate the effects of laryngotracheal stenosis (LTS) on upper airway aerodynamics using computational fluid dynamics simulations. The authors created a three-dimensional model of the upper airway, including the larynx and trachea, with varying degrees of LTS. The results showed that LTS significantly affected upper airway aerodynamics, resulting in increased airway resistance and altered airflow patterns. The simulations also showed that the severity and location of LTS influenced the degree of aerodynamic disturbance. The study highlights the importance of considering the effects of LTS on upper airway aerodynamics when diagnosing and treating respiratory disorders.

2.5.3 *Electrical models of the human respiratory system*

Electrical models of the human respiratory system are mathematical models that represent the respiratory system as an electrical circuit. These models can be used to analyse the electrical properties of the respiratory system and to simulate the behaviour of the system under different conditions [23]. The respiratory system can be represented as an electrical circuit by using electrical components that correspond to the different anatomical structures of the respiratory system. For example, the airways can be represented as a series of resistors, the lungs can be represented as capacitors, and the respiratory muscles can be represented as voltage sources [45]. One of the most commonly used electrical models of the respiratory system is the impedance model, which measures the resistance and reactance of the respiratory system. This model can be used to study the mechanical properties of the respiratory system, such as airway resistance and lung compliance. Other electrical models of the respiratory system include models that simulate the effects of ventilation and perfusion on gas exchange and models that incorporate the effects of respiratory disorders such as asthma and COPD. Electrical models of the respiratory system provide a useful tool for studying the physiology and pathophysiology of the respiratory system, and for developing improved diagnostic and treatment approaches for respiratory disorders. Campbell et al,[46] proposed an electrical analogue of the human lung. The objective of the research work was to show the advantage gained by the use of noncomplex analogues in solving lung mechanics challenges. The formulated lung is to be used in the prediction of optimum ventilatory patterns for patients with respiratory diseases who may require intermittent positive-pressure ventilation. Devesh et al, [47] modelled the human respiratory system using analogies of the electrical model by using a Resistor Inductor Capacitor (RLC) parameter. The analogous electrical model parameters are represented as resistance, inheritance, and compliance respectively. The stability analysis and time domain analysis were performed to identify COPD conditions. Bagchi et al, [48], proposed an electrical model of the human respiratory system that could be applied in the diagnosis of ventilatory diseases. The proposed electrical model is an analogy to the physiological structure of the human respiratory system. The Model is made up of passive electrical components for instance resistor, inductor and capacitor. The input impedance was derived from the electrical model.

2.6 MECHANICAL VENTILATOR MODELING

Tran et al [49], conducted research work whose main goal was to design, control, model, and simulate a mechanical ventilator that is light in weight and portable, and suitable for use at home. [49], modelled the mechanical ventilator as a voltage source. El-Hadj et al [50], applied the fluid-structure Interaction (FSI) to couple the computational fluid dynamics used for fluid flow with finite element analysis for the solid domain. This facilitated the investigation of fluid behaviour, structural behaviour, and interactions. Two designs were proposed for the mechanical ventilator. The first design was reported to be uncontrollable and the second design considers Computational Fluid Dynamics (CDF) with a moving boundary which is applied to the piston cylinder-based ventilator. Tharton et al [51], designed and developed a ventilator prototype to be used by professionals in medical emergencies and in any other context where the regular ventilator is not available. The mechanical ventilator was modelled using the crank rocker mechanism in order to meet specific requirements for mechanical ventilator design. Pivk et al, [52], developed an empirical model for a low-cost mechanical ventilator by observing the response of each of the ventilator subsystems.

The current progress made globally in the development of affordable and effective designs is important. However, research in mechanical ventilator development lacks model development. The Port Hamiltonian approach applied in this research work acts as a modeling template for future energy-based mechanical ventilator modeling and design. Lagrangian modelling and Kane's approach do not emphasize energy routing in the system through a Dirac structure. Kane's method is also limited with regards to modelling of the fluid interaction of the mechanical ventilator –human respiratory system. It is important to develop designs that rest on a solid understanding of a significant aspect of the design. Naggar, [53] developed a piecewise model of a mechanical ventilator which described the artificial behaviour of a mechanical ventilator. A pressure-controlled ventilator is created and simulated. The mechanical ventilator is modelled using a periodic function with inequalities to control the beginning of inspiration and expiration periods. Shi et al, [54] developed a mathematical model of volume-controlled mechanical ventilation. The model is viewed as a pneumatic system where the ventilator is regarded as an air compressor. The exhalation valve is considered a throttle. The compressor and the container represent the ventilator. Naggar et al, [55] proposed an integrated mathematical model of the mechanical ventilator and the lung. Linear quadratic and exponential equations were used to model the system. The integrated model was used to simulate volume-controlled artificial ventilation. Giri et al, [56], proposed a simplified design of a mechanical ventilator, to reduce cost and automate the mechanical ventilation process. The proposed design was simulated on the MATLAB platform. Hannon et al, [57] reviewed the progress in mathematical modelling and simulation of the human anatomy, physiology and, pathophysiology using computers in the context of mechanical ventilation. This study emphasized the clinical applications of computer simulations in various disease states. The research work further discussed the present constraints and the possibility of in-silico modelling. There are currently no existing Port Hamiltonian models of mechanical ventilators.

2.7 APPLICATIONS OF INTEGRATED MECHANICAL VENTILATOR HUMAN LUNG SYSTEM MODELS

Integrated mechanical ventilator human lung system models can be used to simulate the behaviour of the respiratory system and to study the effects of mechanical ventilation on lung function. These models have several applications in research, education, and clinical practice. Overall, integrated mechanical ventilator human lung system models provide a valuable tool for understanding the behaviour of the respiratory system under mechanical ventilation, and for developing improved strategies for the diagnosis and treatment of respiratory disorders. The subsections to follow will provide examples of applications of integrated models of the mechanical ventilator respiratory system.

2.7.1 *Design of controllers for accurate pressure tracking*

Yan et al, [58] proposed a purely pneumatic mathematical model of a MV lung system. The presented model was to be used in the diagnostics and treatment of various lung diseases. El-Hadj et al, [50] designed and simulated a MV system. A finite element method was applied in solving the set of coupled equations. Chellaboina et al, [59], developed a generic mathematical model for the investigation of the dynamic behaviour of a multi-compartment respiratory system. The direct adaptative controller framework was applied to the system. Borello, [60] developed a lumped parameter model to be used in the investigation of pressure-controlled ventilation.

Borello, [61], applied an inverse model of a patient lung. The dynamics of lung circuit mechanics are nonlinear in the model. An analogous linear circuit called an RCC model is applied to define and provide a description of the lung dynamics by assuming the parameters vary with time. In this RCC model, the resistance for the lung circuit which is usually represented as a series input resistance is considered negligible in comparison to the patient's resistance. Scheel et al, [62] used a simple ventilator patient model given by the thermal constitutive equation. The developed model was used for designing an iterative learning controller.

A single-compartment lung was interfaced with a centrifugal blower which represented a mechanical ventilator system. Literature, Lachmann, [63] and Reinders et al, [1] shows that research has been conducted to establish the optimal settings for the MV's modes and settings. However, the current areas of research are focusing on efficient ways to accurately track the target pressure which will assist in indicating whether the patient is being sufficiently supported. Accurate target pressure tracking is very essential in situations where the patient's lung may be large, or when there is an unintentional leak of air for example, during non-invasive ventilation. Pressure tracking may also lead to better patient-ventilator synchrony. Accurate tracking prevents false triggers and it also improves the chances of a patient surviving. In situations where the modes of ventilation are complicated, accurate pressure tracking is important in obtaining the desired standard of assistance, [64], [1].

Conventionally, Linear Time Invariant (LTI) feedback controllers are usually employed in the control of MVs. However, Reinders et al research work [1], has shown LTI to perform sub-optimally in with regards to settling time and overshoot. A satisfactorily performing controller can handle a wide spectrum of patients, from adults to infants as well as any unknown leakages. Various control approaches have been researched to improve MVs. Borrello, [3], presents a review on modelling and control approaches for mechanical ventilation. To reduce overshoots in patient flow, prevent false triggers and improve tracking [64], proposed a variable gain controller. Despite the improvement in patient flow overshoot, the control strategy still needs to be improved. Borello, [61], presents a control technique that applies adaptative feedback to achieve the desired closed-loop transfer function. One of the demerits of this method is that it is not easy to develop an accurate patient model. Laubscher et al, [65] presented an adaptative lung ventilation controller. The controller had a 48 and 81 seconds response to step changes with an overshoot of 5.5 and 7.9 percent respectively.

When the funnel-based control approach is employed on MVs, the obtained gain is constrained in terms of performance [66]. Iterative Learning Control (ILC) is observed to have substantial improvement in the performance of tracking when it is used in the control of mechanical ventilation. However, one of its demerits is the limitation to the repetition of sequences of the initial conditions and the setpoint [67]. The results presented in [67], show a degradation of performance of the ILC in ventilation cases where the patient is breathing spontaneously. Even though the previously presented research work has the potential to improve in terms of tracking performance, it is still lagging in tracking the target pressure accurately.

A model-based control approach is presented in [62] and a Model Predictive control method is presented in [68]. Even though these methods require accurate patient parameters, which may not be readily available in practice, they have a substantial merit of being easy to troubleshoot. This research work presents a fractional proportional derivative and machine learning approach that has the potential to compensate for the pressure drop across the air tubes especially in cases of leaks or large lungs. The main contribution in these research articles is the design of a MV control strategy that will contribute towards ensuring the precise tracking of the human respiratory system air pressure independent of the leakage through the non-invasive ventilation mask or the air tube. The designed controller is an attempt to allow for prompt and precise pressure response while preventing overshoot in the patient flow which leads to false triggering. Sinderby et al,[69] developed a neuro-controller with the potential to improve patient-ventilator interaction and comfort. A neuro-adaptative control framework for MVs was developed by Volyanskyy et al, [70]. The developed architecture automatically adjusts the input pressure to the patient physiological characteristics and it also incorporates the effects of breathing. Mehedi et al, [71], presented the design of a controller using the adaptative sliding mode approach for smooth tracking of the targeted pressure. Classical PID and sliding mode were also developed to benchmark the adaptative sliding mode controller. The fuzzy sliding mode control presented better results in terms of faster convergence, smaller tracking error and less overshoot.

Mohammad et al, [72], proposed a cascaded approach to formulate a robust control system for regulating the states of ventilator units. An active disturbance rejection control structure is proposed for the control of an invasive MV [73]. An active disturbance rejection controller was designed and implemented by Legarda et al, [74] to ensure robustness to the control of continuous dynamics against disturbances. One of the merits of the control structures is that it can be applied to both pressure and volume ventilation. Inspiration and expiration for Intensive Care Unit patient was estimated by applying a fuzzy logic controller [75].

De et al, [76] proposed a feedback vector linear controller for MVs for educational purposes. The objective of the control system was equip students with the knowledge of application of controllers to a system. An evaluation of a nonlinear adaptative fuzzy neural network controller was conducted by Zhu et al [77]. The designed controller was used to regulate flow in a MV and a neural network was applied as well for identification. Gomes et al [78] conducted a study on a mechanical ventilation system to compare the performance of LQG with PID optimized by particle swarm approaches. The objective of Gomes et al [78], research work was to illustrate good practices to researchers with regards to having sufficient suitable theoretical background. The results of Gomes et al [78] research work indicate that LQG outperformed the other controllers. Manne et al, [79], applied a model predictive control approach with the main intention of achieving sufficient gaseous exchange by adjusting the minute volume ventilation. Mehedi et al [80], proposed a fuzzy PID control for the respiratory system. The respiratory system was modelled as a combination of the blower-hose patient system with non-linear lung compliance. There are currently very few studies that have conducted simulations in expiration since a storage possibility for inhaled volume is required during expiration.

2.8 CONCLUSION

The Port Hamiltonian approach is currently an active area of research in various fields. The tools emerging from this approach bring many advantages in the modelling, simulation, and control of complex systems. The main goal of this thesis is to present various abstractions of the integrated Port Hamiltonian model of the mechanical ventilator lung system and its applications.

3

MATHEMATICAL PRELIMINARIES AND NOTATION

3.1 SUMMARY

This chapter provides the background of the Port Hamiltonian method, basic definitions and operations of the Port Hamiltonian approach and the mathematical preliminaries of the method.

3.2 INTRODUCTION

The Port Hamiltonian approach unifies various traditions in physical systems modelling and analysis. In the 1950s Henry Paynter, [81] pioneered the theory of modeling using the port-based approach. Mechanical, electrical, thermal, hydraulic and many other systems belonging to different physical domains are modelled within a unified framework. This is made possible by using energy as the "Lingua franca" between the various physical domains. Energy storage, dissipation and routing are the major physical characteristics captured by the ideal system components. A graphical notation is used in Port-based modelling to emphasize the physical system as a group of ideal components connected by edges which capture the energy flow between them. The edges are referred to as bonds and the graph is called the bond graph. When circuit theory is considered, a pair of variables is used to represent the energy along the bond, in which the product is equal to the power. Examples of such pairs of variables are velocity and forces, voltages and currents, and flows and pressure formulation of bond graph models conducted by Golo et al, [82].

MacFarlane, [81] also presented a further theory of across and through variables which may be viewed as an abstraction of Port-based modelling. The second origin of Port Hamiltonian is rooted in geometric mechanics where the mathematical formulation of classical mechanics is formalized in a geometric way. The Hamiltonian dynamics is represented in a coordinate-free manner using a state space. The geometric approach has resulted in a powerful theory that may be used for the analysis of the intricate dynamical behaviour of Hamiltonian systems. The intrinsic features for instance symmetries and conserved quantities are displayed. The third pillar that forms the foundation of the Port Hamiltonian approach systems and control theory. Dynamical systems are emphasized as being open to interaction with their surroundings via inputs and outputs and being susceptible.

3.3 DEFINITIONS

This section provides the definitions for the building blocks of the Port Hamiltonian approach that have been followed in chapters 4, 5, 6, 7 and 8. These definitions are standard definitions from literature and are mostly derived from the following references: [83], [84], [85] and [86]

Definition 1 (Dirac Structure)
A Dirac Structure (DS) is a pair of elements, $f \in \mathbb{R}^n$ and $e \in \mathbb{R}^n$, that satisfies the set:

$$\mathcal{D} := \left\{ (f, e) \in \mathcal{D},\ (\hat{f}, \hat{e}) \in \mathcal{D} \middle| e^{\mathsf{T}} \hat{f} = -\hat{e}^{\mathsf{T}} f \right\}$$

The DS is a subset $\mathcal{D} \subset \mathcal{F} \times \mathcal{E}$, where $\mathcal{F}$ and $\mathcal{E}$ represent the flows and efforts, respectively.

The DS in electric circuits can be represented as:

Proposition 1:
The subspace

$$\mathcal{D} \subset \mathbb{R}^n \times \mathbb{R}^n$$

is called a DS iff, there exist $A, B \in \mathbb{R}^{n \times n}$ such that

$$AB^{\mathsf{T}} + AB^{\mathsf{T}} = 0 \text{ and } \operatorname{rank}([A\, B]) = n$$

satisfying the condition

$$\mathcal{D} = \{(f, e) \in \mathbb{R}^n \times \mathbb{R}^n | Af = -Be\}$$

Definition 2 (Lagrange Submanifold)
A submanifold $\mathcal{L} \subset \mathbb{R}^n \times \mathbb{R}^n$ of the manifold

$$\mathbb{R}^n \times \mathbb{R}^n$$

is said to be a Lagrange submanifold (LS) if for all points $x \in \mathcal{L}$ and $(y_1, y_2) \in \mathbb{R}^n \times \mathbb{R}^n$ if

$$y_1^{\mathsf{T}} u_2 - y_2^{\mathsf{T}} u_1 = 0$$

is true for all $(y_1, y_2) \in T_x\mathcal{L}$ and $(u_1, u_2) \in T_x\mathcal{L}$.
Proposition 2.
Given a $\mathcal{C}^\infty$ differentiable map, $\mathcal{O} : \mathbb{R}^n \to \mathbb{R}^n$ with graph $\mathcal{O}$, the submanifold $\mathcal{L}_{\mathcal{O}}$

$$\mathcal{L}_{\mathcal{O}} := \{(x, \mathcal{O}(x)) \in \mathbb{R}^n \times \mathbb{R}^n |\ x \in \mathbb{R}^n\}$$

is said to be a Lagrangian submanifold iff there exists a function $H : \mathbb{R}^n \to \mathbb{R}$ that is $\mathcal{C}^2$ differentiable such that

$$\nabla H = \mathcal{O}$$

Proposition 3
A subspace $\mathcal{L} \subset \mathbb{R}^n \times \mathbb{R}^n$ is said to be a Lagrangian submanifold iff there exist $A, B \in \mathbb{R}^{n\times n}$ such that $A^\mathsf{T} B = B^\mathsf{T} A$ and $\text{rank}([A^\mathsf{T} B^\mathsf{T}]) = n$ so that

$$\mathcal{L} = \Big\{(f, e) \in \mathbb{R}^n \times \mathbb{R}^n | A^\mathsf{T} f = B^\mathsf{T} e\Big\}$$

Definition 3 (Resistive Relation)
Any relation $\mathcal{R} \subset \mathbb{R}^n \times \mathbb{R}^n$ is said to be resistive if $\forall(f_\mathcal{R}, e_\mathcal{R}) \in \mathcal{R}$ the

$$e_\mathcal{R}^\mathsf{T} f_\mathcal{R} \le 0$$

is satisfied.

Definition 4 (Port-Hamiltonian (pH) System).
The set $(\mathcal{D}, \mathcal{L}, \mathcal{R})$, defines a pH system where:

- $\mathcal{D} \subset (\mathcal{F}_\mathcal{L} \times \mathcal{F}_\mathcal{R} \times \mathcal{F}_\mathcal{P}) \times (\mathcal{E}_\mathcal{L} \times \mathcal{E}_\mathcal{R} \times \mathcal{E}_\mathcal{P})$ is a DS
- $\mathcal{L} \subset \mathcal{F}_\mathcal{L} \times \mathcal{E}_\mathcal{L}$ is a LS and
- $\mathcal{R} \subset \mathcal{F}_\mathcal{R} \times \mathcal{E}_\mathcal{R}$ a Resistive relation.

The elements of the sets:

- $\mathcal{F}_\mathcal{L} \in \mathbb{R}^{n_\mathcal{L}}$ and $\mathcal{E}_\mathcal{L} \in \mathbb{R}^{n_\mathcal{L}}$ are known as flows and efforts
- $\mathcal{F}_\mathcal{R} \in \mathbb{R}^{n_\mathcal{R}}$ and $\mathcal{E}_\mathcal{R} \in \mathbb{R}^{n_\mathcal{R}}$ are known as resistive flows and efforts
- $\mathcal{F}_\mathcal{P} \in \mathbb{R}^{n_\mathcal{P}}$ and $\mathcal{E}_\mathcal{P} \in \mathbb{R}^{n_\mathcal{P}}$ are known as external flows and efforts, respectively.

where $n_\mathcal{L}, n_\mathcal{R}$ and $n_\mathcal{P} \in \mathbb{N}_0$.
The dynamics of the pH system are given by the differential inclusion

$$\left(-\frac{d}{dt}x(t), f_\mathcal{R}(t), f_\mathcal{P}(t), e_\mathcal{L}(t), e_\mathcal{R}(t), e_\mathcal{P}(t)\right) \in \mathcal{D}$$

where $(x(t), e_\mathcal{L}(t)) \in \mathcal{L}$, $(f_\mathcal{R}(t), e_\mathcal{R}(t)) \in \mathcal{R}$ and $(f_\mathcal{P}(t), e_\mathcal{P}(t)) \in \mathcal{P}$

Definition 5 (Interconnection of n pH Systems)
Let $(\mathcal{D}_i, \mathcal{L}_i, \mathcal{R}_i)$ denote the space of the i^{th} pH system in a set of n pH systems that are to

be interconnected. The space of flows is divided into an external part and a part to be linked and is given by

$$\mathcal{F}_i = \mathcal{F}_{\mathcal{L}_i} \times \mathcal{F}_{\mathcal{R}i} \times \mathcal{F}_{\mathcal{P}i} \times \mathcal{F}_{\mathcal{P}\text{link}}$$

Similarly, the space of efforts is divided into an external part and a part to be linked and is expressed as

$$\mathcal{E}_i = \mathcal{F}_{\mathcal{L}i} \times \mathcal{E}_{\mathcal{R}i} \times \mathcal{E}_{\mathcal{P}i} \times \mathcal{E}_{\mathcal{P}\text{link}}$$

The interconnection of two pH systems $(\mathcal{D}_1, \mathcal{L}_1, \mathcal{R}_1)$ and $(\mathcal{D}_2, \mathcal{L}_2, \mathcal{R}_2)$ with respect to the link $(F_{\mathcal{P}\text{link}}, E_{\mathcal{P}\text{link}})$ results in a new interconnected pH system, $(\mathcal{D}, \mathcal{L}, \mathcal{R})$. This interconnected system is given by the expression

$$(\mathcal{D}_1, \mathcal{L}_1, \mathcal{R}_1) \circ (\mathcal{D}_2, \mathcal{L}_2, \mathcal{R}_2) := (\mathcal{D}, \mathcal{L}, \mathcal{R})$$

Definition 6 (Directed Graph).
A directed graph is a quadruple $\mathcal{G} := (V,\ E,\ \mathrm{l},\ \mathrm{r})$ where

1. V is a set of vertices
2. E is a set of edges
3. $\mathrm{l} : E \rightarrow V$ maps each edge, e, to an initial vertex
4. $\mathrm{r} : E \rightarrow V$ maps each edge, e, to a terminal vertex

Definition 6.1 (Loop-free directed Graph).
If G is a directed graph, then G is said to be loop-free if for all $e \in E$,

$$\mathrm{l}(e) \neq \mathrm{r}(e)$$

Definition 6.2 (Subgraphs).
Given the graphs $\mathcal{G} := (V,\ E,\ \mathrm{l},\ \mathrm{r})$ and $\mathcal{G}' := (V',\ E',\ \mathrm{l},\ \mathrm{r})$, then $\mathcal{G}'$ is said to be a subgraph of $\mathcal{G}'$ if $E' \subset E$ and $V' \subset V$. Furthermore,

1. A subgraph is said to be an induced subgraph on V' if $E' = E|_V'$
2. A subgraph is said to be spanning if $V' = V$
3. A subgraph is said to be a proper subgraph if $E' \neq E$
4. If both V and E are finite, then $\mathcal{G}$ is said to be finite

Definition 7 (Paths, Connectivity and Cycles).
Let $\mathcal{G} = (V, E, \mathrm{l}, \mathrm{r})$ be a directed finite graph.

1. An n-tuple $e = (e_1, \ldots, e_n) \in (E \cup -E)^n$ is called a path from v to ϖ, if
   a) $\mathrm{l}(e_1), \ldots, \mathrm{l}(e_n)$ are distinct
   b) $\mathrm{r}(e_i) = \mathrm{l}(e_{i+1})$ for all $i \in \{1, \ldots, n-1\}$
   c) $\mathrm{l}(e_1) = v \wedge \mathrm{r}(e_n) = \varpi$
2. A path from v to v is called a cycle.
3. Two vertices, v and ϖ are said to be connected if there exists a path from v to ϖ.
4. The existence of paths from vertices gives an equivalence relation on the set of vertices.
5. A subgraph is a component of the graph.
6. A graph with only one component is said to be connected.

Definition 8 (Incidence Matrix).
Let $\mathcal{G} = (V, E, \mathrm{l}, \mathrm{r})$ be a directed graph that is finite and loop-free such that $E = e_1, \ldots, e_m$ and $V = v_1, \ldots, v_n$. Then the j^{th} row and k^{th} columns of the incidence matrix, $A_0 \in \mathbb{R}^{n \times m}$ of $\mathcal{G}$ is given by

$$a_{jk} = \begin{cases} 1 & \mathrm{l}(e_k) = v_j, \\ -1 & \mathrm{r}(e_k) = v_j, \\ 0 & \text{otherwise.} \end{cases}$$

If the $\mathrm{rank}(A_0) = n - k$, then the graph $\mathcal{G}$ has $k \in \mathbb{N}$ components, such that k rows can be removed from A_0 resulting in matrix with same rank.

Definition 9 (Kirchhoff-Dirac Structure, Kirchhoff-Lagrange Submanifold).
The Kirchhoff-Dirac structure of $\mathcal{G}$ can thus be defined by the set

$$\mathcal{D}_K^S(\mathcal{G}) := \left\{ (j, i, \phi, u) \in \mathbb{R}^{n-|S|} \times \mathbb{R}^m \times \mathbb{R}^{n-|S|} \times \mathbb{R}^m \;\middle|\; \begin{bmatrix} I & A \\ 0 & 0 \end{bmatrix} \begin{pmatrix} j \\ i \end{pmatrix} + \begin{bmatrix} I & A \\ 0 & 0 \end{bmatrix} \begin{pmatrix} \phi \\ u \end{pmatrix} = 0 \right\} \tag{3.1}$$

where i and u are the currents and voltages at the edges of the graph, respectively, whereas q and ϕ are the charges and potentials at the vertices of the graph, respectively.

Assuming that $S = \{v_1, \ldots, v_{|S|}\}$, the Kirchhoff-Lagrange submanifold of $\mathcal{G}$ with respect to S is defined as

$$\mathcal{L}_K^S(\mathcal{G}) := 0 \times \mathbb{R}^{n-|S|} \subset \mathbb{R}^{n-|S|} \times \mathbb{R}^{n-|S|} \tag{3.2}$$

where $\mathcal{G} = (V, E, \mathrm{l}, \mathrm{r})$ is a directed graph that

1. Is finite

2. Is loop-free
3. Has an incidence matrix $A_0 \in \mathbb{R}^{n\times m}$

If $\mathcal{G}_1, \dots, \mathcal{G}_k$ are the components of $\mathcal{G}$ with corresponding vertices $V_1, \dots, V_k \subset V$ so that there exists a subset $\mathcal{S} \subset V$ such that $\mathcal{S}$ containing at most one vertex from each component, i.e. $\forall s, s', \quad \in S, i \leq k : v, v' \in V_i \Rightarrow v = v'$, then $A \in \mathcal{R}^{(n-k)\times m}$ can be constructed by deleting the rows corresponding to the vertices $\mathcal{S}$ from $A_0 \in \mathbb{R}^{n\times m}$.

Remark 2. According to Propositions 1 and 3, Equations 4.10 and 4.11 indicate that $\mathcal{D}^S_K(\mathcal{G})$ is a DS and $\mathcal{L}^S_K(\mathcal{G})$ is a LS in the space $\mathbb{R}^{n-|S|} \times \mathbb{R}^{n-|S|}$.

Definition 9 caters for an introduction of a pH system $(\mathcal{D}^S_K(\mathcal{G}), \mathcal{L}^S_K(\mathcal{G}), \{0\})$ with dynamics

$$(-\frac{d}{dt}q(t), i(t), \phi(t), u(t)) \in \mathcal{D}^S_K(\mathcal{G}) \tag{3.3}$$

where $(q(t), \phi(t)) \in \mathcal{L}^S_K(\mathcal{G})$.

Using the equivalence of $(q(t), \phi(t)) \in \mathcal{L}^S_K(\mathcal{G})$ to $q(t) = 0$ and $\phi(t) \in \mathcal{R}^{n-|S|}$, we see that equation 4.12 holds, iff, the condition holds.

$$q(t) = 0 \wedge Ai(t) = 0 \wedge A^{\mathsf{T}}\phi 2(t) = -u(t).$$

$$b_{jl} = \begin{cases} 1 & e_l \in C_j \text{ with orientations that coincide,} \\ -1 & e_l \in C_j \text{ with orientations that do not coincide,} \\ 0 & \text{otherwise} \end{cases}$$

On this basis, one can define a DS

$$\mathcal{D}'_K(\mathcal{G}) := \left\{ (j, i, \phi, u) \in \mathbb{R}^{n-|S|} \times \mathbb{R}^m \times \mathbb{R}^{n-|S|} \times \mathbb{R}^m \;\middle|\; \begin{bmatrix} I & A \\ 0 & 0 \end{bmatrix} \begin{pmatrix} j \\ i \end{pmatrix} + \begin{bmatrix} I & A \\ 0 & 0 \end{bmatrix} \begin{pmatrix} \phi \\ u \end{pmatrix} = 0 \right\}$$

with dynamics

$$\left(-\frac{d}{dt}\psi(t), i(t), \iota(t), u(t)\right) \in \mathcal{D}'_K(\mathcal{G})$$

and an LS

$$\mathcal{L}'_K(\mathcal{G}) := \{0\} \times \mathbb{R}^{n-m+k}$$

with dynamics

$$(\psi(t), \iota(t)) \in \mathcal{L}'_K(\mathcal{G})$$

Together, they form a the pH system defined by the set $(D'_K(\mathcal{G}), \mathcal{L}'_K(\mathcal{G}), \{0\})$.

3.3.1 *Dirac Structure*

A key feature of a Dirac structure is the fact that the standard composition of two Dirac structures is again a Dirac structure. The implication of this statement is that any power-conserving interconnection of a Port Hamiltonian system is also a Port Hamiltonian system itself. This constitutes the foundation feature in the Port Hamiltonian approach to modelling, simulation and control of complex physical systems. The intricate Dirac structure is the guide to the algebraic constraints of the interconnected system as well as its Casimir functions [85]. The Casimir are significant in the set point regulation of Port Hamiltonian systems. The framework for the Port Hamiltonian allows for port-based modelling. Port-based modelling means that we are interconnecting many different elements through ports. Dirac structures are the tools used to connect multiple elements. These various elements are energy-storing elements, energy-dissipating elements and external elements which could be supplying energy. A diagram to demonstrate the connection structure is given in figure 3.1, [85]

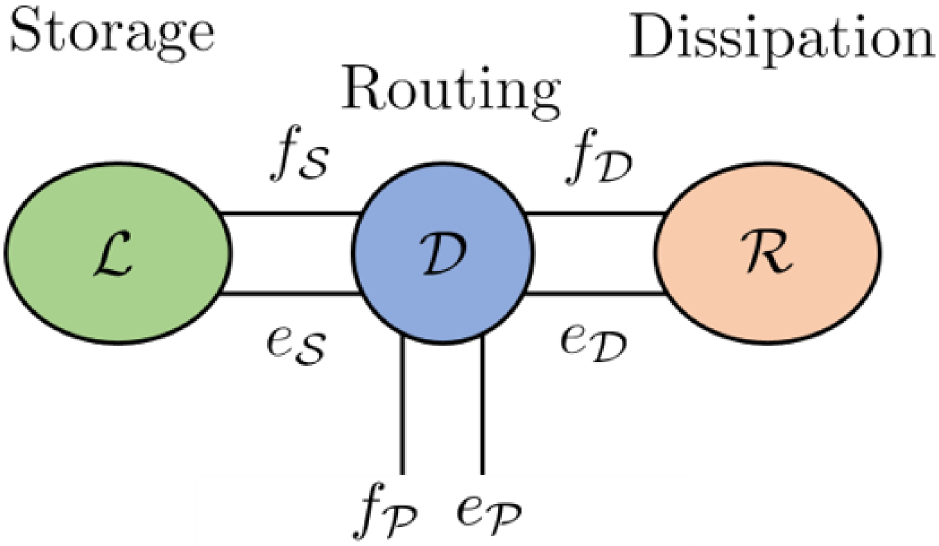

Figure 3.1: The energy storage, routing and dissipation

3.4 CONCLUSION

The preliminaries of the Port Hamiltonian method and the definitions of the concepts to be used in the later sections have been provided. The sections to come will formulate the mechanical ventilator lung model of the respiratory system. Other definitions are presented in the respective sections.

4

COMPOSITIONAL AND GEOMETRIC UNIFYING APPROACH FOR MODELING THE MECHANICAL VENTILATOR-HUMAN RESPIRATORY SYSTEM

4.1 SUMMARY

This chapter presents the modelling of the mechanical ventilator human respiratory system using the conventional method, followed by the Port Hamiltonian integrated model of the mechanical ventilator human respiratory model. Three case scenarios which include a healthy person, a sedated patient, and a spontaneously breathing patient are also presented. The presented formulation of the Port Hamiltonian lumped parameter model can be applied in the design of robust controllers for Mechanical ventilators' patient dynamics.

4.2 INTRODUCTION

Mechanical ventilation is an approach used to assist patients who need support to breathe sufficiently, [1]. These patients are usually in the Intensive Care Unit (ICU) on a mechanical ventilator, which is a machine that is commonly used to assist patients who are partially or unable to breathe on their own for various reasons for instance illnesses or surgical procedures, [2]. The main objective of employing mechanical ventilation is to ensure the patient is sufficiently oxygenated and carbon dioxide is eliminated from their system, [1]. Control Engineering plays a fundamental role in the precise and safe provision of gas to the patient, ([3]). Maintaining human life requires efficient intake and distribution of oxygen to all cells in the body. The distribution is achieved by the heart and the blood vessels whereas the lungs act as the essential interface between the human being and the atmosphere. The lungs facilitate the exchange of carbon dioxide and oxygen in the human body, [3]. When a healthy lung is injured or infected by diseases, the respiratory mechanics become overburdened or strained and the muscles in charge of breathing struggle to maintain the efficiency of gaseous exchange. With extended efforts, the muscles atrophy and they finally cease to function. This results in an urgent need for partial or entire breathing support to be effected. A ventilator is therefore used to facilitate the breathing process through precise control of gas flow, pressure, volume and gas composition, [3]. Adequate ventilation of the patient's lung is maintained sufficiently through a cyclic control of pressure or volume. To achieve an accurate steady-state pressure and to shape the transient reject flow demand disturbances, a feedback controller is usually used for pressure-based ventilators. Positive pressure ventilation is a technique that is normally applied to critical ventilation which entails the generation of an Inspiratory Positive Airway Pressure (IPAP) thus filling the lungs with oxygen air during inspiration. Positive End Expiration Pressure (PEEP) is applied when the medical ventilator reduces the pressure which allows for the air in the lung to be released. Mechatronics systems are used to achieve the objectives of a mechanical ventilation system. Current literature, [2], shows that globally, even before the Covid-19 pandemic, mechanical ventilators have always been in high demand. Thus, improvement of the efficiency of the existing mechanical ventilators is essential and will benefit a greater population across the world.

An overview schematic diagram of a single-compartment mechanical ventilator-lung system is shown in Figure 4.2. Mechanical ventilators can be Pressure-controlled or Volume-controlled. This section of the research work will consider different case scenarios under which a patient may be pressure-controlled ventilated. The first case scenario is represented by a Pressure Controlled ventilation of a sedated patient and the second case scenario is that of a patient who is spontaneously breathing. To benchmark, the presented case scenarios, the third case is that of a healthy person who is not ventilated. For Pressure Controlled Ventilation (PCV), ambient air is compressed by the mechanical ventilator to obtain the profile shown in figure 4.1 near the mouth of the patient. To realize the Inspiratory Positive Airway Pressure (IPAP), the mechanical ventilator pumps air into the patient's airway during the inspiration cycle which results in the filling of the patient's lungs with air. After a predefined time has elapsed, Positive End Expiratory Pressure is achieved due to the decrease in pressure by the mechanical ventilator which results in the lungs being emptied. The objective of Continuous Positive Airway Pressure (CPAP) is for uninterrupted airway pressure to be attained while the patient is breathing through the profile in figure 4.1.

4.3 CONTRIBUTION

Contribution 4.3.1

The main contribution of this chapter is the presentation of a compositional and geometric unifying approach for modelling the mechanical ventilator and the human respiratory system. These types of systems are complex and can be modelled using open graphs in the Port Hamiltonian framework. The directed graph incidence matrix is associated with a Dirac structure. This Dirac structure relates the efforts and flow variables to the edges and vertices of the graph of a mechanical ventilator human respiratory system. In addition to that, the energy dissipating and storing relations between the effort and flow variables of the edges and the internal vertices are also presented. There is an association of state variables to the edges and a formalization of the interconnection of networks. The formulated Hamiltonian structure presents a systematic tool for the control and analysis of the resulting dynamics. From a Port Hamiltonian point of view, this system can be viewed as a Port Hamiltonian lumped Parameter model of the Mechanical ventilator human respiratory system.

4.4 MECHANICAL VENTILATOR-HUMAN RESPIRATORY MODEL

This section presents the conventional or traditional modelling of the mechanical ventilator-human respiratory model. Some of the authors that have previously used the traditional or conventional approach in their works are [25], [1], [64] and [87].

Fig. 4.2 is a diagram of the MV, air-tube, and patient. To begin with, MV required outlet pressure p_{out} is obtained via ambient air compression by the MV. It is important to note that the ambient pressure is used as the reference i.e., $p_{\text{amb}} = 0$. The outlet pressure results in a flow Q_{out} with resistance R_{lin} through the air-tube. Furthermore, the airway pressure of the patient p_{aw} is obtained by measuring using a sensor tube, the pressure in front of the mouth. The exhaled CO_2 rich air is eliminated through a leak in the air tube and it is modelled by using the leak resistance R_{leak}. A one-compartment lung is used in modeling the lung and it has a compliance of C_{lung} with resistance R_{lung}. The patient-air-tube parameters, i.e., R_{lin}, R_{leak}, R_{lung}, and C_{lung}, are all considered as positive. In addition to that, in 4.2 the breathing effort $\dot{p}_{\text{pat}}$, of the patient viewed as an exogenous disturbance on the pressure of the lung, as a result of the patient's respiratory effort. The model in 4.2 provides a description of the relation between p_{out}, the outlet pressure of the MV, the disturbance $\dot{p}_{\text{pat}}$, the state p_{lung}, and the outputs p_{aw} and Q_{out}. The variable to be controlled in this closed-loop system is the airway pressure p_{aw}. It is desired that the airway pressure should track the target pressure p_{target}.

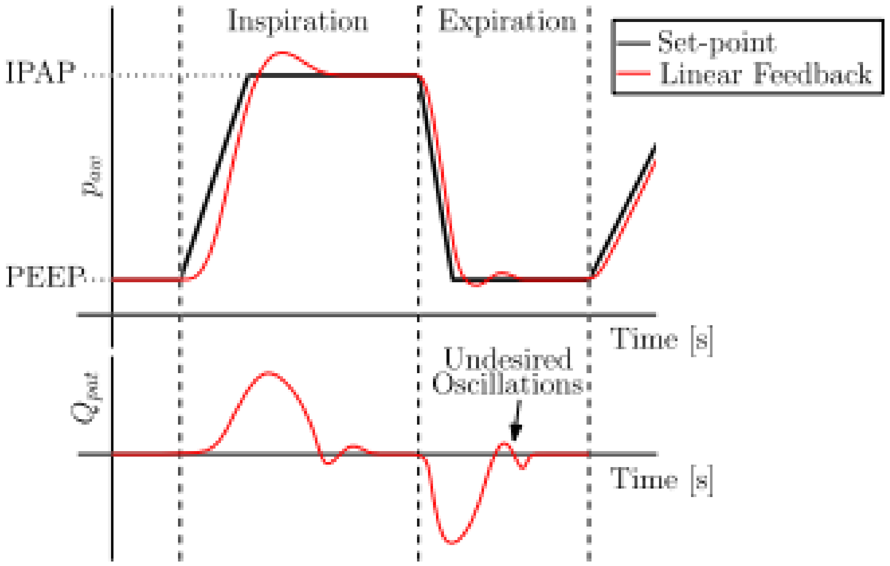

Figure 4.1: Human Airway Pressure and patient flow during one breathing cycle of PC

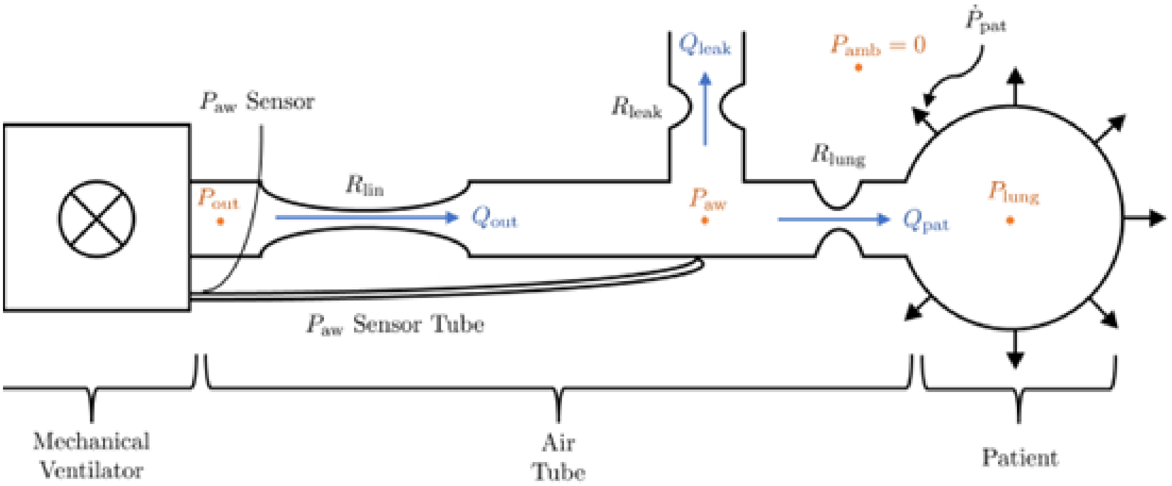

Figure 4.2: Pressure Controlled Mechanical Ventilator

4.5 PHYSICAL MODEL

The model in figure 4.2 describes the relation between p_{out}, outlet pressure of the MV the disturbance $\dot{p}_{\text{pat}}$, the state p_{lung}, and the outputs p_{aw} and Q_{out}.

In this closed-loop system, the airway pressure p_{aw} is the variable to be controlled, i.e., it should track the target pressure p_{target}. The patient airway control system is shown in figure 4.2.

The overall objective in terms of control engineering is to minimize the error in tracking a desired pressure target:

$$e := p_{\text{target}} - p_{\text{aw}} \tag{4.1}$$

Using conservation of flow, the output flow Q_{out}, patient flow Q_{pat}, and leakage flow Q_{leak} are related by:

$$Q_{\text{pat}} = Q_{\text{out}} - Q_{\text{leak}} \tag{4.2}$$

Using the linear resistances R_{lin}, R_{leak}, and R_{lung}, the pressures and flows are related as follows:

$$Q_{\text{out}} = \frac{p_{\text{out}} - p_{\text{aw}}}{R_{\text{lin}}} \qquad Q_{\text{leak}} = \frac{p_{\text{aw}}}{R_{\text{leak}}} \qquad Q_{\text{pat}} = \frac{p_{\text{aw}} - p_{\text{lung}}}{R_{\text{lung}}} \tag{4.3}$$

Lung compliance is defined as [88]:

$$C = \frac{\Delta V}{\Delta p_{\text{trp}}} = \frac{\Delta V}{p_{\text{alv}} - p_{\text{pl}}} \tag{4.4}$$

where

C = Compliance of the lung
ΔV = Volume change
Δp_{trp} = Trans-pulmonary change in pressure
p_{alv} = Alveolar pressure
p_{pl} = Pleural pressure

The lung dynamics can be described by 4.5, with $\dot{p}_{\text{pat}}(t)$ being the patient effort that changes with time. In this research work, the patient effort is viewed and modelled as an unknown disturbance on the lung pressure, which is induced by the respiratory efforts of the patient, such as, it is caused by the contraction of the abdominal muscle or diaphragm. Hence, $p_{\text{lung}}(0)$ provides the pressure of the lung initially, without the patient's effort. The derivative of the lung pressure with time, therefore satisfies:

$$\dot{p}_{\text{lung}} = \frac{1}{C_{\text{lung}}} Q_{\text{pat}} + \dot{p}_{\text{pat}} \tag{4.5}$$

Combining 4.3 and 4.5, the rate of change of pressure in the lung (i.e. the lung dynamics) is:

$$\dot{p}_{\text{lung}} = \frac{p_{\text{aw}} - p_{\text{lung}}}{C_{\text{lung}} R_{\text{lung}}} + \dot{p}_{\text{pat}} \tag{4.6}$$

Using equations 4.2 and 4.3 to determine p_{aw} and then substituting p_{aw} this into 4.6 gives

$$\dot{p}_{\text{lung}} = -\frac{(R_{\text{lin}} + R_{\text{leak}})}{C_{\text{lung}}\bar{R}} p_{\text{lung}} + \frac{R_{\text{leak}}}{C_{\text{lung}}\bar{R}} p_{\text{out}} + \dot{p}_{\text{pat}} \tag{4.7}$$

This is the patient-air-tube differential equation which can be expressed in linear state-space form by defining

$$\begin{aligned} p_{\text{lung}} &= \text{State} \\ p_{\text{out}} &= \text{Input} \\ p_{\text{aw}} &= \text{Output 1} \\ Q_{\text{pat}} &= \text{Output 2} \\ \dot{p}_{\text{pat}} &= \text{Disturbance} \end{aligned}$$

Therefore

$$\dot{p}_{\text{lung}} = -\mathbf{A} p_{\text{lung}} + \mathbf{B} p_{\text{out}} + \dot{p}_{\text{pat}} \tag{4.8}$$

$$\begin{bmatrix} p_{\text{aw}} \\ Q_{\text{pat}} \end{bmatrix} = \mathbf{C} p_{\text{lung}} + \mathbf{D} p_{\text{out}} + \dot{p}_{\text{pat}} \tag{4.9}$$

where

$$\mathbf{A} = -\frac{R_{\text{lin}} + R_{\text{leak}}}{C_{\text{lung}}\bar{R}} \quad \mathbf{B} = \frac{R_{\text{leak}}}{C_{\text{lung}}\bar{R}} \quad \mathbf{C} = \begin{bmatrix} \frac{R_{\text{lin}} R_{\text{leak}}}{\bar{R}} \\ -\frac{R_{\text{lin}} + R_{\text{leak}}}{\bar{R}} \end{bmatrix} \quad \mathbf{D} = \begin{bmatrix} \frac{R_{\text{lin}} R_{\text{leak}}}{\bar{R}} \\ \frac{R_{\text{leak}}}{\bar{R}} \end{bmatrix}$$

4.5.1 *Estimation Parameters for the conventional model*

The parameters used for the traditional model can be found in table 4.1.

4.5.2 *Motivation for the Port Hamiltonian Approach*

They are several observations that are made from the conventional modelling approach presented in the previous section. These observations are summarized below:

- As the complexity of the system is increased, for instance, the Fluid interaction, elasticity of the system, system stability and the power preservation of the system, the presented approach is no longer suitable for modelling of complex dynamical systems since coupling needs to be considered in the development of the model. in addition to that, An integrated mechanical ventilator- human respiratory system can be categorized as a mechano-electro-hydro system which is a Multiphysics system,

Table 4.1: Model parameters for the traditional or conventional model

Parameter	Value	Unit
β	0.7	1/s
$P(0)$	$5 \times 10^{-}8$	s/mL^2
$\hat{R}_{lin}(0)$	0	mbar s/L
m	1	-
R_{leak}	24	mbar s/L
R_{lung}	5	mbar s/L
$R_{lin}(0)$	4.4	mbar s/L
$C_{lung}(0)$	20	mL/mbar

and the traditional techniques provide a limited framework for modelling of such systems.

- The presented modelling method does not emphasize the total energy stored by the system as well as the energy variables. The lack of consideration for the energy of the system is a limitation of the conventional methods because there is a lack of easy assessment of the stability of the system and the power dynamics of the system are not easily accounted for.
- The model does not explicitly account for energy transfer between the different physical domains that govern the MV lung system.

The Sections and the Chapters that follow present the Port Hamiltonian modelling approach which has the following advantages over the traditional approach and seeks to address some of the limitations of the traditional approach:

- The Port Hamiltonian approach provides good structural features, symbolized by distinct physical energy-related interpretations, which makes it easier to define and describe the power systems dynamics, [89].
- The technique applied for the design of controllers for the Port Hamiltonian system is reasonably uncomplicated, logical, and flexible for symbolic computation, [90]

- Complex systems such as power networks, which is one way the integrated mechanical ventilator human respiratory system has been represented can be modelled by means of a modular technique, whereby the Port Hamiltonian models of individual components are combined into a global structure-preserving model that is also in Port Hamiltonian form, [91].

4.6 THE PORT HAMILTONIAN APPROACH

This section will begin with the mathematical preliminaries of the Port Hamiltonian method that will also be applicable in the sections and chapters to follow.

4.6.1 *Assumptions*

The following assumptions are taken in the modelling of the mechanical ventilator and the human respiratory system model presented in the sections to follow.

- The air in the system is assumed to be like an ideal gas
- No chemical reaction occurs during the breathing process
- There is no air leakage during the working process (the dynamic process is quasi-balanced)
- The internal dynamics of the mechanical ventilator are assumed to be negligible and the mechanical ventilator is modelled as a voltage source
- The system is modelled using an electrical analogy and the behaviour of the various subsystems is lumped

4.6.2 *Definitions*

The definitions used in this research work have already been provided in Chapter 3. However, the important definitions that are relevant in this section are provided again for reference purposes. The main reference used in this section is [92]

Definition 1 (Dirac Structure)
A Dirac Structure (DS) is a pair of elements, $f \in \mathbb{R}^n$ and $e \in \mathbb{R}^n$, that satisfies the set:

$$\mathcal{D} := \left\{ (f, e) \in \mathcal{D},\ (\hat{f}, \hat{e}) \in \mathcal{D} \middle| e^{\mathsf{T}} \hat{f} = -\hat{e}^{\mathsf{T}} f \right\}$$

The DS is a subset $\mathcal{D} \subset \mathcal{F} \times \mathcal{E}$, where $\mathcal{F}$ and $\mathcal{E}$ represent the flows and efforts, respectively.

The DS in electric circuits can be represented as:

Proposition 1:
The subspace

$$\mathcal{D} \subset \mathbb{R}^n \times \mathbb{R}^n$$

is called a DS iff, there exist $A, B \in \mathbb{R}^{n \times n}$ such that

$$AB^\mathsf{T} + AB^\mathsf{T} = 0 \text{ and } \operatorname{rank}([A\,B]) = n$$

satisfying the condition

$$\mathcal{D} = \{(f, e) \in \mathbb{R}^n \times \mathbb{R}^n | Af = -Be\}$$

Definition 2 (Lagrange Submanifold)
A submanifold $\mathcal{L} \subset \mathbb{R}^n \times \mathbb{R}^n$ of the manifold

$$\mathbb{R}^n \times \mathbb{R}^n$$

is said to be a Lagrange submanifold (LS) if for all points $x \in \mathcal{L}$ and $(y_1, y_2) \in \mathbb{R}^n \times \mathbb{R}^n$ if

$$y_1^\mathsf{T} u_2 - y_2^\mathsf{T} u_1 = 0$$

is true for all $(y_1, y_2) \in T_x\mathcal{L}$ and $(u_1, u_2) \in T_x\mathcal{L}$.
Proposition 2.
Given a $\mathcal{C}^\infty$ differentiable map, $\mathcal{O} : \mathbb{R}^n \to \mathbb{R}^n$ with graph $\mathcal{O}$, the submanifold $\mathcal{L}_\mathcal{O}$

$$\mathcal{L}_\mathcal{O} := \{(x, \mathcal{O}(x)) \in \mathbb{R}^n \times \mathbb{R}^n |\ x \in \mathbb{R}^n\}$$

is said to be a Lagrangian submanifold iff there exists a function $H : \mathbb{R}^n \to \mathbb{R}$ that is $\mathcal{C}^2$ differentiable such that

$$\nabla H = \mathcal{O}$$

Proposition 3
A subspace $\mathcal{L} \subset \mathbb{R}^n \times \mathbb{R}^n$ is said to be a Lagrangian submanifold iff there exist $A, B \in \mathbb{R}^{n \times n}$ such that $A^\mathsf{T} B = B^\mathsf{T} A$ and $\operatorname{rank}([A^\mathsf{T} B^\mathsf{T}]) = n$ so that

$$\mathcal{L} = \left\{(f, e) \in \mathbb{R}^n \times \mathbb{R}^n | A^\mathsf{T} f = B^\mathsf{T} e\right\}$$

Definition 3 (Resistive Relation)
Any relation $\mathcal{R} \subset \mathbb{R}^n \times \mathbb{R}^n$ is said to be resistive if $\forall (f_\mathcal{R}, e_\mathcal{R}) \in \mathcal{R}$ the

$$e_\mathcal{R}^\mathsf{T} f_\mathcal{R} \leq 0$$

is satisfied.

Definition 4 (Port Hamiltonian (pH) System).
The set $(\mathcal{D}, \mathcal{L}, \mathcal{R})$, defines a pH system where:

- $\mathcal{D} \subset (\mathcal{F}_\mathcal{L} \times \mathcal{F}_\mathcal{R} \times \mathcal{F}_\mathcal{P}) \times (\mathcal{E}_\mathcal{L} \times \mathcal{E}_\mathcal{R} \times \mathcal{E}_\mathcal{P})$ is a DS
- $\mathcal{L} \subset \mathcal{F}_\mathcal{L} \times \mathcal{E}_\mathcal{L}$ is a LS and
- $\mathcal{R} \subset \mathcal{F}_\mathcal{R} \times \mathcal{E}_\mathcal{R}$ a Resistive relation.

The elements of the sets:

- $\mathcal{F}_\mathcal{L} \in \mathbb{R}^{n_\mathcal{L}}$ and $\mathcal{E}_\mathcal{L} \in \mathbb{R}^{n_\mathcal{L}}$ are known as flows and efforts
- $\mathcal{F}_\mathcal{R} \in \mathbb{R}^{n_\mathcal{R}}$ and $\mathcal{E}_\mathcal{R} \in \mathbb{R}^{n_\mathcal{R}}$ are known as resistive flows and efforts
- $\mathcal{F}_\mathcal{P} \in \mathbb{R}^{n_\mathcal{P}}$ and $\mathcal{E}_\mathcal{P} \in \mathbb{R}^{n_\mathcal{P}}$ are known as external flows and efforts, respectively.

where $n_\mathcal{L}, n_\mathcal{R}$ and $n_\mathcal{P} \in \mathbb{N}_0$.
The dynamics of the pH system are given by the differential inclusion

$$\left(-\frac{d}{dt}x(t), f_\mathcal{R}(t), f_\mathcal{P}(t), e_\mathcal{L}(t), e_\mathcal{R}(t), e_\mathcal{P}(t)\right) \in \mathcal{D}$$

where $(x(t), e_\mathcal{L}(t)) \in \mathcal{L}$, $(f_\mathcal{R}(t), e_\mathcal{R}(t)) \in \mathcal{R}$ and $(f_\mathcal{P}(t), e_\mathcal{P}(t)) \in \mathcal{P}$

Definition 5 (Interconnection of n pH Systems)
Let $(\mathcal{D}_i, \mathcal{L}_i, \mathcal{R}_i)$ denote the space of the i^{th} pH system in a set of n pH systems that are to be interconnected. The space of flows is divided into an external part and a part to be linked and is given by

$$\mathcal{F}_i = \mathcal{F}_{\mathcal{L}_i} \times \mathcal{F}_{\mathcal{R}i} \times \mathcal{F}_{\mathcal{P}i} \times \mathcal{F}_{\mathcal{P}\text{link}}$$

Similarly, the space of efforts is divided into an external part and a part to be linked and is expressed as

$$\mathcal{E}_i = \mathcal{F}_{\mathcal{L}i} \times \mathcal{E}_{\mathcal{R}i} \times \mathcal{E}_{\mathcal{P}i} \times \mathcal{E}_{\mathcal{P}\text{link}}$$

The interconnection of two pH systems $(\mathcal{D}_1, \mathcal{L}_1, \mathcal{R}_1)$ and $(\mathcal{D}_2, \mathcal{L}_2, \mathcal{R}_2)$ with respect to the link $(F_{\mathcal{P}\text{link}}, E_{\mathcal{P}\text{link}})$ results in a new interconnected pH system, $(\mathcal{D}, \mathcal{L}, \mathcal{R})$. This interconnected system is given by the expression

$$(\mathcal{D}_1, \mathcal{L}_1, \mathcal{R}_1) \circ (\mathcal{D}_2, \mathcal{L}_2, \mathcal{R}_2) := (\mathcal{D}, \mathcal{L}, \mathcal{R})$$

Definition 6 (Directed Graph).
A directed graph is a quadruple $\mathcal{G} := (V,\, E,\, \mathrm{l},\, \mathrm{r})$ where

1. V is a set of vertices
2. E is a set of edges
3. $\mathrm{l} : E \to V$ maps each edge, e, to an initial vertex
4. $\mathrm{r} : E \to V$ maps each edge, e, to a terminal vertex

Definition 6.1 (Loop-free directed Graph).
If G is a directed graph, then G is said to be loop-free if for all $e \in E$,

$$\mathrm{l}(e) \neq \mathrm{r}(e)$$

Definition 6.2 (Subgraphs).
Given the graphs $\mathcal{G} := (V,\, E,\, \mathrm{l},\, \mathrm{r})$ and $\mathcal{G}' := (V',\, E',\, \mathrm{l},\, \mathrm{r})$, then $\mathcal{G}'$ is said to be a subgraph of $\mathcal{G}'$ if $E' \subset E$ and $V' \subset V$. Furthermore,

1. A subgraph is said to be an induced subgraph on V' if $E' = E|_V'$
2. A subgraph is said to be spanning if $V' = V$
3. A subgraph is said to be a proper subgraph if $E' \neq E$
4. If both V and E are finite, then $\mathcal{G}$ is said to be finite

Definition 7 (Paths, Connectivity and Cycles).
Let $\mathcal{G} = (V, E, \mathrm{l}, \mathrm{r})$ be a directed finite graph.

1. An n-tuple $e = (e_1, \ldots, e_n) \in (E \cup -E)^n$ is called a path from v to ϖ, if
    a) $\mathrm{l}(e_1), \ldots, \mathrm{l}(e_n)$ are distinct
    b) $\mathrm{r}(e_i) = \mathrm{l}(e_{i+1})$ for all $i \in \{1,\, \ldots,\, n-1\}$
    c) $\mathrm{l}(e_1) = v \wedge \mathrm{r}(e_n) = \varpi$
2. A path from v to v is called a cycle.
3. Two vertices, v and ϖ are said to be connected if there exists a path from v to ϖ.
4. The existence of paths from vertices gives an equivalence relation on the set of vertices.
5. A subgraph is a component of the graph.
6. A graph with only one component is said to be connected.

Definition 8 (Incidence Matrix).
Let $\mathcal{G} = (V, E, \mathrm{l}, \mathrm{r})$ be a directed graph that is finite and loop-free such that $E = e_1, \dots, e_m$ and $V = v_1, \dots, v_n$. Then the j^{th} row and k^{th} columns of the incidence matrix, $A_0 \in \mathbb{R}^{n \times m}$ of $\mathcal{G}$ is given by

$$a_{jk} = \begin{cases} 1 & \mathrm{l}(e_k) = v_j, \\ -1 & \mathrm{r}(e_k) = v_j, \\ 0 & \text{otherwise.} \end{cases}$$

If the rank$(A_0) = n - k$, then the graph $\mathcal{G}$ has $k \in \mathbb{N}$ components, such that k rows can be removed from A_0 resulting in matrix with same rank.

Definition 9 (Kirchhoff-Dirac Structure, Kirchhoff-Lagrange Submanifold).
The Kirchhoff-Dirac structure of $\mathcal{G}$ can thus be defined by the set

$$\mathcal{D}_K^S(\mathcal{G}) := \left\{ (j,\, i,\, \phi, u) \in \mathbb{R}^{n-|S|} \times \mathbb{R}^m \times \mathbb{R}^{n-|S|} \times \mathbb{R}^m \middle| \begin{bmatrix} I & A \\ 0 & 0 \end{bmatrix} \begin{pmatrix} j \\ i \end{pmatrix} + \begin{bmatrix} I & A \\ 0 & 0 \end{bmatrix} \begin{pmatrix} \phi \\ u \end{pmatrix} = 0 \right\} \tag{4.10}$$

where i and u are the currents and voltages at the edges of the graph, respectively, whereas q and ϕ are the charges and potentials at the vertices of the graph, respectively.

Assuming that $S = \{v_1,\, \dots,\, v_{|S|}\}$, the Kirchhoff-Lagrange submanifold of $\mathcal{G}$ with respect to S is defined as

$$\mathcal{L}_K^S(\mathcal{G}) := 0 \times \mathbb{R}^{n-|S|} \subset \mathbb{R}^{n-|S|} \times \mathbb{R}^{n-|S|} \tag{4.11}$$

where $\mathcal{G} = (V, E, \mathrm{l}, \mathrm{r})$ is a directed graph that

1. Is finite
2. Is loop-free
3. Has an incidence matrix $A_0 \in \mathbb{R}^{n \times m}$

If $\mathcal{G}_1, \dots, \mathcal{G}_k$ are the components of $\mathcal{G}$ with corresponding vertices $V_1, \dots, V_k \subset V$ so that there exists a subset $\mathcal{S} \subset V$ such that $\mathcal{S}$ containing at most one vertex from each component, i.e. $\forall s, s', \in S, i \leq k : v, v' \in V_i \Rightarrow v = v'$, then $A \in \mathcal{R}^{(n-k) \times m}$ can be constructed by deleting the rows corresponding to the vertices $\mathcal{S}$ from $A_0 \in \mathbb{R}^{n \times m}$.

Remark 2. According to Propositions 1 and 3, Equations 4.10 and 4.11 indicate that $\mathcal{D}_K^S(\mathcal{G})$ is a DS and $\mathcal{L}_K^S(\mathcal{G})$ is a LS in the space $R^{n-|S|} \times R^{n-|S|}$.

In Definition 9 canters for introduction of a pH system $(\mathcal{D}_K^S(\mathcal{G}), \mathcal{L}_K^S(\mathcal{G}), \{0\})$ with dynamics

$$(-\frac{d}{dt}q(t), i(t), \phi(t), u(t)) \in \mathcal{D}_K^S(\mathcal{G}) \tag{4.12}$$

where $(q(t), \phi(t)) \in \mathcal{L}_K^S(\mathcal{G})$.

Using the equivalence of $(q(t), \phi(t)) \in \mathcal{L}_K^S(\mathcal{G})$ to $q(t) = 0$ and $\phi(t) \in \mathcal{R}^{n-|S|}$, we see that equation 4.12 holds, iff, the condition holds.

$$q(t) = 0 \wedge Ai(t) = 0 \wedge A^{\mathsf{T}}\phi 2(t) = -u(t).$$

$$b_{jl} = \begin{cases} 1 & e_l \in C_j \text{ with orientations that coincide,} \\ -1 & e_l \in C_j \text{ with orientations that do not coincide,} \\ 0 & \text{otherwise} \end{cases}$$

On this basis, one can define a DS

$$\mathcal{D}_K'(\mathcal{G}) := \left\{ (j, i, \phi, u) \in \mathbb{R}^{n-|S|} \times \mathbb{R}^m \times \mathbb{R}^{n-|S|} \times \mathbb{R}^m \,\middle|\, \begin{bmatrix} I & A \\ 0 & 0 \end{bmatrix} \begin{pmatrix} j \\ i \end{pmatrix} + \begin{bmatrix} I & A \\ 0 & 0 \end{bmatrix} \begin{pmatrix} \phi \\ u \end{pmatrix} = 0 \right\}$$

with dynamics

$$\left(-\frac{d}{dt}\psi(t), i(t), \iota(t), u(t)\right) \in \mathcal{D}_K'(\mathcal{G})$$

and an LS

$$\mathcal{L}_K'(\mathcal{G}) := \{0\} \times \mathbb{R}^{n-m+k}$$

with dynamics

$$(\psi(t), \iota(t)) \in \mathcal{L}_K'(\mathcal{G})$$

Together, they form a the pH system defined by the set $(D_K'(\mathcal{G}), \mathcal{L}_K'(\mathcal{G}), \{0\})$.

4.7 PORT HAMILTONIAN MODELING OF MECHANICAL VENTILATOR HUMAN RESPIRATORY SYSTEM

The Port Hamiltonian model of the mechanical ventilator human respiratory system is now presented in this section.

4.7.1 *Physical system description with assumptions*

Consider a human lung system consisting of a series arrangement of four segments, namely the larynx, trachea, bronchi, and alveoli as shown in figure 4.3 and 4.4. Linear compliance (elastic forces) and linear resistance (dissipative forces) are used to represent each segment. The human respiratory system experiences these forces during normal breathing. The inertial forces are assumed to have negligible impacts within the physiological breathing frequencies, [93], [94].

- For a spontaneous breathing patient: V1 denotes the pressure from the mechanical ventilator, and it is external while V2 denotes pressure generated internally by the respiratory muscles.
- A passive-compliant element is used to model the chest walls. The characteristics of this passive compliant element are assumed to be linear, and they are defined by a constant compliance term namely, the chest-wall compliance (C5). The assumption is taken with consideration to the sigmoidal PV relationship. It is a valid approximation considering the volume range of quiet breathing (2.5-3 Liters), [93], [94].
- For both diseased and healthy lung states the resistance to flow of the chest wall is assumed to have a negligible effect to the overall respiratory system resistance, [93], [94].
- The diaphragm is assumed to be connected to C5 and it acts on the pleural space. The internal pressure is transferred to the trachea, bronchi, alveoli and any other segment that lies within the chest cavity, [93], [94].
- The resistances are represented as follows: Mouth to Larynx (R1), Larynx to trachea (R2), Trachea to bronchea (R3) and bronchea to alveoli (R4). and C1, C2, C3 and C4 are their respective elastic forces.

In the present study, three case scenarios are considered:

- For the healthy person, the action of the V1 is nullified, and the airway opening pressure (Pairway) is always assumed to be equal to the atmospheric pressure.
- In the second case scenario, representing a sedated patient, V1 is applied to simulate artificial ventilation conditions. The action of the V2 is ignored since it is assumed that the patient cannot breathe on their own.
- The third case scenario is for a patient who is both on a mechanical ventilator but can still breathe to some extent on their own, therefore, V1 action is superimposed on the action of V2 for simultaneously natural and artificial breathing.

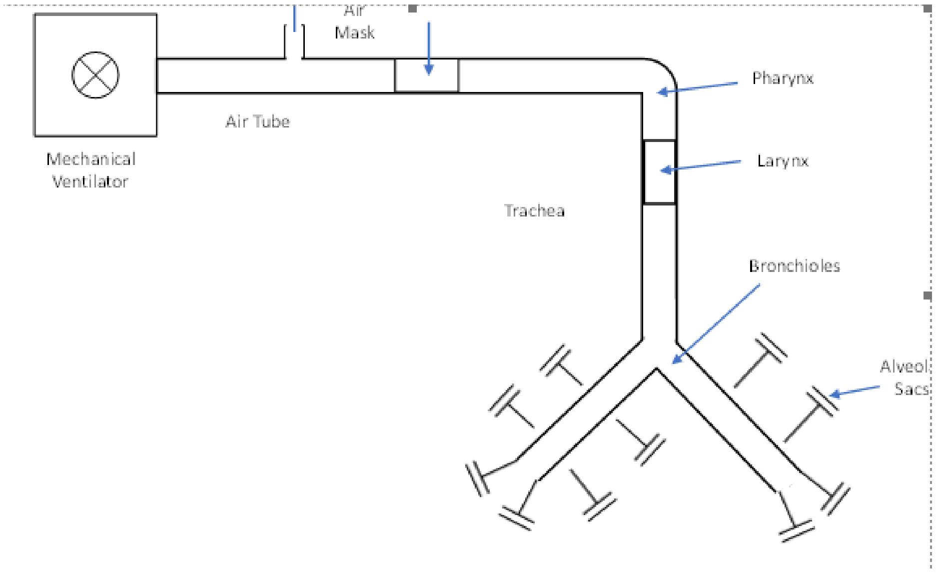

Figure 4.3: Physical system diagram

4.7.2 *Electrical analogy*

The physical model of the mechanical ventilator and the human respiratory system may be represented by the electrical equivalent representation as shown in figure 4.4. The pressure measurements related to compliance for each of the four segments in the human lung system are modelled as voltages. The driving sources of pressure are introduced as voltage sources: the principle of superposition is used to realize the three case scenarios as presented.

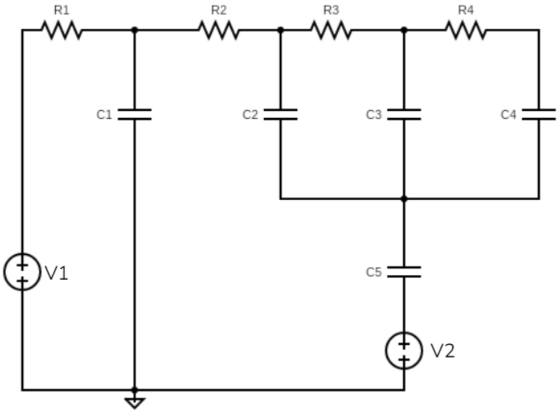

Figure 4.4: Electrical Analogy diagram

4.7.3 *Scenario with sedated patients:* $V_1 \neq 0, V_2 = 0$

This case scenario is for a patient who is depending entirely on the mechanical ventilator for respiratory support. The mechanical ventilator is represented as a voltage source. Since the patient is not breathing on their own, the effects of the diaphragm action are not included. The assumption made is that the pressure source from the patient's natural breathing is effectively nullified. The modified circuit representation as shown in Figure 4.5 has a single voltage source (the external ventilator source).

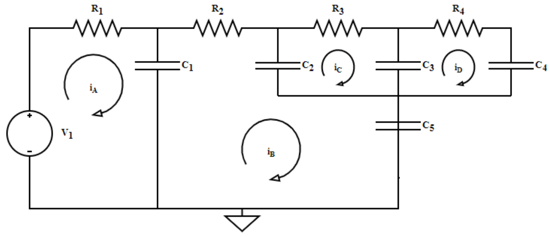

Figure 4.5: Sedated Patient

A loop analysis based on Kirchhoff's Voltage Law (KVL) which states that the vector sum of voltage in an electrical loop is equal to zero, following the general law of conservation of energy. The principle of cause and effect may be translated as the voltage source inducing a current in the first loop (larynx segment) which in turn couples with the second loop (trachea segment) via the trachea capacitance. This effect is applied throughout the segments and the following segment KVL loop equations are determined.

$$V_1 - i_A R_1 - V_{C_1} = 0$$

$$V_{C_1} - i_B R_2 - V_{C_2} - V_{C_5} = 0$$

$$V_{C_2} - i_C R_3 - V_{C_3} = 0$$

$$V_{C_3} - i_D R_4 - V_{C_4} = 0$$

By solving for the current in each loop, the mathematical model determined is represented by five differential equations, each describing the dynamics of the energy storage elements. This is done by applying the linear capacitor voltage equation and determining the expression for current as a derivative of the voltage across each capacitor. For each of the segments, the following capacitor voltage expressions are used to model the lung system equivalent.

$$V_{C_1} = \frac{1}{C_1}\int (i_A - i_B)dt \tag{4.13}$$

$$V_{C_2} = \frac{1}{C_2}\int (i_B - i_C)dt \tag{4.14}$$

$$V_{C_3} = \frac{1}{C_3}\int (i_C - i_D)dt \tag{4.15}$$

$$V_{C_4} = \frac{1}{C_4}\int (i_D)dt \tag{4.16}$$

$$V_{C_5} = \frac{1}{C_5}\int (i_B)dt \tag{4.17}$$

The following state equations are presented as the mathematical model for this case scenario. The state variables are denoted as follows: $(x_1 = V_{C_1}, x_2 = V_{C_2}, x_3 = V_{C_3}, x_4 = V_{C_4}, x_5 = V_{C_5})$

$$\frac{dV_{C_1}}{dt} = \dot{x_1} = a_{11}x_1 + a_{12}x_2 + a_{15}x_5 + b_{11}V_1 \tag{4.18}$$

$$\frac{dV_{C_2}}{dt} = \dot{x_2} = a_{21}x_1 + a_{22}x_2 + a_{23}x_3 + a_{25}x_5 \tag{4.19}$$

$$\frac{dV_{C_3}}{dt} = \dot{x_3} = a_{32}x_2 + a_{33}x_3 + a_{34}x_4 \tag{4.20}$$

$$\frac{dV_{C_4}}{dt} = \dot{x_4} = a_{43}x_3 + a_{44}x_4 \tag{4.21}$$

$$\frac{dV_{C_5}}{dt} = \dot{x_5} = a_{51}x_1 + a_{52}x_2 + a_{55}x_5 \tag{4.22}$$

Where each of the state variable and input coefficients are derived to be:

$$a_{11} = -\frac{1}{R_1C_1} - \frac{1}{R_2C_1}, a_{12} = \frac{1}{R_2C_1}$$
$$a_{15} = \frac{1}{R_2C_1}, b_{11} = \frac{1}{R_1C_1}$$
$$a_{21} = \frac{1}{R_2C_2}, a_{22} = -\frac{1}{R_2C_2} - \frac{1}{R_3C_2}$$
$$a_{23} = \frac{1}{R_3C_2}, a_{25} = -\frac{1}{R_2C_2}$$
$$a_{32} = \frac{1}{R_3C_3}, a_{33} = -\frac{1}{R_3C_3} - \frac{1}{R_4C_3}$$
$$a_{34} = \frac{1}{R_4C_3}, a_{43} = \frac{1}{R_4C_4}, a_{44} = -\frac{1}{R_4C_4},$$
$$a_{51} = \frac{1}{R_2C_5}, a_{52} = -\frac{1}{R_2C_5}, a_{55} = -\frac{1}{R_2C_5}$$

4.7.4 *Scenario with healthy person:* $V_1 = 0, V_2 \neq 0$

The same approach used for the scenario with sedated patients is employed for the case of a healthy person. Since this is a healthy person with respect to respiratory mechanics, the effects of the ventilator are not included in this model. The only source of the equivalent system is the human's natural breathing action represented by the diaphragm which acts as a voltage source as shown in figure 4.6.

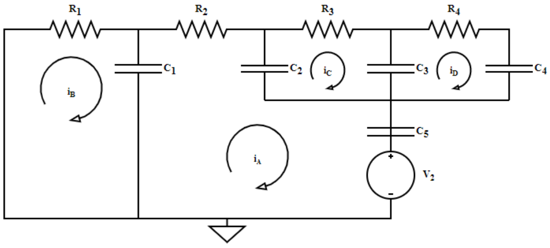

Figure 4.6: Healthy Person

The five energy storage elements as previously stated are evaluated in a similar fashion by using the linear capacitor voltage equation to determine the individual loop current expressions as derivatives of the voltage across each capacitor. For each of the segments, the following capacitor voltage expressions are used to model the lung system equivalent.

$$V_{C_1} = \frac{1}{C_1} \int (i_B - i_A) dt \tag{4.23}$$

$$V_{C_2} = \frac{1}{C_2} \int (i_A - i_C) dt \tag{4.24}$$

$$V_{C_3} = \frac{1}{C_3} \int (i_C - i_D) dt \tag{4.25}$$

$$V_{C_4} = \frac{1}{C_4} \int (i_D) dt \tag{4.26}$$

$$V_{C_5} = \frac{1}{C_5} \int (i_A) dt \tag{4.27}$$

The following state equations are presented as the mathematical model for this case scenario. The state variables are denoted as follows: $(x_1 = V_{C_1}, x_2 = V_{C_2}, x_3 = V_{C_3}, x_4 = V_{C_4}, x_5 = V_{C_5})$

$$\frac{dV_{C_1}}{dt} = \dot{x_1} = a_{11}x_1 + a_{12}x_2 + a_{15}x_5 + b_{11}V_2 \tag{4.28}$$

$$\frac{dV_{C_2}}{dt} = \dot{x_2} = a_{21}x_1 + a_{22}x_2 + a_{23}x_3 + a_{25}x_5 + b_{21}V_2 \tag{4.29}$$

$$\frac{dV_{C_3}}{dt} = \dot{x_3} = a_{32}x_2 + a_{33}x_3 + a_{34}x_4 \tag{4.30}$$

$$\frac{dV_{C_4}}{dt} = \dot{x_4} = a_{43}x_3 + a_{44}x_4 \tag{4.31}$$

$$\frac{dV_{C_5}}{dt} = \dot{x_5} = a_{51}x_1 + a_{52}x_2 + a_{55}x_5 + b_{51}V_2 \tag{4.32}$$

Where each of the state variable and input coefficients are derived to be:

$$a_{11} = -\frac{1}{R_1C_1} - \frac{1}{R_2C_1}, a_{12} = -\frac{1}{R_2C_1}$$

$$a_{15} = -\frac{1}{R_2C_1}, b_{11} = \frac{1}{R_2C_1}, a_{21} = -\frac{1}{R_2C_2}$$

$$a_{22} = -\frac{1}{R_2C_2} - \frac{1}{R_3C_2}, a_{23} = -\frac{1}{R_3C_2}$$

$$a_{25} = -\frac{1}{R_2C_2}, b_{21} = \frac{1}{R_2C_2}, a_{32} = \frac{1}{R_3C_3},$$

$$a_{33} = -\frac{1}{R_3C_3} - \frac{1}{R_4C_3} a_{34} = \frac{1}{R_4C_3},$$

$$a_{43} = \frac{1}{R_4C_4} a_{44} = -\frac{1}{R_4C_4}, a_{51} = -\frac{1}{R_2C_5}$$

$$a_{52} = -\frac{1}{R_2C_5}, a_{55} = -\frac{1}{R_2C_5} b_{51} = \frac{1}{R_2C_5}$$

4.7.5 *Scenario with spontaneously breathing patients:*

The more complex scenario in comparison to the previous two is the spontaneous case where both the mechanical ventilator and the diaphragm are working together to ensure the patient is breathing sufficiently. This is represented by the presence of two voltage sources in the system as shown in figure 4.7.

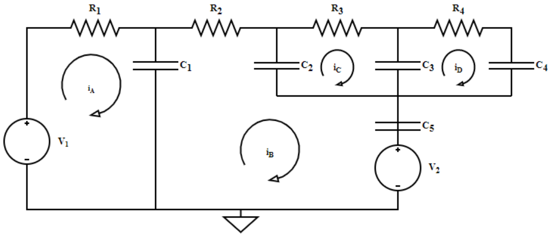

Figure 4.7: Spontaneously breathing patients

Likewise, the process of solving the vector or algebraic current in each segment loop is implemented to both determine the current expressions and to account for the effect of both pressure sources. Notably, if one source is chosen as positive, in this case the external ventilator drive, the other inherently becomes negative due to superposition. This is a knock-off result of modelling based on a cause and effect basis. For each of the segments, the following capacitor voltage expressions are used to model the lumped lung system equivalent.

$$V_{C_1} = \frac{1}{C_1}\int (i_A - i_B)dt \tag{4.33}$$

$$V_{C_2} = \frac{1}{C_2}\int (i_B - i_C)dt \tag{4.34}$$

$$V_{C_3} = \frac{1}{C_3}\int (i_C - i_D)dt \tag{4.35}$$

$$V_{C_4} = \frac{1}{C_4}\int (i_D)dt \tag{4.36}$$

$$V_{C_5} = \frac{1}{C_5}\int (i_B)dt \tag{4.37}$$

The following state equations are presented as the mathematical model for this case scenario. The state variables are denoted as follows: $(x_1 = V_{C_1}, x_2 = V_{C_2}, x_3 = V_{C_3}, x_4 = V_{C_4}, x_5 = V_{C_5})$

$$\frac{dV_{C_1}}{dt} = \tag{4.38}$$

$$\frac{dV_{C_2}}{dt} = \tag{4.39}$$

$$\frac{dV_{C_3}}{dt} = \tag{4.40}$$

$$\frac{dV_{C_4}}{dt} = \tag{4.41}$$

$$\frac{dV_{C_5}}{dt} = \tag{4.42}$$

Where each of the state variable and input coefficients are derived to be:

$$\begin{aligned}
a_{11} &= -\frac{1}{R_1C_1} - \frac{1}{R_2C_1}, a_{12} = -\frac{1}{R_2C_1} \\
a_{15} &= -\frac{1}{R_2C_1}, b_{11} = \frac{1}{R_2C_1}, a_{21} = -\frac{1}{R_2C_2} \\
a_{22} &= -\frac{1}{R_2C_2} - \frac{1}{R_3C_2}, a_{23} = -\frac{1}{R_3C_2} \\
a_{25} &= -\frac{1}{R_2C_2}, b_{21} = \frac{1}{R_2C_2}, a_{32} = \frac{1}{R_3C_3}, \\
a_{33} &= -\frac{1}{R_3C_3} - \frac{1}{R_4C_3} a_{34} = \frac{1}{R_4C_3}, \\
a_{43} &= \frac{1}{R_4C_4} a_{44} = -\frac{1}{R_4C_4}, a_{51} = -\frac{1}{R_2C_5} \\
a_{52} &= -\frac{1}{R_2C_5}, a_{55} = -\frac{1}{R_2C_5} b_{51} = \frac{1}{R_2C_5}
\end{aligned}$$

4.7.6 *The Port Hamiltonian model*

The three case scenarios can therefore be represented in the Hamiltonian framework using the following circuit dynamics:

dynamics of the resistors in the pH system are given by the following:

$$\left(-\frac{d}{dt}x(t), f_{\mathcal{R}}(t), f_{\mathcal{P}}(t), e_{\mathcal{L}}(t), e_{\mathcal{R}}(t), e_{\mathcal{P}}(t)\right) \in \mathcal{D}$$

where $(x(t), e_{\mathcal{L}}(t)) \in \mathcal{L}$, $(f_{\mathcal{R}}(t), e_{\mathcal{R}}(t)) \in \mathcal{R}$ and $(f_{\mathcal{P}}(t), e_{\mathcal{P}}(t)) \in \mathcal{P}$

dynamics of the capacitors in the pH system are given by the following:

Let $H_{\mathcal{C}} \in \mathcal{C}^1(\mathbb{R}^{\ell_p}, \mathbb{R})$. A capacitance with ℓ_p ports is modeled as a pH system $(D_{\mathcal{C}}, L_{\mathcal{C}}, R_{\mathcal{C}})$, where $D_{\mathcal{C}} = D_{\ell_p}$ with D_{ℓ_p} as in (9), $R_{\mathcal{C}} = 0$, and

$$L_{\mathcal{C}} = (u_{\mathcal{C}}, q_{\mathcal{C}}) \in R^{2\ell_p} | q_{\mathcal{C}} = \nabla H_{\mathcal{C}}(u_{\mathcal{C}}).$$

The dynamics consequently read

$$(-\frac{d}{dt} q_{\mathcal{C}}(t), i_{\mathcal{C}}(t), u_{\mathcal{C}}(t), u_{\mathcal{C}}(t)) \in D_{\mathcal{C}}, (q_{\mathcal{C}}(t), u_{\mathcal{C}}(t)) \in L_{\mathcal{C}}.$$

Here, $q_{\mathcal{C}}$ represents the charge of the capacitance and the Hamiltonian $H_{\mathcal{C}}$ represents the energy storage function of the system. From this pH system, one can derive

$$i_{\mathcal{C}}(t) = \frac{d}{dt} q_{\mathcal{C}}(t), u_{\mathcal{C}}(t) = \nabla H_{\mathcal{C}}(q_{\mathcal{C}}(t)).$$

If the capacitance has two terminals, then we obtain a conventional capacitance with one port.

The dynamics of the inductance are represented as follows:

Let $H_{\mathcal{L}} \in \mathcal{C}^1(\mathbb{R}^{\ell_p}, \mathbb{R})$. An inductance with ℓ_p ports is modeled as a pH system $(\mathcal{D}_{\mathcal{L}}, \mathcal{L}_{\mathcal{L}}, \mathcal{R}_{\mathcal{L}})$ with

$$\mathcal{D}_{\mathcal{L}} = \left\{ \begin{pmatrix} -u_{\mathcal{L}} \\ i_{\mathcal{L}} \\ i_{\mathcal{L}} \\ u_{\mathcal{L}} \end{pmatrix} \in \mathbb{R}^{4\ell_p} \middle| u_{\mathcal{L}}, i_{\mathcal{L}} \in \mathbb{R}^{\ell_p} \right\}$$

$$L_{\mathcal{L}} = \left\{ (\psi_{\mathcal{L}}, i_{\mathcal{L}}) \in R^{2\ell_p} | i_{\mathcal{L}} = \Delta H_{\mathcal{L}}(\psi_{\mathcal{L}}) \right\}, \qquad R_{\mathcal{L}} = 0$$

The dynamics are now given by

$$(-\frac{d}{dt} \psi_{\mathcal{L}}(t), i_{\mathcal{L}}(t), i_{\mathcal{L}}(t), u_{\mathcal{L}}(t)) \in D_{\mathcal{L}}, (\psi_{\mathcal{L}}(t), i_{\mathcal{L}}(t)) \in \mathcal{L}_{\mathcal{L}},$$

Here, $\psi_{\mathcal{L}}$ represents the magnetic flux of the inductance and the Hamiltonian $H_{\mathcal{L}} \in \mathcal{C}^1(\mathbb{R}^{\ell_p}, \mathbb{R})$ represents the energy storage function of the system. From this pH system, one can derive

$$u_{\mathcal{L}}(t) = \frac{d}{dt} \psi_{\mathcal{L}}(t), i_{\mathcal{L}}(t) = \Delta H_{\mathcal{L}}(\psi_{\mathcal{L}}(t)).$$

If the inductance has two terminals, then we obtain a conventional inductance with one port.

The dynamics of the voltage source are represented as follows:

$\mathcal{D}_S = \mathcal{D}_1$ with $\mathcal{D}_1$ as defined in (9), and the Lagrange submanifold and resistive relation are trivial, i.e., $\mathcal{L}_S = \mathcal{R}_S = 0$. The dynamics are

$$(-i_{\mathcal{S}}(t), i_{\mathcal{S}}(t), u_{\mathcal{S}}(t), u_{\mathcal{S}}(t)) \in \mathcal{D}_S.$$

4.8 DIRAC STRUCTURE

The incidence matrix of a directed graph defines the Dirac structure known as the vertex edge Dirac structure which is applied in defining Port Hamiltonian dynamics of the Mechanical ventilator-respiratory system dynamics. Usually, for a standard consensus algorithm, the energy storage corresponds to the vertices and energy dissipation corresponds to the edges while for coordination control, energy storage is both at the vertices and on the edges. In this section of the thesis, Kirchhoff's current laws have been applied to derive a Kirchhoff-Dirac Structure of the integrated mechanical ventilator-human respiratory system dynamics. The sections to follow present, the equivalent graph, the netlist, and the incidence matrix for the spontaneously breathing patient. For the case scenarios of the sedated patient and healthy person, the Dirac structure formulation follows the same pattern as presented in the sections that follow.

4.8.1 *The spontaneous breathing patient Dirac structure*

This diagram presents the integrated mechanical ventilator with the human respiratory system. It is also a representation of the spontaneously breathing patient.

4.8.1.1 *Equivalent graph*

The equivalent graph of the spontaneously breathing patient is provided in figure 4.8. The remaining case scenarios closely follow the same methodology and they will therefore not be demonstrated.

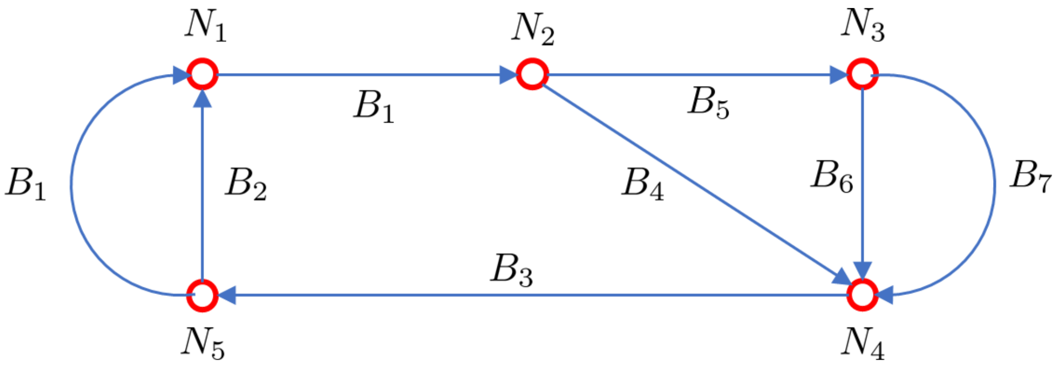

Figure 4.8: Equivalent Graph for a spontaneously breathing patient

4.8.1.2 *The net list*

The netlist of spontaneously breathing patients is provided in table 4.2

Table 4.2: Spontaneously breathing patient net list

R_1	N_1, N_1
R_2	N_1, N_2
R_3	N_2, N_3
R_4	N_3, N_4
C_1	N_1, N_5
C_2	N_2, N_4
C_3	N_3, N_4
C_4	N_3, N_4
C_5	N_4, N_5

4.8.1.3 *The unconnected incidence Matrix*

The unconnected incidence Matrix is provided in the table 4.4

Table 4.3: Spontaneously breathing patient incidence matrix

B_1	B_2	B_3	B_4	B_5	B_6	B_7	B_8	B_9	
-1	1	0	0	1	0	0	0	0	N_1
0	-1	1	0	0	1	0	0	0	N_2
0	0	-1	1	0	0	1	1	0	N_3
0	0	0	-1	0	-1	-1	-1	-1	N_4
1	0	0	0	-1	0	0	0	-1	N_5

4.8.1.4 *The incidence Matrix*

The connected incidence matrix is provided in table 4.3. The interconnection constraints are given by the presented graph incidence matrix which captures the interconnection structure of the mechanical ventilator respiratory system dynamics.

Table 4.4: Spontaneously breathing patient unconnected incidence matrix

B_1	B_2	B_3	B_4	B_5	B_6	B_7	B_8	B_9	
1	0	0	0	0	0	0	0	0	N_5
-1	0	0	0	0	0	0	0	0	N_1
0	1	0	0	0	0	0	0	0	N_1
0	-1	0	0	0	0	0	0	0	N_2
0	0	1	0	0	0	0	0	0	N_2
0	0	-1	0	0	0	0	0	0	N_3
0	0	0	1	0	0	0	0	0	N_3
0	0	0	-1	0	0	0	0	0	N_4
0	0	0	0	1	0	0	0	0	N_1
0	0	0	0	-1	0	0	0	0	N_5
0	0	0	0	0	1	0	0	0	N_2
0	0	0	0	0	-1	0	0	0	N_4
0	0	0	0	0	0	1	0	0	N_3
0	0	0	0	0	0	-1	0	0	N_4
0	0	0	0	0	0	0	1	0	N_3
0	0	0	0	0	0	0	-1	0	N_4
0	0	0	0	0	0	0	0	1	N_4
0	0	0	0	0	0	0	0	-1	N_5

4.8.2 *Model validation*

The model is validated using the parameters listed in tables 4.5, 4.6,4.7 and 4.8 obtained from [93], [94].

4.8.2.1 *Model Parameters*

Table 4.5 provides the resistances

Table 4.7 provides unstressed volume

Table 4.5: Resistance (Units: $CmH_2O.S.1^-1$)

Parameter	Description	Value
R_1	Mouth to larynx	1.021
R_2	Larynx to Trachea	0.3369
R_3	Trachea to Bronchi	0.3063
R_4	Bronchi to Alveoli	0.0817

Table 4.6: Compliance (L/CmH_2O)

Table 4.6 provides the compliance Parameter	Description	Value
C_1	Larynx	0.00127
C_2	Trachea	0.00238
C_3	Bronchi	0.0131
C_4	Alveoli	0.2
C_5	Chest wall compliance	0.2445

Table 4.8 provides other important parameters used.

4.8.3 *Results and discussion of results*

The results for the various case scenarios are now presented:

For each of the presented case scenarios, the current represents the flow of fluid and the voltage which represents the pressure. The presented curves are found to have similar patterns to those presented by [95] in literature as shown in figure 4.21.

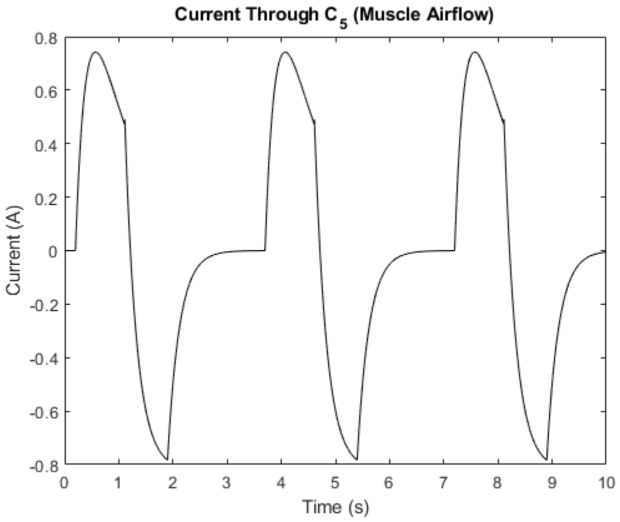

Figure 4.9: Current waveform at the diaphragm versus time

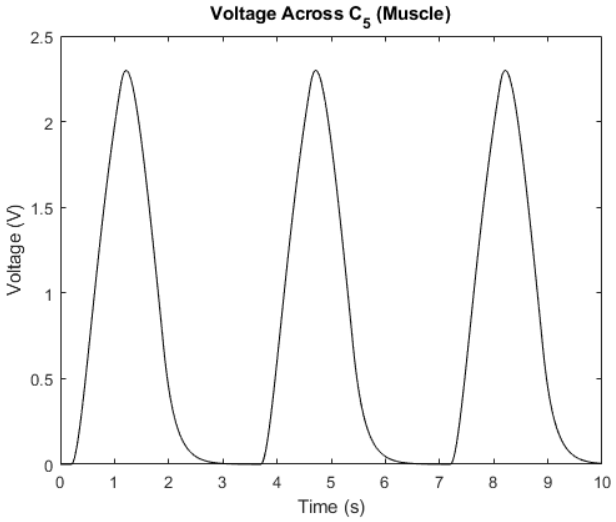

Figure 4.10: Voltage waveform at the diaphragm versus time

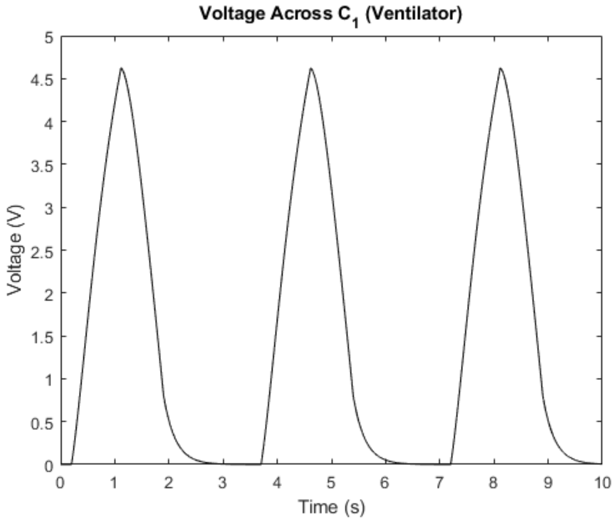

Figure 4.11: voltage waveform at the mouth to the Larynx versus time

Table 4.7: Unstressed volume (ml)

Parameter	Description	Value
V_{UL}	Larynx	34.4
V_{Ut}	Trachea	6.63
V_{Ub}	Bronchi	18.7
V_{UA}	Alveoli	1.263

Table 4.8: Other Parameters

Parameter	Description	Value
$V_{2|}CmH_2O$	Internal pressure generator	-5
$P_{atm}(mmHg$	Atmospheric Pressure	760
$FRC(litres)$	Functional Residue Capacity	2.4
RR (Breaths/min)	Respiratory Rate	12
IE Ratio	Proportions of each breath cycle devoted to the inspiratory and expiratory phases	0.6

Figure 4.9, 4.10 and 4.11, represents the simulated results of a sedated patient. These results are obtained by putting into consideration that when the patient is sedated the is very little to no effort by the diaphragm muscles. The only source of supply of pressure or voltage is the mechanical ventilator.

The simulated results of a healthy person are represented with the following graphs 4.12, 4.13, 4.14 and 4.15. The healthy person is not on a mechanical ventilator and hence the effects of the mechanical ventilation are not included in the simulation. However, the healthy person has the atmospheric air and pressure which supports and aids in the breathing process.

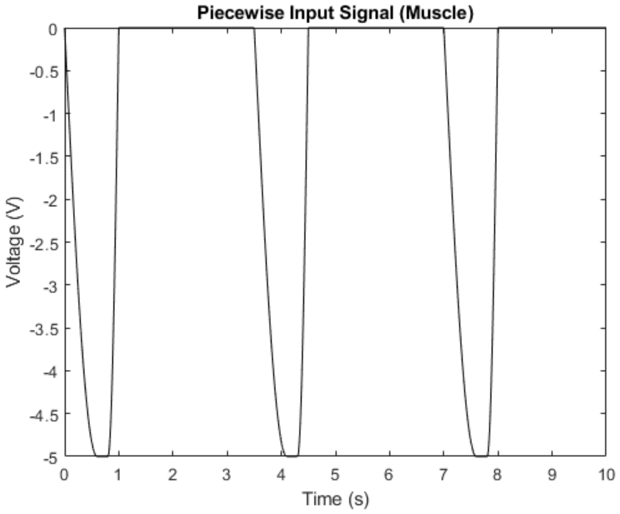

Figure 4.12: Healthy person Input Signal

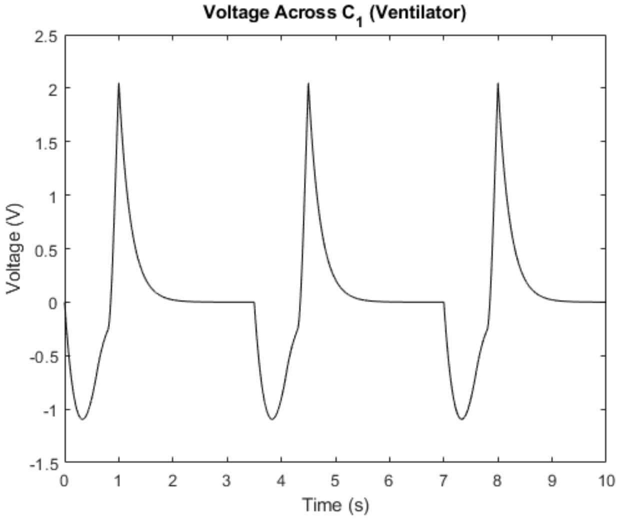

Figure 4.13: Healthy Person Pressure versus time at the Ventilator

For a patient who is both on the mechanical ventilator and can breathe on their own, the simulated results are represented by figures 4.16, 4.17, 4.18, 4.19 and 4.20. This patient requires both the mechanical ventilator and their internal muscles in order to breathe.

The presented Port Hamiltonian lumped parameter model of the respiratory system with the mechanical ventilator modelled as a voltage source represents a lumped parameter model of the human respiratory system. Even though the alveoli are modelled using a single compartment, the proposed model is still sufficiently detailed enough to reproduce human respiratory responses to be applied in different representations of positive pressure while still maintaining low computational costs. The black box approach applied in the representation of the respiratory muscles, has the merit of correctly fitting the observed signal, however, it is limited in its ability to provide the contribution of each

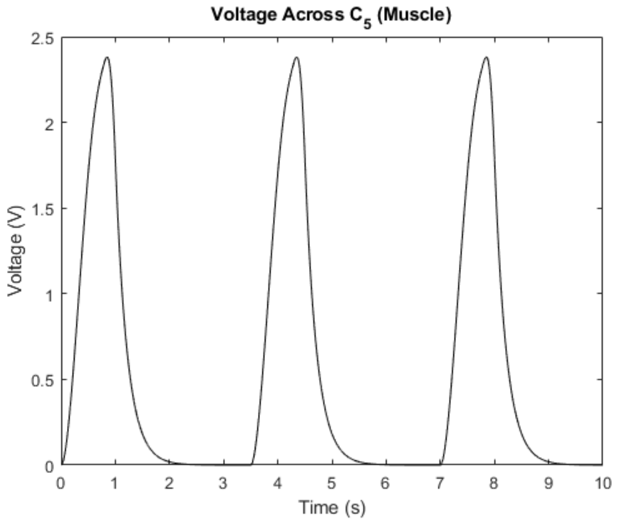

Figure 4.14: Healthy Person Pressure versus time at the diaphragm muscle

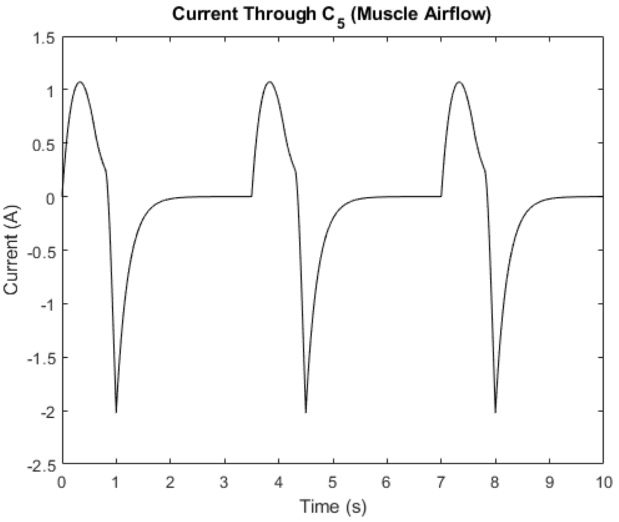

Figure 4.15: Healthy Person air flow verses time at the diaphragm muscle

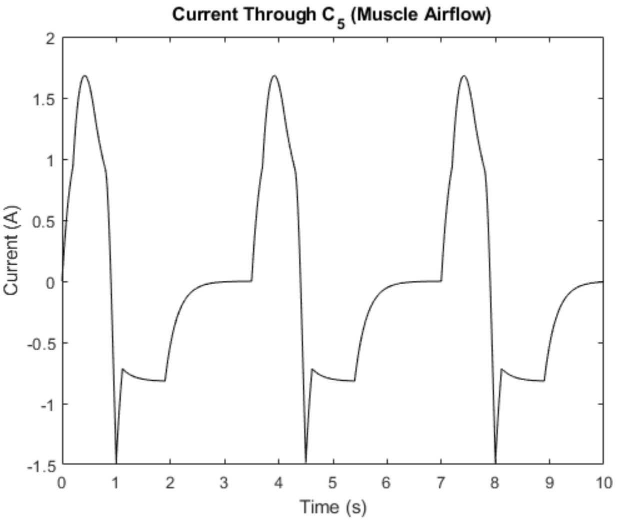

Figure 4.16: Spontaneusly breathing patient airflow for the Muscles

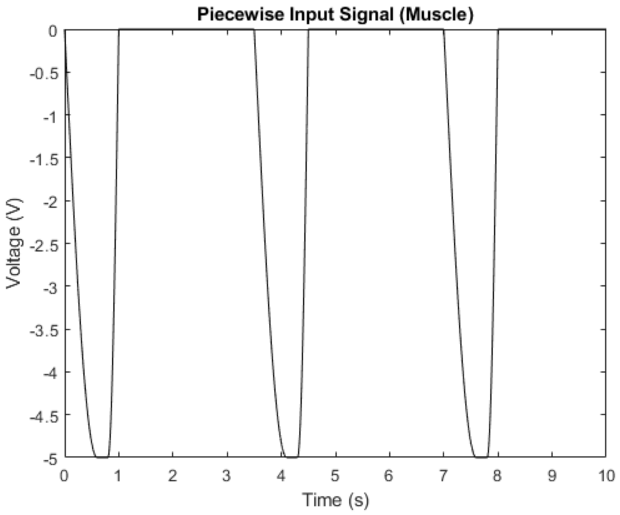

Figure 4.17: Input signal for a spontaneously breathing patient at the Muscles

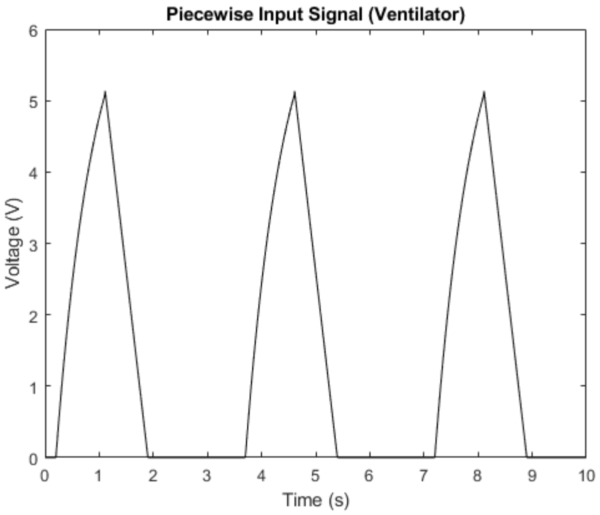

Figure 4.18: Spontaneously breathing patient input signal at the ventilator

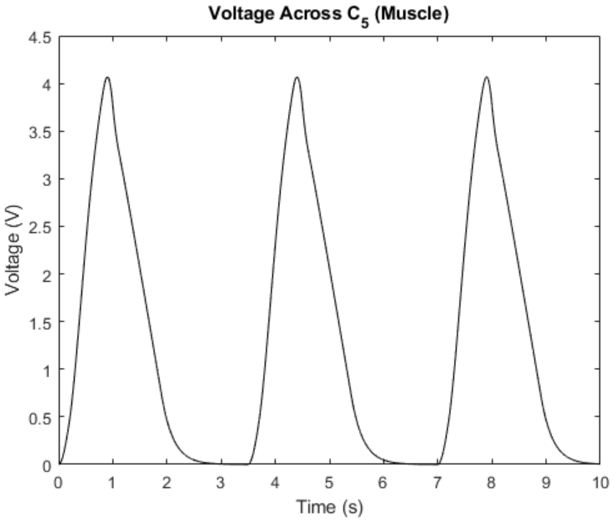

Figure 4.19: Spontaneously breathing patient pressure at the the Muscles

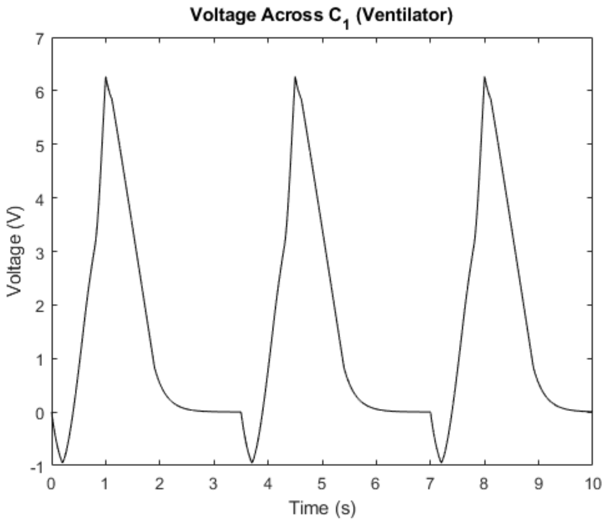

Figure 4.20: Spontaneously breathing patient airflow pressure

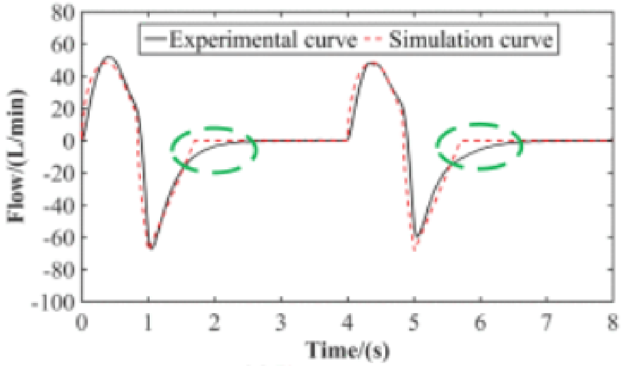

(a) Flow curve

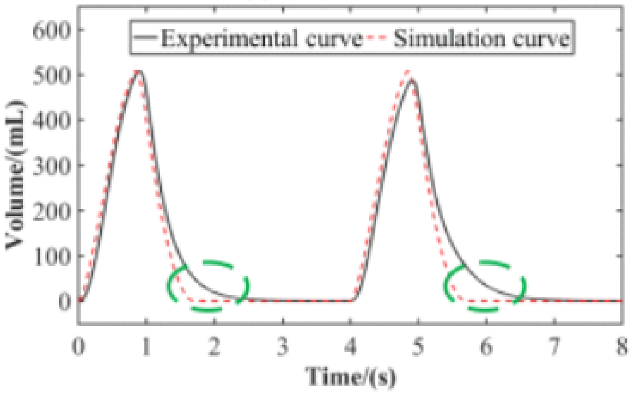

Figure 4.21: Flow verses time curves from the literature

muscle. This level of representation in modelling the Mechanical Ventilator human respiratory system model applied in this chapter is sufficient for controller design. However, it is limited in representation of certain pathologies and phenomena; for instance investigation of the accumulated pressure effects in the alveoli and the impacts of the airway secretion in the mechanical ventilator system. The chapters that follow provide more in-depth models that can address the limitations observed with the presented model.

4.8.4 *Reflection on the contribution for the chapter*

The main contribution in this chapter was a formulation of a lumped parameter Port Hamiltonian human respiratory system model connected to a pressure source which represents the mechanical ventilator. The contribution introduces a paradigm shift from the traditional modelling of the mechanical ventilator human respiratory system to the introduction of a novel energy-based modelling of the human respiratory system with a unique interconnection.

4.9 CONCLUSION

This section has presented a Port Hamiltonian formulation of a mechanical ventilator human respiratory system using the Port Hamiltonian dynamics graphing approach. The conventional method of modeling the mechanical ventilator lung system has been presented followed by a motivation for using the Port Hamiltonian approach to model the mechanical ventilator human respiratory system. The developed model provides a structure or a tool that can be used in the development of robust controllers in the Port Hamiltonian framework. Future work could include the design, development and implementation of robust controllers for the Mechanical ventilator Human respiratory system.

5

FORMULATION OF A COMPREHENSIVE INTEGRATED MODEL OF THE HUMAN RESPIRATORY SYSTEM VIA THE PORT HAMILTONIAN APPROACH

5.1 SUMMARY

This Chapter builds on the concepts presented in Chapter 4 and provides a more detailed model of the human respiratory system. The detailed model is obtained by expanding parts of the human respiratory system that were previously lumped. The human respiratory system is extended to include the effects of the alveoli and the diaphragm. The experimental validation of the results was conducted at the University of the Witwatersrand, Faculty of Health Science, School of Physiology, in the Human Nutrition Research Laboratory. The extended model can be applied in the illustration of the breathing mechanism and in simulating respiratory pathologies for instance: Acute Lung Injury (ALI) and Acute Respiratory Distress Syndrome (ARDS).

5.2 INTRODUCTION

Model-based Mechanical Ventilator treatment in Mechanical Ventilation stipulates the availability of a lung model which is normally used to establish the state of the lung and thereafter, the optimal MV settings are determined. This is important for clinicians to be able to detect lung diseases. Model-based MV treatment requires that the complexities of the lung dynamics to be captured accurately. However, the developed model should be simple enough for easy evaluation and model parameter accessibility. Barbin et al, [96], formulated a dynamic model of the lung for investigation of the expiration flow limitation in mechanical ventilators. Jandre et al, [97], used one non-linear lung model to simulate the impacts of low pass filtering, filter inter-channel delay and mismatch. Babuska et al, derived a mathematical model of a non-linear single-compartment model. During inspiration, the ventilator is modelled as a flow source and during expiration, it is modelled as an effort. Rosa et al, [98], formulated the bond graph model of the human esophagus and the researcher also conducted the analysis in the satiation of an individual. Tabrizi, [99] formulated the acoustic behaviour of the respiratory system using bond graph. The airways were represented using distributed dynamics while the lower passage generation was modelled using lumped resistance and compliance effects. [96], [97], [100], [98], presented the model of a single dynamic lung. In reality, a human being has two lungs, and the left lung is smaller than the right lung and therefore for accurate modeling both lungs are supposed to be considered. Shi et al, [54], proposed a mathematical formulation of volume controlled mechanically ventilated respiratory system with two different lungs. The main parts of the human respiratory system are the trachea, main bronchi, bronchioles and alveoli. It is estimated that the human body, has approximately 480 million alveoli [101]. The alveolar is one of the factors that structurally limits the diffusing capacity of the lung. Within the respiratory parenchyma, the alveolar is the smallest gaseous exchange unit. The alveoli may be viewed as pronounced surface irregularities with opening [101]. These alveoli act as the interface for gaseous exchange such that carbon dioxide is eliminated and oxygen is transferred through the blood capillary vessels that lead to the pulmonary vein.

5.3 CONTRIBUTION

Contribution 5.3.1

The contribution in this chapter is the formulation of a comprehensive integrated Port Hamiltonian model of the human respiratory system which includes the alveoli and the diaphragm. The previously lumped parameter system is now represented using a Port Hamiltonian distributed resistor model. The human respiratory system is modelled using distributed resistors and the alveoli is included in the detailed model. The distributed resistors are terminated with a voltage source (it represents a pressure source) which acts as a collector for all the summed up pressures produced by the numerous alveoli in the lung. This model can be used in the investigation and illustration of the breathing mechanism which involves inspiration and expiration. Another application would be the pressure analysis for patients with COPD and it can also be used for design of robust controllers for the mechanical ventilation system

5.4 DETAILED PORT HAMILTONIAN MODELING OF THE RESPIRATORY SYSTEM

This section provides a detailed port Hamiltonian modeling of the human respiratory system including the alveoli.

5.4.1 *Physical model of the lung*

Here, under certain assumptions, an analogy between an electric circuit and the flow of fluid with pressure, P, flow rate Q, density ρ, through a cylinder of cross-sectional area A and length L_E. Take note that

$$L_E = \int dx \tag{5.1}$$

where dx is the infinitesimal change in length along the cylinder.

Assuming the density is constant over the length L_E, the inertance of the fluid L, is given by

$$L = \int \frac{\rho L_E}{A} \tag{5.2}$$

Hence the relations between the flow rate and pressure are given by

$$P = \frac{dQ}{dt} \tag{5.3}$$

$$P = \frac{1}{C} \int Q dt \tag{5.4}$$

$$P = RQ \tag{5.5}$$

where R and C are the resistance and capacitance of the flow.

Under these assumptions, the flow through a cylinder over an infinitesimal length dx is illustrated in figure 5.1

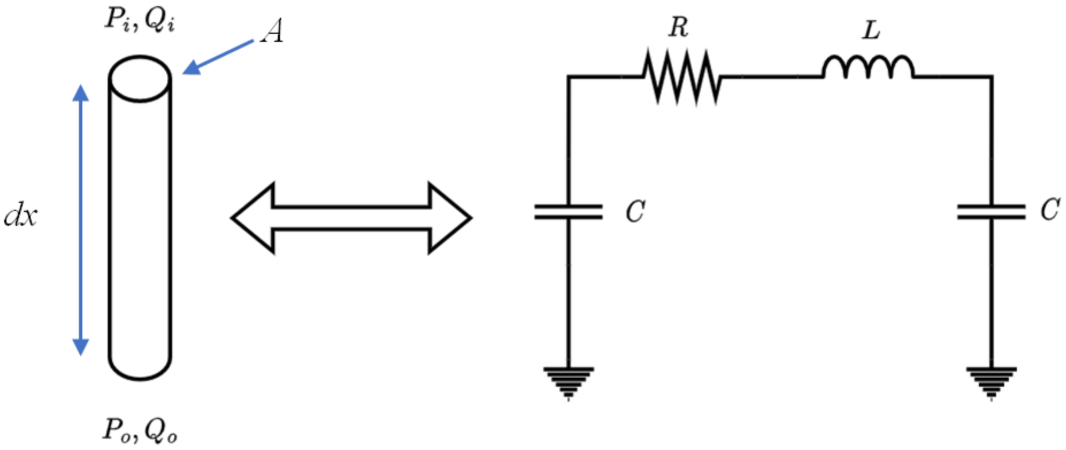

Figure 5.1: Fluid-Electrical analogy of flow through a cylinder

The lung model consists of two parts, the airway and the respiratory zone. The airway is broken down into the upper and lower airways. The upper airway consists of the nostrils, nose, pharynx and larynx. While the lower airway is made up of the right and left bronchioles, the bronchus and the terminal bronchioles. All these can be thought of as a network of connected cylinders of varying length which form a tree-like network structure. For simplicity it is assumed that each section of the lower airway splits into into two branches at each generation, see figure 5.2.

The alveoli can be modelled as capacitors at the endpoints of the trees representing the terminal bronchioles. In order to model the action of the diaphragm of a normal breathing patient, all the capacitors representing the alveoli are connected at the same node which is connected to a source. This represents the pressure change due to the movement of the diaphragm, see figure 5.3.

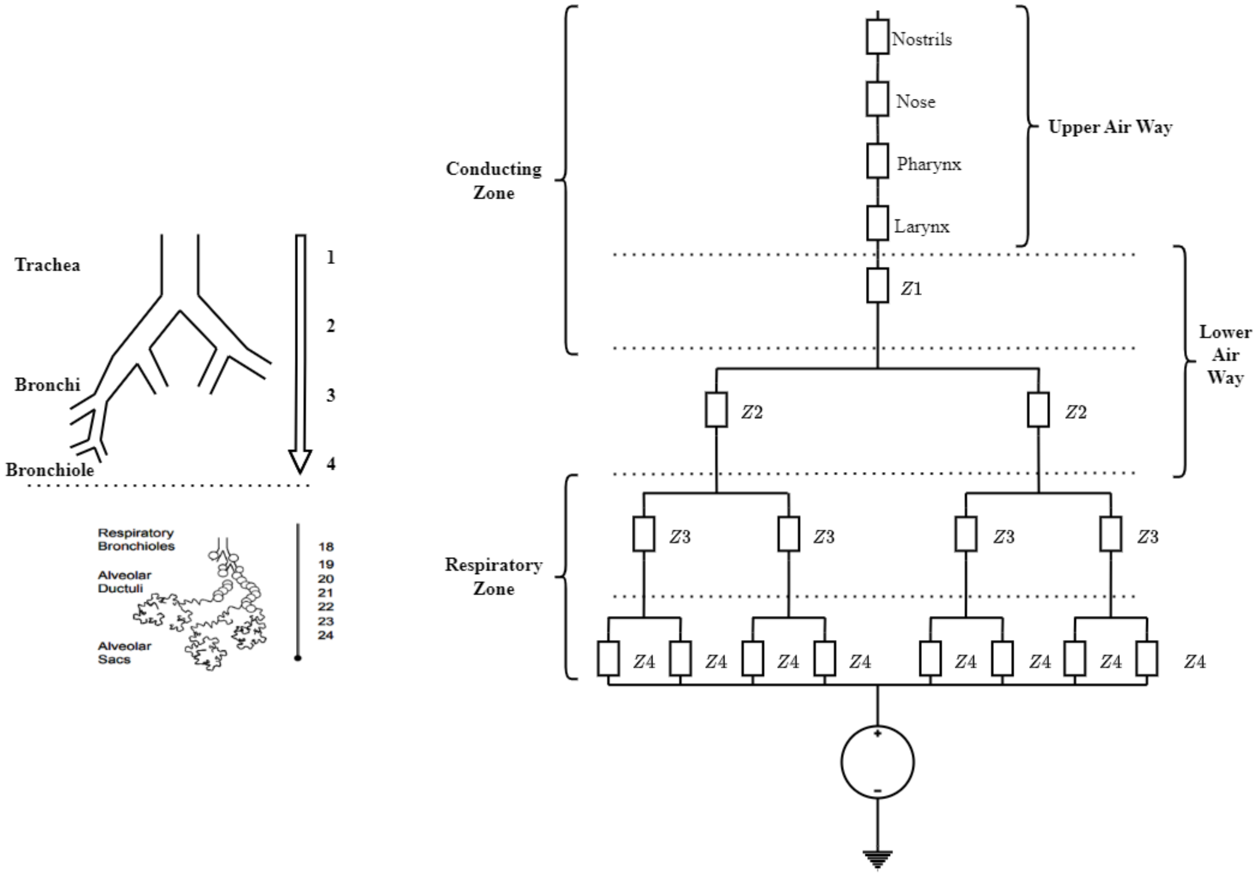

Figure 5.2: Distributed resistor model

5.5 ELECTRICAL ANALOGY OF THE ENTIRE SYSTEM

The comprehensive electrical analogy of the entire system is presented in figure 5.4.

For the sake of illustration, a simplified model is presented in figure 5.6.

The total number of branches, n_B, is

$$n_B = n_S + n_P + n_D \tag{5.6}$$

where n_S is the number of branches with storage elements, n_P is the number of branches with ports and n_D is the number of branches with dissipative elements. From figure 5.6, the number of storage branches is $n_S = 11$, i.e. five capacitors and six inductors, since there are five resistors, the number of dissipative branches $n_D = 5$ and the number of ports is $n_P = 2$. The simplified graphical representation is presented in figure 5.7

5.6 THE GRAPHICAL REPRESENTATION OF THE SYSTEM

The simplified model of the system and the graphical equivalence is provided:

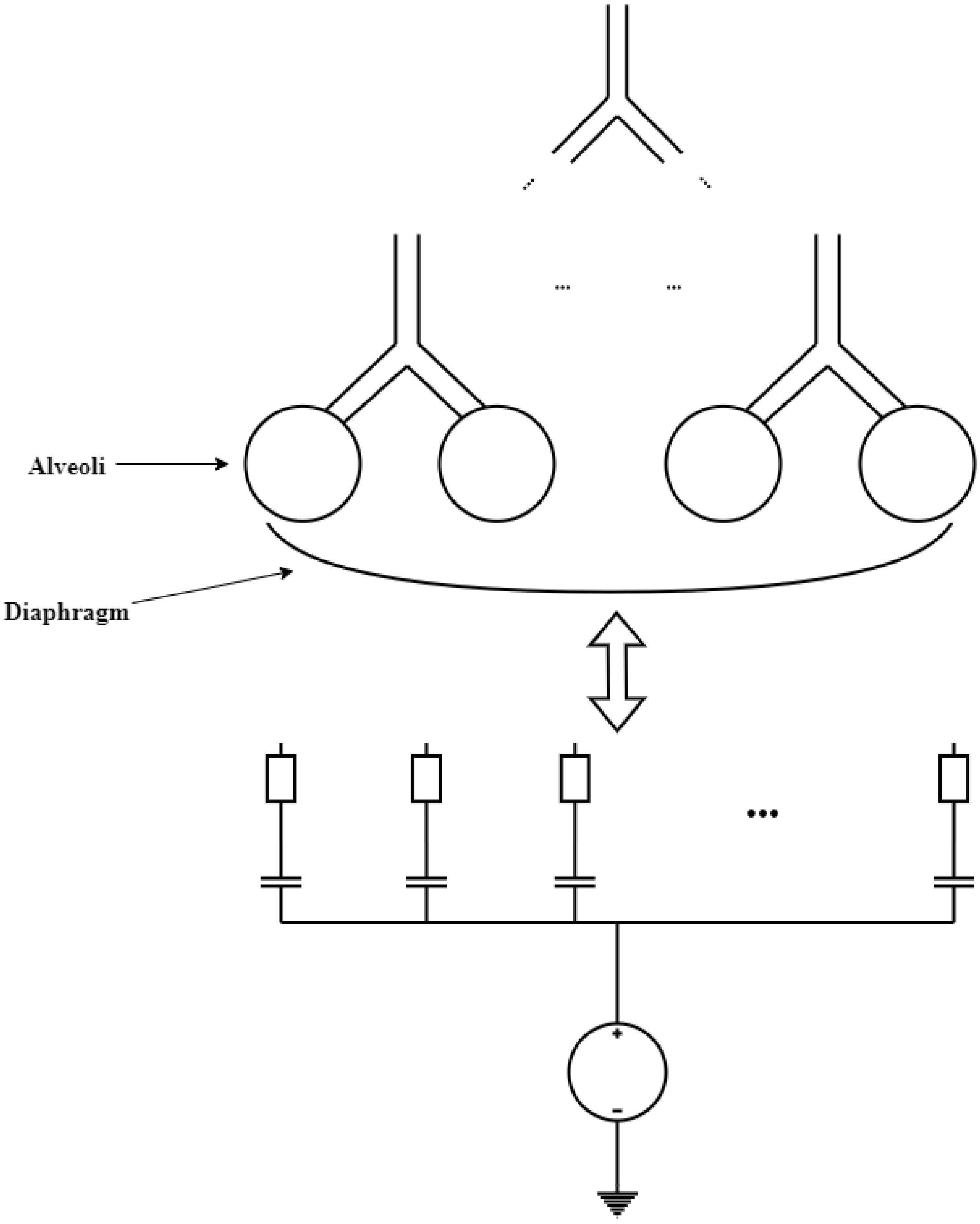

Figure 5.3: Fluid-electric analogy at the alveoli

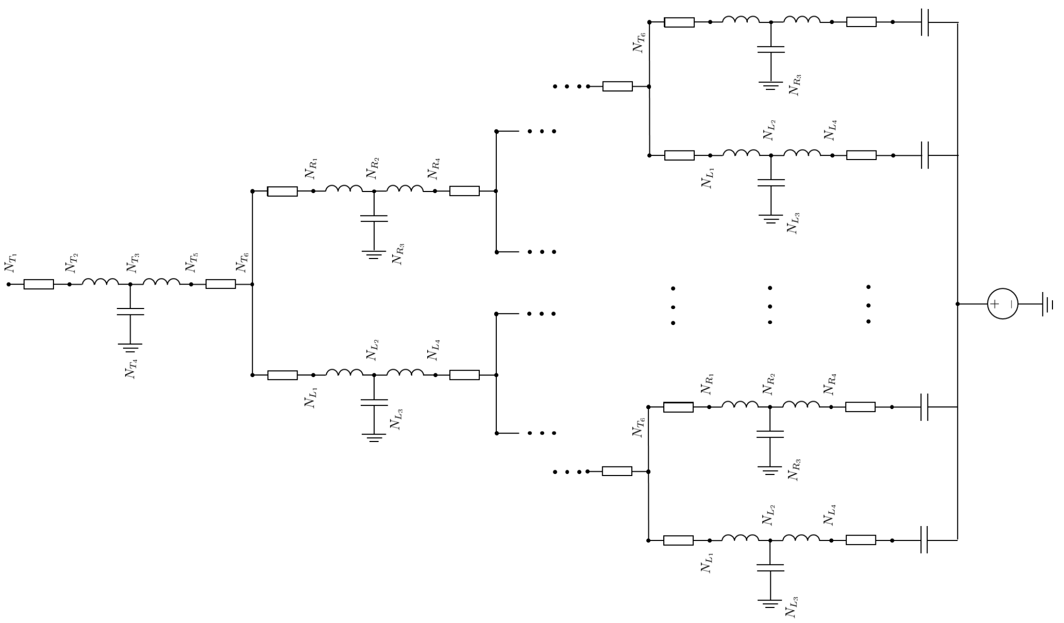

Figure 5.4: Electrical analogy of the detailed model of the respiratory system

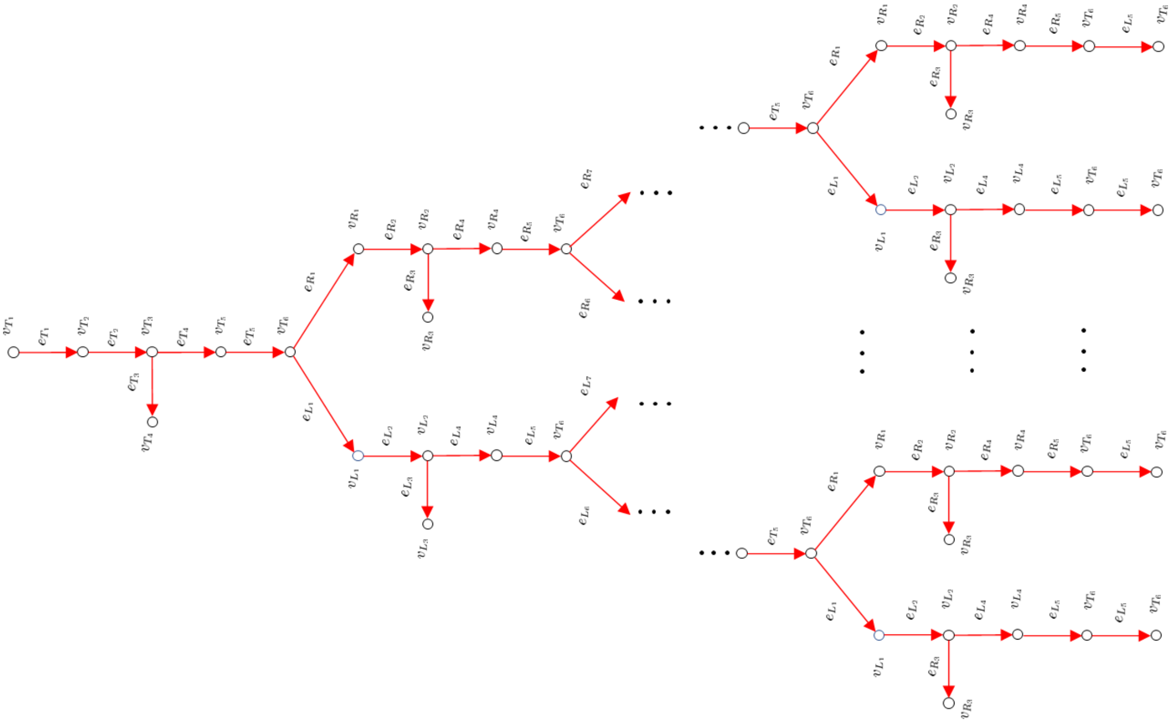

Figure 5.5: Graph theoretical model with source node

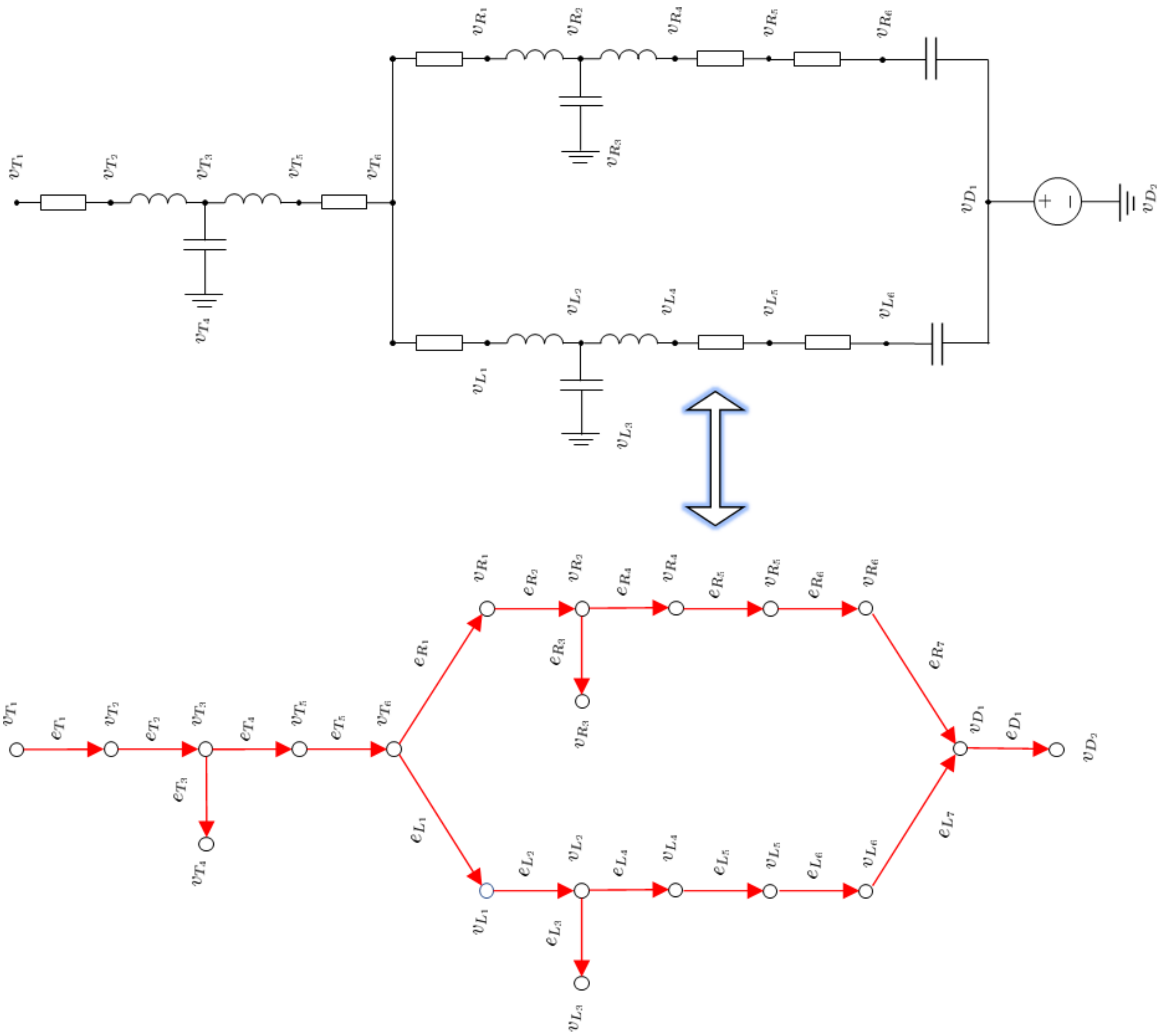

Figure 5.6: Simplified model

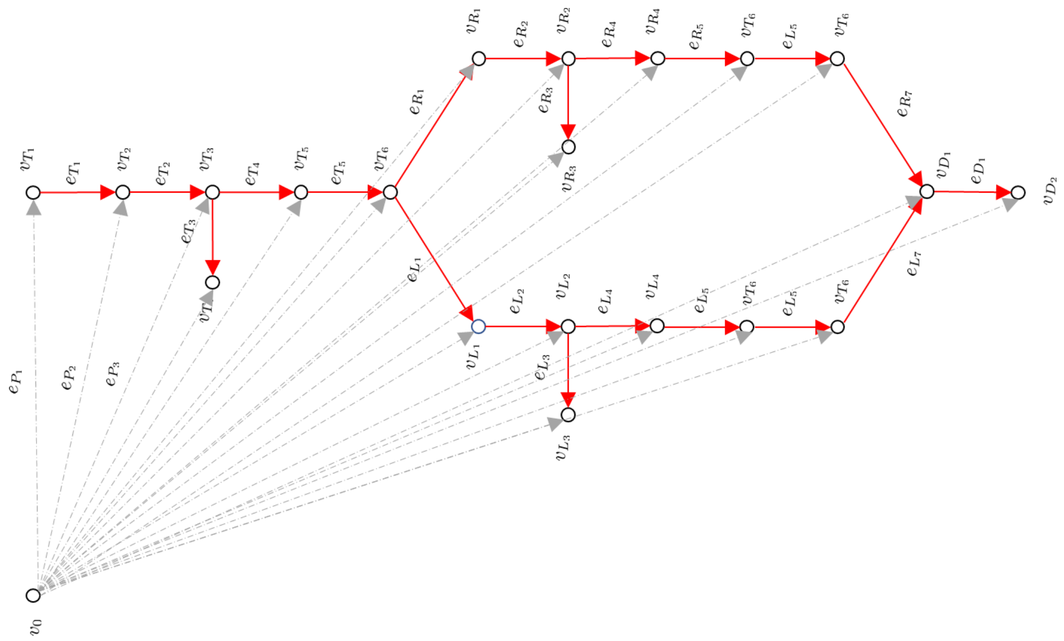

Figure 5.7: Simplified graphical representation

5.6.1 *The unconnected and connected incidence matrix*

The incidence matrix when the components are not connected to each other is

$$\gamma = \begin{array}{cccccccccccccccccccc|c}
e_{t_1} & e_{t_2} & e_{t_3} & e_{t_4} & e_{t_5} & e_{l_1} & e_{l_2} & e_{l_3} & e_{l_4} & e_{l_5} & e_{l_6} & e_{l_7} & e_{r_1} & e_{r_2} & e_{r_3} & e_{r_4} & e_{r_5} & e_{r_6} & e_{r_7} & e_{D_1} & \\
1 & 0 & 0 & 0 & 0 & 0 & 0 & 0 & 0 & 0 & 0 & 0 & 0 & 0 & 0 & 0 & 0 & 0 & 0 & 0 & v_{t_1} \\
-1 & 0 & 0 & 0 & 0 & 0 & 0 & 0 & 0 & 0 & 0 & 0 & 0 & 0 & 0 & 0 & 0 & 0 & 0 & 0 & v_{t_2} \\
0 & 1 & 0 & 0 & 0 & 0 & 0 & 0 & 0 & 0 & 0 & 0 & 0 & 0 & 0 & 0 & 0 & 0 & 0 & 0 & v_{t_2} \\
0 & -1 & 0 & 0 & 0 & 0 & 0 & 0 & 0 & 0 & 0 & 0 & 0 & 0 & 0 & 0 & 0 & 0 & 0 & 0 & v_{t_3} \\
0 & 0 & 1 & 0 & 0 & 0 & 0 & 0 & 0 & 0 & 0 & 0 & 0 & 0 & 0 & 0 & 0 & 0 & 0 & 0 & v_{t_3} \\
0 & 0 & -1 & 0 & 0 & 0 & 0 & 0 & 0 & 0 & 0 & 0 & 0 & 0 & 0 & 0 & 0 & 0 & 0 & 0 & v_{t_4} \\
0 & 0 & 0 & 1 & 0 & 0 & 0 & 0 & 0 & 0 & 0 & 0 & 0 & 0 & 0 & 0 & 0 & 0 & 0 & 0 & v_{t_3} \\
0 & 0 & 0 & -1 & 0 & 0 & 0 & 0 & 0 & 0 & 0 & 0 & 0 & 0 & 0 & 0 & 0 & 0 & 0 & 0 & v_{t_5} \\
0 & 0 & 0 & 0 & 1 & 0 & 0 & 0 & 0 & 0 & 0 & 0 & 0 & 0 & 0 & 0 & 0 & 0 & 0 & 0 & v_{t_5} \\
0 & 0 & 0 & 0 & -1 & 0 & 0 & 0 & 0 & 0 & 0 & 0 & 0 & 0 & 0 & 0 & 0 & 0 & 0 & 0 & v_{t_6} \\
0 & 0 & 0 & 0 & 0 & 1 & 0 & 0 & 0 & 0 & 0 & 0 & 0 & 0 & 0 & 0 & 0 & 0 & 0 & 0 & v_{t_6} \\
0 & 0 & 0 & 0 & 0 & -1 & 0 & 0 & 0 & 0 & 0 & 0 & 0 & 0 & 0 & 0 & 0 & 0 & 0 & 0 & v_{l_1} \\
0 & 0 & 0 & 0 & 0 & 0 & 1 & 0 & 0 & 0 & 0 & 0 & 0 & 0 & 0 & 0 & 0 & 0 & 0 & 0 & v_{l_1} \\
0 & 0 & 0 & 0 & 0 & 0 & -1 & 0 & 0 & 0 & 0 & 0 & 0 & 0 & 0 & 0 & 0 & 0 & 0 & 0 & v_{l_2} \\
0 & 0 & 0 & 0 & 0 & 0 & 0 & 1 & 0 & 0 & 0 & 0 & 0 & 0 & 0 & 0 & 0 & 0 & 0 & 0 & v_{l_2} \\
0 & 0 & 0 & 0 & 0 & 0 & 0 & -1 & 0 & 0 & 0 & 0 & 0 & 0 & 0 & 0 & 0 & 0 & 0 & 0 & v_{l_3} \\
0 & 0 & 0 & 0 & 0 & 0 & 0 & 0 & 1 & 0 & 0 & 0 & 0 & 0 & 0 & 0 & 0 & 0 & 0 & 0 & v_{l_2} \\
0 & 0 & 0 & 0 & 0 & 0 & 0 & 0 & -1 & 0 & 0 & 0 & 0 & 0 & 0 & 0 & 0 & 0 & 0 & 0 & v_{l_4} \\
0 & 0 & 0 & 0 & 0 & 0 & 0 & 0 & 0 & 1 & 0 & 0 & 0 & 0 & 0 & 0 & 0 & 0 & 0 & 0 & v_{l_4} \\
0 & 0 & 0 & 0 & 0 & 0 & 0 & 0 & 0 & -1 & 0 & 0 & 0 & 0 & 0 & 0 & 0 & 0 & 0 & 0 & v_{l_5} \\
0 & 0 & 0 & 0 & 0 & 0 & 0 & 0 & 0 & 0 & 1 & 0 & 0 & 0 & 0 & 0 & 0 & 0 & 0 & 0 & v_{l_5} \\
0 & 0 & 0 & 0 & 0 & 0 & 0 & 0 & 0 & 0 & -1 & 0 & 0 & 0 & 0 & 0 & 0 & 0 & 0 & 0 & v_{l_6} \\
0 & 0 & 0 & 0 & 0 & 0 & 0 & 0 & 0 & 0 & 0 & 1 & 0 & 0 & 0 & 0 & 0 & 0 & 0 & 0 & v_{l_6} \\
0 & 0 & 0 & 0 & 0 & 0 & 0 & 0 & 0 & 0 & 0 & -1 & 0 & 0 & 0 & 0 & 0 & 0 & 0 & 0 & v_{D_1} \\
0 & 0 & 0 & 0 & 0 & 0 & 0 & 0 & 0 & 0 & 0 & 0 & 1 & 0 & 0 & 0 & 0 & 0 & 0 & 0 & v_{D_1} \\
0 & 0 & 0 & 0 & 0 & 0 & 0 & 0 & 0 & 0 & 0 & 0 & -1 & 0 & 0 & 0 & 0 & 0 & 0 & 0 & v_{D_2} \\
0 & 0 & 0 & 0 & 0 & 0 & 0 & 0 & 0 & 0 & 0 & 0 & 0 & 1 & 0 & 0 & 0 & 0 & 0 & 0 & v_{t_6} \\
0 & 0 & 0 & 0 & 0 & 0 & 0 & 0 & 0 & 0 & 0 & 0 & 0 & -1 & 0 & 0 & 0 & 0 & 0 & 0 & v_{r_1} \\
0 & 0 & 0 & 0 & 0 & 0 & 0 & 0 & 0 & 0 & 0 & 0 & 0 & 0 & 1 & 0 & 0 & 0 & 0 & 0 & v_{r_1} \\
0 & 0 & 0 & 0 & 0 & 0 & 0 & 0 & 0 & 0 & 0 & 0 & 0 & 0 & -1 & 0 & 0 & 0 & 0 & 0 & v_{r_2} \\
0 & 0 & 0 & 0 & 0 & 0 & 0 & 0 & 0 & 0 & 0 & 0 & 0 & 0 & 0 & 1 & 0 & 0 & 0 & 0 & v_{r_2} \\
0 & 0 & 0 & 0 & 0 & 0 & 0 & 0 & 0 & 0 & 0 & 0 & 0 & 0 & 0 & -1 & 0 & 0 & 0 & 0 & v_{r_3} \\
0 & 0 & 0 & 0 & 0 & 0 & 0 & 0 & 0 & 0 & 0 & 0 & 0 & 0 & 0 & 0 & 1 & 0 & 0 & 0 & v_{r_2} \\
0 & 0 & 0 & 0 & 0 & 0 & 0 & 0 & 0 & 0 & 0 & 0 & 0 & 0 & 0 & 0 & -1 & 0 & 0 & 0 & v_{r_4} \\
0 & 0 & 0 & 0 & 0 & 0 & 0 & 0 & 0 & 0 & 0 & 0 & 0 & 0 & 0 & 0 & 0 & 1 & 0 & 0 & v_{r_4} \\
0 & 0 & 0 & 0 & 0 & 0 & 0 & 0 & 0 & 0 & 0 & 0 & 0 & 0 & 0 & 0 & 0 & -1 & 0 & 0 & v_{r_5} \\
0 & 0 & 0 & 0 & 0 & 0 & 0 & 0 & 0 & 0 & 0 & 0 & 0 & 0 & 0 & 0 & 0 & 0 & 1 & 0 & v_{r_5} \\
0 & 0 & 0 & 0 & 0 & 0 & 0 & 0 & 0 & 0 & 0 & 0 & 0 & 0 & 0 & 0 & 0 & 0 & -1 & 0 & v_{r_6} \\
0 & 0 & 0 & 0 & 0 & 0 & 0 & 0 & 0 & 0 & 0 & 0 & 0 & 0 & 0 & 0 & 0 & 0 & 0 & 1 & v_{r_6} \\
0 & 0 & 0 & 0 & 0 & 0 & 0 & 0 & 0 & 0 & 0 & 0 & 0 & 0 & 0 & 0 & 0 & 0 & 0 & -1 & v_{D_1}
\end{array} \tag{5.7}$$

Adding the rows with repeating nodal labels, γ reduces to

$$\gamma = \begin{array}{cccccccccccccccccccc|c}
e_{t_1} & e_{t_2} & e_{t_3} & e_{t_4} & e_{t_5} & e_{l_1} & e_{l_2} & e_{l_3} & e_{l_4} & e_{l_5} & e_{l_6} & e_{l_7} & e_{r_1} & e_{r_2} & e_{r_3} & e_{r_4} & e_{r_5} & e_{r_6} & e_{r_7} & e_{D_1} & \\
1 & 0 & 0 & 0 & 0 & 0 & 0 & 0 & 0 & 0 & 0 & 0 & 0 & 0 & 0 & 0 & 0 & 0 & 0 & 0 & v_{t_1} \\
-1 & 1 & 0 & 0 & 0 & 0 & 0 & 0 & 0 & 0 & 0 & 0 & 0 & 0 & 0 & 0 & 0 & 0 & 0 & 0 & v_{t_2} \\
0 & -1 & 1 & 1 & 0 & 0 & 0 & 0 & 0 & 0 & 0 & 0 & 0 & 0 & 0 & 0 & 0 & 0 & 0 & 0 & v_{t_3} \\
0 & 0 & -1 & 0 & 0 & 0 & 0 & 0 & 0 & 0 & 0 & 0 & 0 & 0 & 0 & 0 & 0 & 0 & 0 & 0 & v_{t_4} \\
0 & 0 & 0 & -1 & 1 & 0 & 0 & 0 & 0 & 0 & 0 & 0 & 0 & 0 & 0 & 0 & 0 & 0 & 0 & 0 & v_{t_5} \\
0 & 0 & 0 & 0 & -1 & 1 & 0 & 0 & 0 & 0 & 0 & 0 & 0 & 1 & 0 & 0 & 0 & 0 & 0 & 0 & v_{t_6} \\
0 & 0 & 0 & 0 & 0 & -1 & 1 & 0 & 0 & 0 & 0 & 0 & 0 & 0 & 0 & 0 & 0 & 0 & 0 & 0 & v_{l_1} \\
0 & 0 & 0 & 0 & 0 & 0 & -1 & 1 & 1 & 0 & 0 & 0 & 0 & 0 & 0 & 0 & 0 & 0 & 0 & 0 & v_{l_2} \\
0 & 0 & 0 & 0 & 0 & 0 & 0 & -1 & 0 & 0 & 0 & 0 & 0 & 0 & 0 & 0 & 0 & 0 & 0 & 0 & v_{l_3} \\
0 & 0 & 0 & 0 & 0 & 0 & 0 & 0 & -1 & 1 & 0 & 0 & 0 & 0 & 0 & 0 & 0 & 0 & 0 & 0 & v_{l_4} \\
0 & 0 & 0 & 0 & 0 & 0 & 0 & 0 & 0 & -1 & 1 & 0 & 0 & 0 & 0 & 0 & 0 & 0 & 0 & 0 & v_{l_5} \\
0 & 0 & 0 & 0 & 0 & 0 & 0 & 0 & 0 & 0 & -1 & 1 & 0 & 0 & 0 & 0 & 0 & 0 & 0 & 0 & v_{l_6} \\
0 & 0 & 0 & 0 & 0 & 0 & 0 & 0 & 0 & 0 & 0 & -1 & 1 & 0 & 0 & 0 & 0 & 0 & 0 & -1 & v_{D_1} \\
0 & 0 & 0 & 0 & 0 & 0 & 0 & 0 & 0 & 0 & 0 & 0 & -1 & 0 & 0 & 0 & 0 & 0 & 0 & 0 & v_{D_2} \\
0 & 0 & 0 & 0 & 0 & 0 & 0 & 0 & 0 & 0 & 0 & 0 & 0 & -1 & 1 & 0 & 0 & 0 & 0 & 0 & v_{r_1} \\
0 & 0 & 0 & 0 & 0 & 0 & 0 & 0 & 0 & 0 & 0 & 0 & 0 & 0 & -1 & 1 & 1 & 0 & 0 & 0 & v_{r_2} \\
0 & 0 & 0 & 0 & 0 & 0 & 0 & 0 & 0 & 0 & 0 & 0 & 0 & 0 & 0 & -1 & 0 & 0 & 0 & 0 & v_{r_3} \\
0 & 0 & 0 & 0 & 0 & 0 & 0 & 0 & 0 & 0 & 0 & 0 & 0 & 0 & 0 & 0 & -1 & 1 & 0 & 0 & v_{r_4} \\
0 & 0 & 0 & 0 & 0 & 0 & 0 & 0 & 0 & 0 & 0 & 0 & 0 & 0 & 0 & 0 & 0 & -1 & 1 & 0 & v_{r_5} \\
0 & 0 & 0 & 0 & 0 & 0 & 0 & 0 & 0 & 0 & 0 & 0 & 0 & 0 & 0 & 0 & 0 & 0 & -1 & 1 & v_{r_6}
\end{array} \tag{5.8}$$

The incidence matrix can be re-arranged according to the nature of the elements in the circuit, that is whether they are storage, dissipative or ports, so that

$$\gamma = \left[\begin{array}{ccc} \gamma_S & \gamma_D & \gamma_P \end{array}\right] = \begin{array}{ccccccccccccccccccccc}
e_{t_1} & e_{t_2} & e_{t_3} & e_{t_4} & e_{t_5} & e_{l_1} & e_{l_2} & e_{l_3} & e_{l_4} & e_{l_5} & e_{l_6} & e_{l_7} & e_{r_1} & e_{r_2} & e_{r_3} & e_{r_4} & e_{r_5} & e_{r_6} & e_{r_7} & e_{d_1} & \\
1 & 0 & 0 & 0 & 0 & 0 & 0 & 0 & 0 & 0 & 0 & 0 & 0 & 0 & 0 & 0 & 0 & 0 & 0 & 0 & v_{t_1} \\
-1 & 1 & 0 & 0 & 0 & 0 & 0 & 0 & 0 & 0 & 0 & 0 & 0 & 0 & 0 & 0 & 0 & 0 & 0 & 0 & v_{t_2} \\
0 & -1 & 1 & 1 & 0 & 0 & 0 & 0 & 0 & 0 & 0 & 0 & 0 & 0 & 0 & 0 & 0 & 0 & 0 & 0 & v_{t_3} \\
0 & 0 & -1 & 0 & 0 & 0 & 0 & 0 & 0 & 0 & 0 & 0 & 0 & 0 & 0 & 0 & 0 & 0 & 0 & 0 & v_{t_4} \\
0 & 0 & 0 & -1 & 1 & 0 & 0 & 0 & 0 & 0 & 0 & 0 & 0 & 0 & 0 & 0 & 0 & 0 & 0 & 0 & v_{t_5} \\
0 & 0 & 0 & 0 & -1 & 1 & 0 & 0 & 0 & 0 & 0 & 0 & 0 & 1 & 0 & 0 & 0 & 0 & 0 & 0 & v_{t_6} \\
0 & 0 & 0 & 0 & 0 & -1 & 1 & 0 & 0 & 0 & 0 & 0 & 0 & 0 & 0 & 0 & 0 & 0 & 0 & 0 & v_{l_1} \\
0 & 0 & 0 & 0 & 0 & 0 & -1 & 1 & 1 & 0 & 0 & 0 & 0 & 0 & 0 & 0 & 0 & 0 & 0 & 0 & v_{l_2} \\
0 & 0 & 0 & 0 & 0 & 0 & 0 & -1 & 0 & 0 & 0 & 0 & 0 & 0 & 0 & 0 & 0 & 0 & 0 & 0 & v_{l_3} \\
0 & 0 & 0 & 0 & 0 & 0 & 0 & 0 & -1 & 1 & 0 & 0 & 0 & 0 & 0 & 0 & 0 & 0 & 0 & 0 & v_{l_4} \\
0 & 0 & 0 & 0 & 0 & 0 & 0 & 0 & 0 & -1 & 1 & 0 & 0 & 0 & 0 & 0 & 0 & 0 & 0 & 0 & v_{l_5} \\
0 & 0 & 0 & 0 & 0 & 0 & 0 & 0 & 0 & 0 & -1 & 1 & 0 & 0 & 0 & 0 & 0 & 0 & 0 & 0 & v_{l_6} \\
0 & 0 & 0 & 0 & 0 & 0 & 0 & 0 & 0 & 0 & 0 & -1 & 1 & 0 & 0 & 0 & 0 & 0 & 0 & -1 & v_{D_1} \\
0 & 0 & 0 & 0 & 0 & 0 & 0 & 0 & 0 & 0 & 0 & 0 & -1 & 0 & 0 & 0 & 0 & 0 & 0 & 0 & v_{D_2} \\
0 & 0 & 0 & 0 & 0 & 0 & 0 & 0 & 0 & 0 & 0 & 0 & 0 & -1 & 1 & 0 & 0 & 0 & 0 & 0 & v_{r_1} \\
0 & 0 & 0 & 0 & 0 & 0 & 0 & 0 & 0 & 0 & 0 & 0 & 0 & 0 & -1 & 1 & 1 & 0 & 0 & 0 & v_{r_2} \\
0 & 0 & 0 & 0 & 0 & 0 & 0 & 0 & 0 & 0 & 0 & 0 & 0 & 0 & 0 & -1 & 0 & 0 & 0 & 0 & v_{r_3} \\
0 & 0 & 0 & 0 & 0 & 0 & 0 & 0 & 0 & 0 & 0 & 0 & 0 & 0 & 0 & 0 & -1 & 1 & 0 & 0 & v_{r_4} \\
0 & 0 & 0 & 0 & 0 & 0 & 0 & 0 & 0 & 0 & 0 & 0 & 0 & 0 & 0 & 0 & 0 & -1 & 1 & 0 & v_{r_5} \\
0 & 0 & 0 & 0 & 0 & 0 & 0 & 0 & 0 & 0 & 0 & 0 & 0 & 0 & 0 & 0 & 0 & 0 & -1 & 1 & v_{r_6}
\end{array} \tag{5.9}$$

The current and voltage vectors are given by

$$v = \left[\begin{array}{ccc} v_S & v_D & v_P \end{array}\right]^T = \left[\begin{array}{cccccccccccccccccccc} v_{\mathcal{L}_1} & v_{\mathcal{L}_2} & v_{\mathcal{L}_3} & v_{\mathcal{L}_4} & v_{\mathcal{L}_5} & v_{\mathcal{L}_6} & v_{\mathcal{C}_1} & v_{\mathcal{C}_2} & v_{\mathcal{C}_3} & v_{\mathcal{C}_4} & v_{\mathcal{C}_5} & v_{\mathcal{R}_1} & v_{\mathcal{R}_2} & v_{\mathcal{R}_3} & v_{\mathcal{R}_4} & v_{\mathcal{R}_5} & v_{\mathcal{R}_6} & v_{\mathcal{R}_7} & v_{\mathcal{R}_8} & v_{\mathcal{O}_1} \end{array}\right]^T \tag{5.10}$$

and

$$i = \left[\begin{array}{ccc} i_S & i_D & i_P \end{array}\right]^T = \left[\begin{array}{cccccccccccccccccccc} i_{\mathcal{L}_1} & i_{\mathcal{L}_2} & i_{\mathcal{L}_3} & i_{\mathcal{L}_4} & i_{\mathcal{L}_5} & i_{\mathcal{L}_6} & i_{\mathcal{C}_1} & i_{\mathcal{C}_2} & i_{\mathcal{C}_3} & i_{\mathcal{C}_4} & i_{\mathcal{C}_5} & i_{\mathcal{R}_1} & i_{\mathcal{R}_2} & i_{\mathcal{R}_3} & i_{\mathcal{R}_4} & i_{\mathcal{R}_5} & i_{\mathcal{R}_6} & i_{\mathcal{R}_7} & i_{\mathcal{R}_8} & i_{\mathcal{O}_1} \end{array}\right]^T \tag{5.11}$$

The incidence matrix can be re-arranged according to the nature of the elements in the circuit, that is whether they are storage, dissipative or ports, so that

$$\gamma = \left[\begin{array}{ccc} \gamma_S & \gamma_D & \gamma_P \end{array}\right] = \begin{array}{cccccccccccccccccccc|c}
e_{t_1} & e_{t_2} & e_{t_3} & e_{t_4} & e_{t_5} & e_{l_1} & e_{l_2} & e_{l_3} & e_{l_4} & e_{l_5} & e_{l_6} & e_{l_7} & e_{r_1} & e_{r_2} & e_{r_3} & e_{r_4} & e_{r_5} & e_{r_6} & e_{r_7} & e_{d_1} & \\
-1 & 1 & 0 & 0 & 0 & 0 & 0 & 0 & 0 & 0 & 0 & 0 & 0 & 0 & 0 & 0 & 0 & 0 & 0 & 0 & L_1 \\
0 & 0 & -1 & 0 & 0 & 0 & 0 & 0 & 0 & 0 & 0 & 0 & 0 & 0 & 0 & 0 & 0 & 0 & 0 & 0 & L_2 \\
0 & 0 & 0 & 0 & 0 & -1 & 1 & 0 & 0 & 0 & 0 & 0 & 0 & 0 & 0 & 0 & 0 & 0 & 0 & 0 & L_3 \\
0 & 0 & 0 & 0 & 0 & 0 & 0 & -1 & 0 & 0 & 0 & 0 & 0 & 0 & 0 & 0 & 0 & 0 & 0 & 0 & L_4 \\
0 & 0 & 0 & 0 & 0 & 0 & 0 & 0 & 0 & 0 & 0 & 0 & -1 & 0 & 0 & 0 & 0 & 0 & 0 & 0 & L_5 \\
0 & 0 & 0 & 0 & 0 & 0 & 0 & 0 & 0 & 0 & 0 & 0 & 0 & 0 & -1 & 1 & 1 & 0 & 0 & 0 & L_6 \\
0 & -1 & 1 & 1 & 0 & 0 & 0 & 0 & 0 & 0 & 0 & 0 & 0 & 0 & 0 & 0 & 0 & 0 & 0 & 0 & C_1 \\
0 & 0 & 0 & 0 & 0 & 0 & -1 & 1 & 1 & 0 & 0 & 0 & 0 & 0 & 0 & 0 & 0 & 0 & 0 & 0 & C_2 \\
0 & 0 & 0 & 0 & 0 & 0 & 0 & 0 & 0 & 0 & -1 & 1 & 0 & 0 & 0 & 0 & 0 & 0 & 0 & 0 & C_3 \\
0 & 0 & 0 & 0 & 0 & 0 & 0 & 0 & 0 & 0 & 0 & 0 & 0 & -1 & 1 & 0 & 0 & 0 & 0 & 0 & C_4 \\
0 & 0 & 0 & 0 & 0 & 0 & 0 & 0 & 0 & 0 & 0 & 0 & 0 & 0 & 0 & 0 & 0 & -1 & 1 & 0 & C_5 \\
1 & 0 & 0 & 0 & 0 & 0 & 0 & 0 & 0 & 0 & 0 & 0 & 0 & 0 & 0 & 0 & 0 & 0 & 0 & 0 & R_1 \\
0 & 0 & 0 & -1 & 1 & 0 & 0 & 0 & 0 & 0 & 0 & 0 & 0 & 0 & 0 & 0 & 0 & 0 & 0 & 0 & R_2 \\
0 & 0 & 0 & 0 & -1 & 1 & 0 & 0 & 0 & 0 & 0 & 0 & 0 & 1 & 0 & 0 & 0 & 0 & 0 & 0 & R_3 \\
0 & 0 & 0 & 0 & 0 & 0 & 0 & 0 & -1 & 1 & 0 & 0 & 0 & 0 & 0 & 0 & 0 & 0 & 0 & 0 & R_4 \\
0 & 0 & 0 & 0 & 0 & 0 & 0 & 0 & 0 & -1 & 1 & 0 & 0 & 0 & 0 & 0 & 0 & 0 & 0 & 0 & R_5 \\
0 & 0 & 0 & 0 & 0 & 0 & 0 & 0 & 0 & 0 & 0 & -1 & 1 & 0 & 0 & 0 & 0 & 0 & 0 & -1 & R_6 \\
0 & 0 & 0 & 0 & 0 & 0 & 0 & 0 & 0 & 0 & 0 & 0 & 0 & 0 & 0 & -1 & 0 & 0 & 0 & 0 & R_7 \\
0 & 0 & 0 & 0 & 0 & 0 & 0 & 0 & 0 & 0 & 0 & 0 & 0 & 0 & 0 & 0 & -1 & 1 & 0 & 0 & R_8 \\
0 & 0 & 0 & 0 & 0 & 0 & 0 & 0 & 0 & 0 & 0 & 0 & 0 & 0 & 0 & 0 & 0 & 0 & -1 & 1 & O_1
\end{array} \tag{5.12}$$

5.6.2 *Model Validation*

The parameters in table 5.1 are used for model validation of the presented model, [96].

Table 5.1: Airway dimensions and branch parameters in generations of the conductive zone. [96]

Generation number	d^a_{bnmax} (mm)	I_{bn} (mm)	k_{bn} (sl)	γ_{1bn} (CmH_2O)	γ_{2bn} (CmH_2O)	γ_{3bn} (CmH_2O)
1	14.1	47.6	10.68	5.567	6080	64.03
2	9.58	19.0	12.15	25.77	2527	28.58
3	6.47	7.60	13.79	33.59	1351	16.90
4	5.20	12.7	6.767	46.34	835.8	11.25
5	4.04	10.7	4.819	52.01	534.5	7.738
6	3.23	9.00	3.323	58.52	370.2	5.737
7	2.66	7.60	2.162	58.72	263/7	4.564
8	2.15	6.40	1.272	59.90	192.9	3.749
9	1.78	5.40	0.585	59.90	192.9	3.749
10	1.50	4.60	0.047	59.90	192.9	3.749
11	1.26	3.90	0	59.90	192.9	3.749
12	1.10	3.30	0	59.90	192.9	3.749
13	0.95	2.70	0	59.90	192.9	3.749
14	0.85	2.30	0	59.90	192.9	3.749
15	0.76	2.00	0	59.90	192.9	3.749
16	0.69	1.65	0	59.90	192.9	3.749

5.6.3 *Simulation results*

The proposed model was tested using various patients' datasets obtained with various participants in the experimental study. The curve of the normal participant showed the same behaviour as the inspiration – expiration curves obtained during the experimental study. The curves with the participant with mild constriction had changing compliance values fit to the estimated data sets. There is continuously changing lung dynamics which explains the difference in the curves. The simulated results are shown in figure 5.8 and 5.9.

5.6.3.1 *Interpretation of the graphs*

The green line and blue line represent the trials with varying simulated parameters. The pink line shows the trend of the theoretical values.

5.7 EXPERIMENTAL STUDY

Considering the successful formulation of the Port Hamiltonian model of the human respiratory system, an experiment was set up to illustrate the lung function results and bench mark the physical performance of the proposed Port Hamiltonian model. The experiment

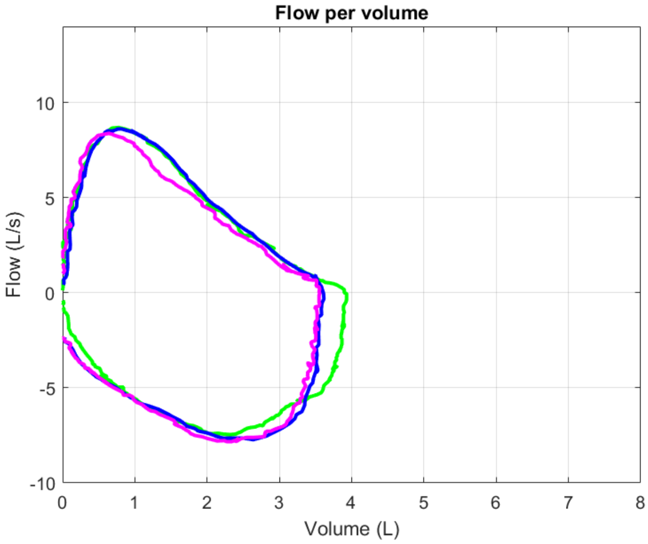

Figure 5.8: Flow per volume breathing profile of a normal participant

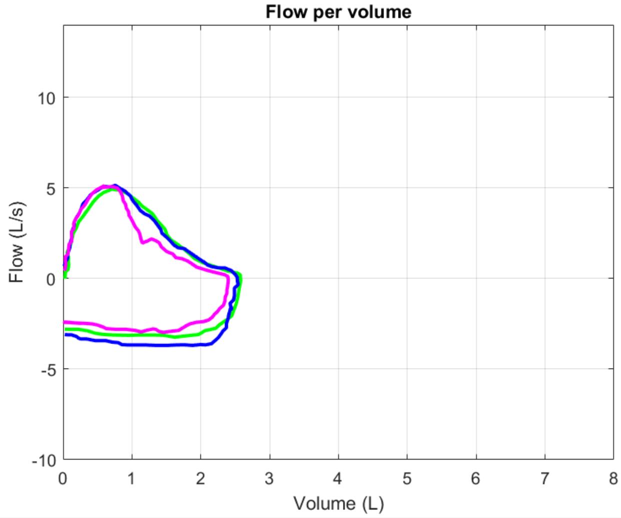

Figure 5.9: Flow per volume breathing Profile of a participant with a constriction

is performed on adult participants and the resultant curves demonstrate their lung performance. The experimental study was conducted at the University of the Witwatersrand, Faculty of Health Sciences, School of Physiology, in the Human Nutrition Laboratory. All procedures contributing to this work complied with the relevant national institutional guidelines for research on human subjects and adhered to the Helsinki Declaration of 1975 revised in 2008. Permission to conduct the study at the laboratory was obtained from the head of the department. Furthermore, approval was obtained from the University of the Witwatersrand research ethics committee and an ethical clearance certificate was obtained prior to the commencement of the experimental study.

In these section a brief description of the experimental set up is provided, the limitations and the results of the experimental results.

5.7.1 *Experimental Setup*

For static and dynamic flow volumes, the normal spirometry tests were conducted and to determine flow volume loops, the flow meter, Winspiro was used. Figure 5.10, shows the experimental set up and 5.11 is the cup like breathing mask that the participants inhale and exhale through.

Figure 5.10: Experimental Set up

5.7.1.1 *Interpretation of the graphs*

The green line shows the trend of the BEST PRE trials of the selected parameter on the left side of the graph. The pink line shows the trend of the theoretical values for the selected parameter on the left side of the graph. The blue line is also one of the pretrials.

Figure 5.11: Cup like breathing Mask

5.7.2 *Description and Limitations*

The spirometer is a piece of equipment that is used to measure the functioning of the human lungs by measuring airflow into and out of the human lungs. It is commonly used in the diagnosis of asthma, COPD, restrictive lung diseases and any other lung disorders.

5.7.3 *Experimental Procedure*

The following procedure was followed for the experimentation on the dynamic flow of air into and out of the lung by participants:

- The participant sat on a chair in the laboratory.
- A clip was placed on the participants nose to keep both nostrils closed.
- A cup-like breathing mask was placed around the participant's mouth.
- The participant was instructed to take a deep breath in, and to hold their breath for a few seconds, and then exhale as hard as they can into the breathing mask.
- The tests were repeated at least three times to make sure that the results were consistent. The highest value from three close test readings was considered the result.

The following are the limitations of the experimental set up:

- The ability to obtain correct results is dependent on the participant being able to clearly take the instructions.

5.7.4 *Experimental Results*

5.7.4.1 *Interpretation of the graphs*

The green line shows the trend of the BEST PRE trials of the selected parameter on the left side of the graph. The green dot on the graph shows the values of the BEST post trials (if

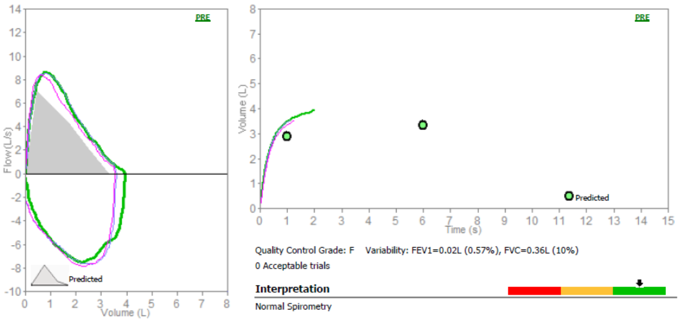

Figure 5.12: Breathing Profile of a Normal Participant

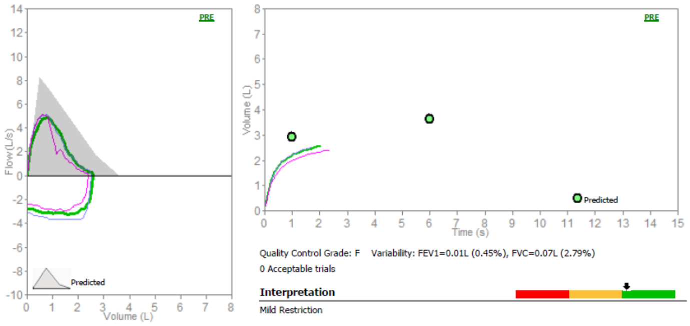

Figure 5.13: Breathing Profile of a Participant with Mild restriction

detected) The pink line shows the trend of the theoretical values for the selected parameter on the left side of the graph.

5.7.5 *Discussion of Experimental results*

The obtained experimental results also show the FVC which gives the maximum possible exhalation of the patient after the patient has inhaled maximally. FEV1 which is the first second exhalation volume and the PEF which refers to the Peak Expiratory Flow or the speed of the airflow when the participant is exhaling. The simulated results follow the same pattern as the experimental results. The normal graph, there is a linearity in the expiratory limb. The inspiratory limb loop is convex and symmetric. In the graph that shows a patient with mild restriction, the loop has a narrowing shape which is an indication of the diminished lung volumes. The upsurge in elastic recoil of the lungs sustains or ensures the airways are open. In the mild constriction case, the airflow is greater than the normal graph at Comparable Lung volumes.

5.7.6 *Reflection on the Contribution for the chapter*

The contribution in this chapter is the expansion of the research work conducted in the previous chapter on the formulation of a human respiratory system model. In this chapter, the previously lumped resistors are now broken further using distributed resistors, the model also includes the modeling of the alveoli. The Port Hamiltonian modeling approach provides a unified energy modelling of the system which is useful for the stability studies of the human respiratory system. The current model captures the structure and dissipation of the system and is easily scalable.

5.8 CONCLUSION

A detailed model of the human respiratory system which includes the alveoli has been presented. The incidence matrix of a directed graph has been used to define the Dirac structure known as the vertex edge Dirac structure. The presented model can be used in pressure analysis for COPD patients and also in the design of robust controllers for the mechanical ventilator used to ventilate these patients. The sections to follow present a detailed model of the mechanical ventilator, followed by a multiphysics model of the human respiratory system which includes the action of the diaphragm. A generalized approach to modeling the fluid flow in the mechanical ventilator and the respiratory system would provide more insights into the pressure analysis in the alveoli and it is also presented in the coming chapters.

6

A MIXED FINITE/INFINITE DIMENSIONAL PORT-HAMILTONIAN MODEL OF A MECHANICAL VENTILATOR

6.1 SUMMARY

In chapters 4 and 5, the mechanical ventilator has been assumed to be a single pressure or voltage source. While this is true and sufficient in capturing the details of the applications presented in chapters 4 and 5, the mechanical ventilator in actual sense is more intricate and detailed in its structure and function. This chapter presents a detailed model of a mechanical ventilator system. This is followed by a formulation of a multi-physics, multi-scale port Hamiltonian model of the human respiratory system. The two systems are integrated to provide the overall detailed model of the Mechanical ventilator human respiratory system model.

6.2 INTRODUCTION

The World Health Organization (WHO) has "access to oxygen" on its model list as one of the essentials required by an individual, especially when they are in a critical condition health-wise and they are unable to breathe on their own. Access to oxygen is the only medicine listed that does not have a substitute. Access to oxygen even after the worldwide pandemic is still a major dilemma in middle and low-income countries [102]. A mechanical ventilator is a medical device that is employed in assisting patients in cases where their respiratory system is not functioning well, thus the patient has challenges in breathing or has shortness of breath. The mechanical ventilator can also be used in cases where a patient has been sedated and is undergoing surgery.

The basic operation of a mechanical ventilator is to control a high-pressure region during the inspiration stage. In the inspiration stage, the mechanical ventilator is paused. During expiration, air flows out due to the lung's natural recoil which creates a higher pressure in the alveoli. Due to the high demand for mechanical ventilators both in the past and at present, it is imperative that efficient and affordable mechanical ventilators should be researched, modelled, designed and implemented. To ensure that robust mechanical ventilators are designed, it is important to formulate new models that can be used in the research and testing stages of the mechanical ventilators.

6.3 MODELING OF MECHANICAL VENTILATORS

Tran et al, [49], conducted research whose main goal was to design, control, model, and simulate a mechanical ventilator that is light in weight, portable, and suitable for use at home. [49], modelled the mechanical ventilator as a voltage source. El-Hadj et al [103], applied the fluid-structure Interaction (FSI) to a couple of computational fluid dynamics used for fluid flow with finite element analysis for the solid domain. This facilitated the investigation of fluid behaviour, structural behavior, and interactions. Two designs were proposed for the mechanical ventilator. The first design was reported to be uncontrollable and the second design considers Computational Fluid Dynamics (CDF) with a moving boundary which is applied to the piston cylinder based ventilator. Tharton et al [51], designed and developed a ventilator prototype to be used by professionals in medical emergencies and in any other context where the regular ventilator is not available. The mechanical ventilator was modelled using the crank rocker mechanism in order to meet specific requirements for mechanical ventilator design. Pivk et al, [52], developed an empirical model for a low-cost mechanical ventilator by observing the response of each of the ventilator subsystems. The current progress made globally in the development of affordable and effective designs is important. However, research in mechanical ventilator development lacks model development. The Port-Hamiltonian approach applied in this research work acts as a modelling template for future energy-based mechanical ventilator modelling and design. It is important to develop designs that rest on a solid understanding of a significant aspect of the design. Naggar, [53] developed a piecewise model of a mechanical ventilator which described the artificial behaviour of a mechanical ventilator. A pressure-controlled ventilator is created and simulated. The mechanical ventilator is modelled using a periodic function with inequalities to control the beginning of inspiration and expiration periods. Shi et al, [54] developed a mathematical model of volume-controlled mechanical ventilation. The model is viewed as a pneumatic system where the ventilator is regarded as an air compressor. The exhalation valve is considered as throttle. The compressor and the container represent the ventilator. Naggar et al, [55] proposed an integrated mathematical model of the mechanical ventilator and the lung. Linear quadratic and exponential equations were used to model the system. The integrated model was used to simulate volume-controlled artificial ventilation. Giri et al, [56], proposed a simplified design of a mechanical ventilator, to reduce cost and automate the mechanical ventilation process. The proposed design was simulated on the MATLAB platform. Hannon et al, [57] presented a review on the advancement in the modelling of human anatomy, physiology and pathophysiology via mathematical modelling and computer simulation. Clinical applications in various disease states were emphasized. The research work discussed the current limitations and potential of in-silico modelling. There are currently no existing Port Hamiltonian models of mechanical ventilators.

Contribution 6.3.1

This section presents a two-fold contribution.

- Firstly, the development of a Port-Hamiltonian model representation of a mechanical ventilator. The model consists of electromechanical and electromagnetic components modelled in the finite-dimensional representation, interconnected with fluid components in the infinite-dimensional representation. As a result, this Port-Hamiltonian model is of a mixed finite/infinite dimensional nature.
- Secondly, formulation of a multi-physics and multi-scale Port Hamiltonian model of the human respiratory system. The formulated Port Hamiltonian ventilator and the detailed respiratory system are interconnected to form a detailed integrated system that can be used for various applications for instance investigation of the response to air pressure stimuli of the various segments of the respiratory system for a ventilated patient.

6.4 DETAILED PORT-HAMILTONIAN MODEL OF A MECHANICAL VENTILATOR

The mathematical preliminaries and background for this chapter have already been provided in Chapter 3.

6.4.1 *Description of the system*

The overall mechanical ventilator system diagram is provided in figure 6.1. The entire system consists of various subsystems. In this research work, the main subsystem that contributes to the flow of air and consequently the air pressure are discussed. Therefore, the following main subsystems will be discussed: the DC Motor subsystem, Turbine pump/blower subsystem, Pump-shaft/impeller subsystem and Solenoid valve subsystem,

6.4.2 *Blower model*

In this section, the dynamical system model equations for the blower model are presented in the port-Hamiltonian framework. The blower model comprises three sub-systems, namely a DC Motor which drives the blower-shaft/impeller, a blower-shaft/impeller that couples the DC motor to the fluid, using the rotational motion of the motor to accelerate the fluid and finally the fluid being driven.

In the Port-Hamiltonian perspective, the state vector $\mathcal{X}_b \in \mathbb{R}^4$, given by

$$\mathcal{X}_b := \begin{bmatrix} p_m, & \phi_m, & P_b, & Q_b \end{bmatrix}^\top \tag{6.1}$$

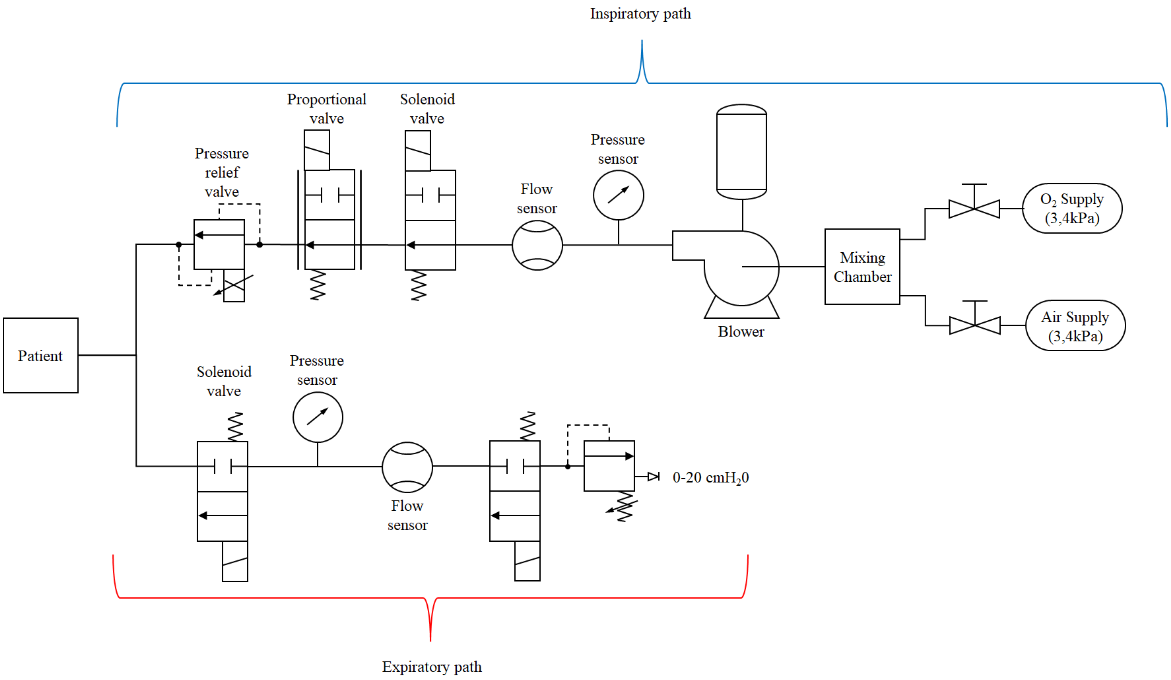

Figure 6.1: Schematic diagram of a Mechanical Ventilator

where $p_m \in \mathbb{R}^1$ and $\phi_m \in \mathbb{R}^1$ are the angular momentum and magnetic flux of the DC motor, respectively, while $P_b \in \mathbb{R}^1$ and $Q_b \in \mathbb{R}^1$ are the pressure and flow rate of the blower.

The total energy of the blower is given by the Hamiltonian

$$\mathcal{H}_b\left[\mathcal{X}_b\right] = \frac{1}{2}\left(\frac{p_m^2}{I_m} + \frac{\phi_m^2}{L_m} + C_b P_b^2 + I_b Q_b^2\right) \tag{6.2}$$

where $I_m \in \mathbb{R}^1_+$ is the inertia and $L_m \in \mathbb{R}^1_+$ is the inductance of the DC motor, while $C_b \in \mathbb{R}^1_+$ and $I_b \in \mathbb{R}^1_+$ is the hydraulic capacitance and inertance of the air in the blower, respectively.

Thus, the Port-Hamiltonian model of a blower is given by

$$\dot{\mathcal{X}}_b = \left(\mathcal{J}_b - \mathcal{R}_b\right)\nabla\mathcal{H}_b\left[\mathcal{X}_b\right] + \mathcal{G}_b u_b \tag{6.3}$$

$$\mathcal{Y}_b = \mathcal{G}_b^* \nabla\mathcal{H}_b\left[\mathcal{X}_b\right] \tag{6.4}$$

where

$$\begin{aligned}
\mathcal{J}_b &:= \begin{bmatrix} 0 & K_m & 0 & -(K_o p_m)/I_m \\ -K_m & 0 & 0 & 0 \\ 0 & 0 & 0 & 1/(C_b I_b) \\ (K_o p_m)/I_m & 0 & -1/(C_b I_b) & 0 \end{bmatrix} \in \mathbb{R}^{4\times 4} \\
\mathcal{R}_b &:= \operatorname{diag}\left(\begin{bmatrix} b_m & R_m & 0 & (R_b p_m)/(I_b I_m) \end{bmatrix}\right) \in \mathbb{R}^{4\times 4} \\
\nabla \mathcal{H}_b\left[\mathcal{X}_b\right] &:= \begin{bmatrix} p_m/I_m & \phi_m/L_m & C_b P_b & I_b Q_b \end{bmatrix} \in \mathbb{R}^{4\times 1} \\
\mathcal{G}_b &:= \begin{bmatrix} 1 & 0 & 0 \\ 0 & 0 & 0 \\ 0 & -(1/C_b) & 0 \\ 0 & 0 & (1/I_b) \end{bmatrix} \in \mathbb{R}^{4\times 3} \\
u_b &:= \begin{bmatrix} V_m & Q_{in} & P_{in} \end{bmatrix} \in \mathbb{R}^{3\times 1}
\end{aligned}$$

where $K_m \in \mathbb{R}^1_+$ is the motor torque constant, $b_m \in \mathbb{R}^1_+$ is the viscous damping, $R_m \in \mathbb{R}^1_+$ is the armature resistance and $K_o \in \mathbb{R}^1_+$ is the motor angular momentum/pressure coupling constant. The inputs to the system are the DC motor voltage, the input volumetric flow rate and pressure given by $V \in \mathbb{R}^1$, $Q_{in} \in \mathbb{R}^1$ and $P_{in} \in \mathbb{R}^1$. One can easily show that $\mathcal{J}_m = -\mathcal{J}_m^\top$ and $\mathcal{R}_m = \mathcal{R}_m^\top \succeq 0$.

Taking the time derivative of the Hamiltonian

$$\dot{\mathcal{H}}_b[\chi_b] = u_b \cdot \mathcal{Y}_b - \nabla \mathcal{H}_b[\mathcal{X}_b] \cdot (\mathcal{R}_b \nabla \mathcal{H}_b[\mathcal{X}_b]) \tag{6.5}$$

This system has power and resistive ports.

6.5 SOLENOID VALVE SUBSYSTEM

Figure 6.2 shows a solenoid valve in the open and closed position. It is assumed that the air gaps are sufficiently small such that the effect of fringing of the magnetic flux is negligible. Consider a solenoid in which the permeability of the core and the length of the part of the magnetic circuit inside the core are denoted by $\mu_c \in \mathbb{R}^1_+$ and $l_c \in \mathbb{R}^1_+$, respectively. The equivalent length of the solenoid's magnetic circuit, $l_{eq}\left[\cdot\right] : \mathbb{R} \to \mathbb{R}$ is dependent on the displacement of the spool, $q_s \in \mathbb{R}$, and can be written as

$$l_{eq}\left[q_s\right] = l_c + \frac{\mu_c}{\mu_0}(q_{s_{\text{tot}}} - q_s) \tag{6.6}$$

where $\mu_0 \in \mathbb{R}^1_+$ are the permeability of air and $q_{s_{\text{tot}}} \in \mathbb{R}^1_+$ is the total air-gap. The solenoid coordinate systems is represented in Figure 6.3. Thus, the inductance of the solenoid varies

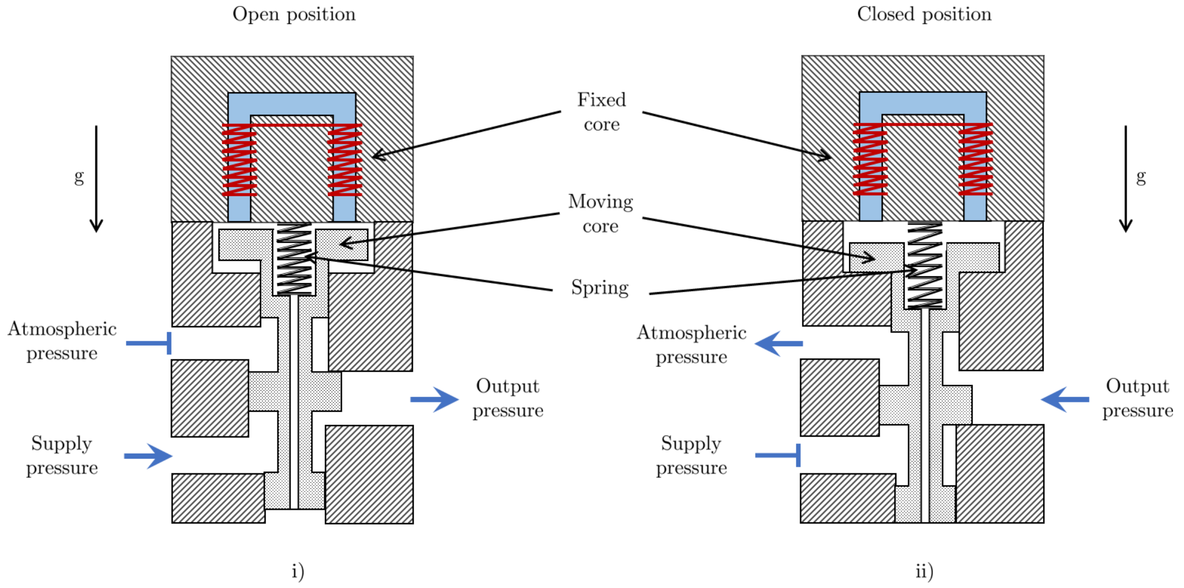

i) ii)

Figure 6.2: Diagram of a Solenoid valve in the i) open position which allows fluid flow and ii) closed position which stops fluid flow

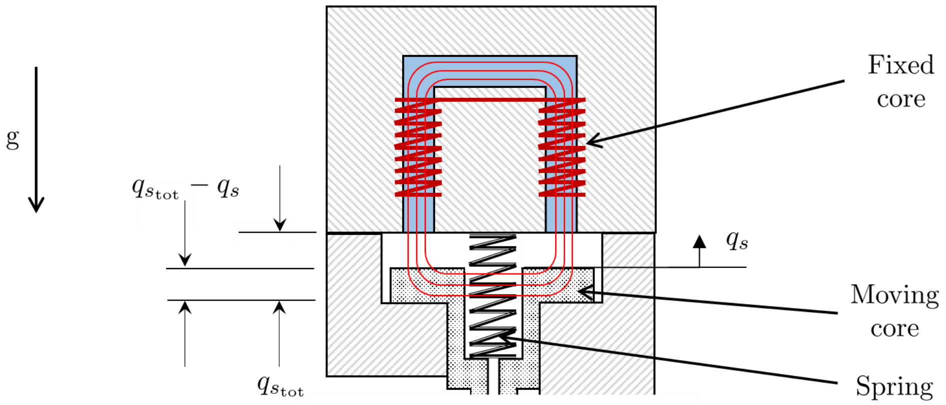

Figure 6.3: Solenoid coordinate system

with displacement of the spool and hence can be expressed by the function $L_s\left[\cdot\right] : \mathbb{R} \to \mathbb{R}$ given by

$$L_s\left[q_s\right] = \frac{N^2 A_e \mu_c}{l_{eq}\left[q_s\right]} \tag{6.7}$$

where $N \in \mathbb{R}^1_+$ is the number of turns in the coil of the solenoid and $A_e \in \mathbb{R}^1_+$ is the effective cross-sectional area of the path of the magnetic flux. The magnetic and mechanical subsystems in the solenoid valve are therefore coupled magnetically due to the dependence of the inductance on the displacement of the spool.

The total energy of the solenoid is given by the Hamiltonian, $\mathcal{H}_s\left[\cdot\right] : \mathbb{R}^3 \to \mathbb{R}$, which is a function of the state vector $\mathcal{X}_s = \begin{bmatrix}\phi_s, & p_s, & q_s\end{bmatrix}^\top \in \mathbb{R}^3$, expressed as the sum of the magnetic, kinetic and potential energies denoted by $\mathcal{H}_{\text{magnetic}}\left[\phi_s, q_s\right] : \mathbb{R}^2 \rightarrow \mathbb{R}$, $\mathcal{H}_{\text{kinetic}}\left[p_s\right] : \mathbb{R} \rightarrow \mathbb{R}$ and $\mathcal{H}_{\text{potential}}\left[q_s\right] : \mathbb{R} \rightarrow \mathbb{R}$, respectively. Thus

$$\mathcal{H}_s\left[\mathcal{X}_s\right] = \mathcal{H}_{\text{magnetic}}\left[\phi_s, q_s\right] + \mathcal{H}_{\text{kinetic}}\left[p_s\right] + \mathcal{H}_{\text{potential}}\left[q_s\right] \tag{6.8}$$

given a magnetic flux $\phi_s \in \mathbb{R}$.

Assuming that the pretension of the spring is set to $q_0 \in \mathbb{R}$, the Hamiltonian is

$$\mathcal{H}_s\left[\mathcal{X}_s\right] = \frac{1}{2}\left(\frac{\phi_s^2}{L[q_s]} + \frac{p_s^2}{m_s} + k_s(q_s + q_{s_0})^2\right) + m_s q_s g \tag{6.9}$$

where $p_s \in \mathbb{R}$ is the momentum of the spool, $m_s \in \mathbb{R}^1_+$ is the mass of the spool, $k_s \in \mathbb{R}^1_+$ is the spring stiffness and $g \in \mathbb{R}^1_+$ is the acceleration due to gravity.

Hence, the solenoid's state and output dynamics are expressed in Port-Hamiltonian form in equations 6.10 and 6.11 respectively

$$\begin{aligned} \dot{\mathcal{X}}_s &= \left(\mathcal{J}_s - \mathcal{R}_s\right)\nabla\mathcal{H}_s\left[\mathcal{X}_s\right] + \mathcal{G}_s u_s & (6.10)\\ \mathcal{Y}_s &= \mathcal{G}_s^* u_s & (6.11) \end{aligned}$$

where

$$\begin{aligned} \mathcal{J}_s &= \begin{bmatrix} 0 & 0 & 0 \\ 0 & 0 & -1 \\ 0 & 1 & 0 \end{bmatrix}, \quad \mathcal{R}_s = \begin{bmatrix} R_s & 0 & 0 \\ 0 & b_s & 0 \\ 0 & 0 & 0 \end{bmatrix}, \quad \mathcal{G}_s = \begin{bmatrix} 1 & 0 & \\ 0 & 0 & 0 \\ 0 & (A_{s_1} - A_{s_2}) & (A_{s_3} - A_{s_4}) \end{bmatrix}, \\ \mathcal{G}_s^* &= \mathcal{G}_s^\top, \quad u_s = \begin{bmatrix} V_s \\ p_s \end{bmatrix} \quad \text{and} \quad \nabla\mathcal{H}_s\left[\mathcal{X}_s\right] = \begin{bmatrix} \frac{\phi_s}{A_e N^2 \mu_c}\left(l_c - \frac{\mu_c(q_s - q_{s_{\text{tot}}})}{\mu_0}\right) \\ \frac{p_s}{m_s} \\ \frac{A_e N^2 \mu_c^2 \mu_0}{\left(\mu_0 l_c - \mu_c(q_s - q_{s_{\text{tot}}})\right)^2} + k_s(q_s + q_{s_0}) + m_s g \end{bmatrix} \end{aligned}$$

where $R_s \in \mathbb{R}^1_+$ is the resistance of the coil, $b_s \in \mathbb{R}^1_+$ is the viscous damping acting on the spool and ∇ is the gradient operator. $A_{s_1}, A_{s_2} \in \mathbb{R}^1_+$ are the various cross-sectional areas of the lands of the spool and the input vector $u_s \in \mathbb{R}^2$ consists of the input voltage $V_s \in \mathbb{R}^1$ and the supply pressure $p_s \in \mathbb{R}^1$. It can be seen that $\mathcal{J}_s = -\mathcal{J}_s^\top \in \mathbb{R}^{3\times3}$ possesses skew-symmetry, while $\mathcal{R}_s = \mathcal{R}_s^\top \in \mathbb{R}^{3\times3}$ is positive semi-definite.

Taking the time derivative of the Hamiltonian

$$\dot{\mathcal{H}}_s[\chi_s] = u_s \cdot \mathcal{Y}_s - \nabla\mathcal{H}_s[\mathcal{X}_s] \cdot (\mathcal{R}_s \nabla\mathcal{H}_s[\mathcal{X}_s]) \tag{6.12}$$

This system has power and resistive ports.

6.5.1 *Pipe model*

In this section, a port-Hamiltonian model of a single pipe segment is developed. The basis of these developments is the Navier Stokes equations for one-dimensional non-stationary flow of gas in a pipe. The following assumptions are taken for the sake of model simplification [104], [105]:

1. The pipe is taken as rigid (it does not expand in cross-section as a result of fluid flow).
2. Frictional and gravitational effects are neglected (this will be relaxed in future works in this research area),
3. The model parameters of the gas remain constant along the pipe cross-section but vary in time along the pipe length. Thus they can be averaged about the cross-section and thus the gas flow is one-dimensional.
4. The temperatures of the pipe walls are assumed to be constant and equal to the ambient room temperature. Hence temperature effects are ignored.

Taking into account these assumptions, the coordinate system attached to a segment of pipe is illustrated in figure 6.4. Thus, for a given time interval $t_s \leq t < t_f$ with start time t_s and finish time t_f, the length normalized one-dimensional Euler equations for gas of density $\rho(t,z) : (t_s, t_f] \times (0, \ell) \to \mathbb{R}^1$ flowing at a velocity $v(t,z) : (t_s, t_f] \times (0, \ell) \to \mathbb{R}^1$ through a pipe of length $\ell \in \mathbb{R}^1_+$ and cross-sectional area $A_p \in \mathbb{R}^1_+$ are given by:

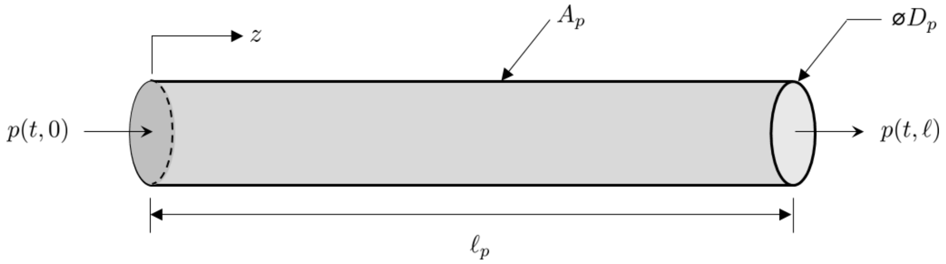

Figure 6.4: Pipe segment coordinate system

$$\partial_t(\rho A_p) + \partial_z(\rho A_p v) = 0 \tag{6.13a}$$

$$\partial_t(\rho A_p v) + \partial_z(\rho A_p v^2 + p A_p) = 0 \tag{6.13b}$$

where $p(t,z) : (t_s, t_f] \times (0, \ell) \to \mathbb{R}^1$ is the pressure and $\partial_i := \partial/\partial_i$ is the partial derivative with respect to the temporal and spatial variables given by the subscripts $i \in \{t, z\}$.

6.5.1.1 *Port-Hamiltonian formulation of pipe-flow model*

The fluid dynamics can be written in terms of mass per unit length, i.e. $\varrho := \rho A_p$, as well as the fluid momentum, $m := \varrho v$. Thus equations 6.13a and 6.13b can be expressed as

$$\partial_t \varrho = -\partial_z m \tag{6.14a}$$

$$\partial_t m = -\partial_z \left(\frac{m^2}{\varrho} + p A_p \right) \tag{6.14b}$$

Defining the state vector of the gas flow through a pipe segment as $\chi_p := \begin{bmatrix} \varrho \\ m \end{bmatrix}$, the energy of the gas can be expressed in form of a Hamiltonian $\mathcal{H}_p \left[\chi_p\right] : \mathbb{R}^2 \to \mathbb{R}^1$ given by

$$\mathcal{H}_p \left[\chi_p\right] = \int_0^\ell H_p \left[\chi_p\right] \, \mathrm{d}x = \int_0^\ell \left(\frac{m^2}{2\varrho} + \varrho U \left[\varrho / A_p\right] \right) \, \mathrm{d}x \tag{6.15}$$

where $H_p\left[\cdot\right] : \mathbb{R}^2 \to \mathbb{R}^1$ is the Hamiltonian density and $U\left[\cdot\right] : \mathbb{R}^1 \to \mathbb{R}^1$ is the internal energy of the gas which in the case of an isentropic fluid, can be expressed as a function of density.

The port-Hamiltonian dynamics take the following form

$$\partial_t \chi_p = \mathcal{J} \left[\chi_p\right] \delta_{\chi_p} \mathcal{H}_p \left[\chi_p\right] \tag{6.16}$$

where $\mathcal{J}\left[\chi_p\right]$, the formally skew-symmetric operator and $\delta_{\chi_p} \mathcal{H}\left[\chi_p\right]$, the variational derivative of the Hamiltonian density are expressed as

$$\mathcal{J} \left[\chi_p\right] = - \begin{bmatrix} 0 & \partial_z \\ \partial_z & 0 \end{bmatrix} \quad \text{and} \quad \delta_{\chi_p} \mathcal{H}_p \left[\chi_p\right] = \begin{bmatrix} h - \frac{m^2}{2\varrho^2} \\ \frac{m}{\varrho} \end{bmatrix} \tag{6.17}$$

where h is the enthalpy, and $\mathcal{J}\left[\chi_p\right]$ is a formally skew-symmetric operator.

The rate of change of the Hamiltonian can be found as

$$\dot{\mathcal{H}}_p = \mathbf{u}_p^\top \mathbf{y}_p \tag{6.18}$$

where

$$\mathbf{u}_p = W_B R_{\text{ext}} \begin{bmatrix} \delta_{\chi_p} \mathcal{H}_p|_0 \\ \delta_{\chi_p} \mathcal{H}_p|_\ell \end{bmatrix} \quad \text{and} \quad \mathbf{y}_p = W_C R_{\text{ext}} \begin{bmatrix} \delta_{\chi_p} \mathcal{H}_p|_0 \\ \delta_{\chi_p} \mathcal{H}_p|_\ell \end{bmatrix} \tag{6.19}$$

with components given by

$$W_B = \frac{1}{\sqrt{2}} \begin{bmatrix} 1 & 0 & 0 & 1 \\ 0 & -1 & 1 & 0 \end{bmatrix}, \quad W_C = \frac{1}{\sqrt{2}} \begin{bmatrix} 0 & 1 & 1 & 0 \\ 1 & 0 & 0 & -1 \end{bmatrix}, \quad R_{\text{ext}} = \frac{1}{\sqrt{2}} \begin{bmatrix} 0 & -1 & 0 & 1 \\ -1 & 0 & 1 & 0 \\ 1 & 0 & 1 & 0 \\ 0 & 1 & 0 & 1 \end{bmatrix}$$

$$\text{and} \quad \begin{bmatrix} \delta_{\chi_p} \mathcal{H}_p|_0 \\ \delta_{\chi_p} \mathcal{H}_p|_\ell \end{bmatrix} = \begin{bmatrix} \left(h - \frac{m^2}{2\varrho^2}\right)\Big|_0 \\ \left(\frac{m}{\varrho}\right)\Big|_0 \\ \left(h - \frac{m^2}{2\varrho^2}\right)\Big|_\ell \\ \left(\frac{m}{\varrho}\right)\Big|_\ell \end{bmatrix}$$

Expanding $\mathbf{u}_p$ and $\mathbf{y}_p$

$$\mathbf{u}_p = \begin{bmatrix} \left(\frac{m}{\varrho}\right)\Big|_\ell \\ \left(h - \frac{m^2}{2\varrho^2}\right)\Big|_0 \end{bmatrix} \quad \text{and} \quad \mathbf{y}_p = \begin{bmatrix} \left(h - \frac{m^2}{2\varrho^2}\right)\Big|_\ell \\ -\left(\frac{m}{\varrho}\right)\Big|_0 \end{bmatrix} \tag{6.20}$$

Thus, the rate of change of the Hamiltonian is

$$\dot{\mathcal{H}}_p = \left(h - \frac{m^2}{2\varrho^2}\right)\Big|_\ell \left(\frac{m}{\varrho}\right)\Big|_\ell - \left(\frac{m}{\varrho}\right)\Big|_0 \left(h - \frac{m^2}{2\varrho^2}\right)\Big|_0 \tag{6.21}$$

6.5.2 *Electric Circuit Model of the Lung*

The port Hamiltonian formulation for nonlinear electric circuits is presented in this section. Since the main focus of this article is on the mechanical ventilator model, the lung model is simplified by considering an electric circuit analogy. The model under consideration is that of a fully sedated patient who relies completely on the mechanical ventilator to breathe. The circuit model is shown in Figure 6.5. The circuit can be represented in the form of a network graph using graph theory. The graph of the circuit given in Figure 6.5 is given in Figure 6.6. The model has $n = |\mathcal{V}| = 7$ vertices.

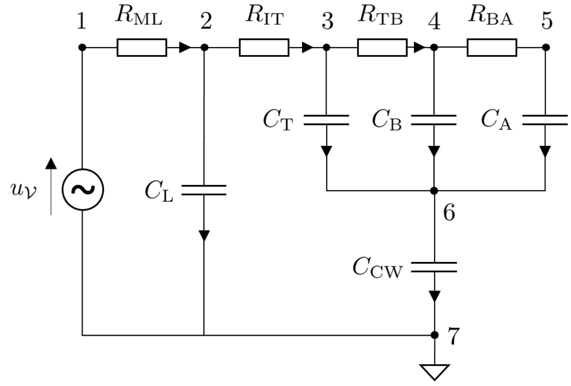

Figure 6.5: Circuit diagram of an electric model of a lung of a fully sedated patient [94]

The complete graph of the circuit, A_0, is

$$\mathcal{A}_0 = \begin{array}{cccc|ccccc|cc} R_{ML} & R_{IT} & R_{TB} & R_{BA} & C_T & C_B & C_A & C_L & C_{CW} & u_{\mathcal{V}} & \\ 1 & 0 & 0 & 0 & 0 & 0 & 0 & 0 & 0 & -1 & 1 \\ -1 & 1 & 0 & 0 & 0 & 0 & 0 & 1 & 0 & 0 & 2 \\ 0 & -1 & 1 & 0 & 1 & 0 & 0 & 0 & 0 & 0 & 3 \\ 0 & 0 & -1 & 1 & 0 & 1 & 0 & 0 & 0 & 0 & 4 \\ 0 & 0 & 0 & -1 & 0 & 0 & 1 & 0 & 0 & 0 & 5 \\ 0 & 0 & 0 & 0 & -1 & -1 & -1 & 0 & 1 & 0 & 6 \\ 0 & 0 & 0 & 0 & 0 & 0 & 0 & -1 & -1 & 1 & 7 \end{array} \tag{6.22}$$

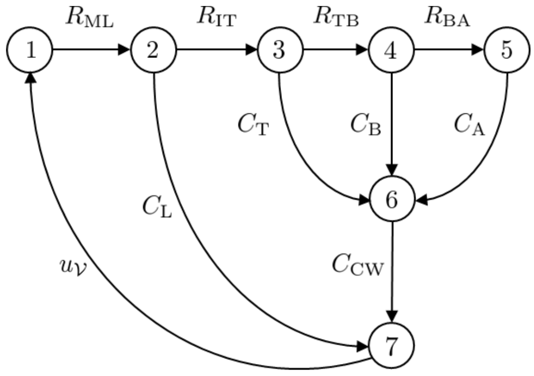

Figure 6.6: The graph associated with the circuit diagram given in Figure 6.5

The ventilator input voltage is represented as a source $\mathcal{S} = (\mathcal{D}_{\mathcal{S}}, \mathcal{L}_{\mathcal{S}}, \mathcal{R}_{\mathcal{S}})$. The set of sources is $\mathcal{S} = \{v_7\}$ and the dimension $|\mathcal{S}| = 1$ source. The circuit also consists of $m_{\mathcal{C}} = 5$ capacitors (storage elements) that are represented as $\mathcal{C}_i = (\mathcal{D}_{\mathcal{C}_i}, \mathcal{L}_{\mathcal{C}_i}, \mathcal{R}_{\mathcal{C}_i})$ where the i^{th} index is used to distinguish between the components is $i = \left\{C_{\mathrm{L}},\ C_{\mathrm{T}},\ C_{\mathrm{B}},\ C_{\mathrm{A}},\ C_{\mathrm{CW}}\right\}$. Furthermore there are $m_{\mathcal{R}} = 4$ resistors (dissipative elements) that are represented as $\mathcal{R}_i = (\mathcal{D}_{\mathcal{R}_i}, \mathcal{L}_{\mathcal{R}_i}, \mathcal{R}_{\mathcal{R}_i})$ where the i^{th} index is given by $i = \left\{R_{\mathrm{ML}},\ R_{\mathrm{IT}},\ R_{\mathrm{TB}},\ R_{\mathrm{BA}}\right\}$.

Selecting node 7 as the ground, the reduced incidence matrix, $\mathcal{A}$, is given by

$$A = \begin{bmatrix} A_{\mathcal{R}} & A_{\mathcal{C}} & A_{\mathcal{S}} \end{bmatrix} = \left(\underbrace{\begin{matrix} 1 & 0 & 0 & 0 \\ -1 & 1 & 0 & 0 \\ 0 & -1 & 1 & 0 \\ 0 & 0 & -1 & 1 \\ 0 & 0 & 0 & -1 \\ 0 & 0 & 0 & 0 \end{matrix}}_{A_{\mathcal{R}}} \middle| \underbrace{\begin{matrix} 0 & 0 & 0 & 0 & 0 \\ 0 & 0 & 0 & 1 & 0 \\ 1 & 0 & 0 & 0 & 0 \\ 0 & 1 & 0 & 0 & 0 \\ 0 & 0 & 1 & 0 & 0 \\ -1 & -1 & -1 & 0 & 1 \end{matrix}}_{A_{\mathcal{C}}} \middle| \underbrace{\begin{matrix} -1 \\ 0 \\ 0 \\ 0 \\ 0 \\ 0 \end{matrix}}_{A_{\mathcal{S}}} \right) \tag{6.23}$$

where the dimensions of the components of $\mathcal{A}$ are $\dim(A_{\mathcal{R}}) = (n - |S|) \times m_{\mathcal{R}} = 6 \times 4$, $\dim(A_{\mathcal{C}}) = (n - |S|) \times m_{\mathcal{C}} = 6 \times 5$ and $\dim(A_{\mathcal{S}}) = (n - |S|) \times m_{\mathcal{S}} = 6 \times 1$.

The total energy of the circuit is given by the Hamiltonian

$$\mathcal{H}_C = \sum_{\forall i} \mathcal{H}_{C_i}(q_{C_i}) = \frac{1}{2} \sum_{\forall i} \frac{q_{C_i}}{C_i} \tag{6.24}$$

where $q_{C_i} \in \mathbb{R}^1$ is the charge of the i^{th} capacitor for $i = \left\{C_{\mathrm{L}},\ C_{\mathrm{T}},\ C_{\mathrm{B}},\ C_{\mathrm{A}},\ C_{\mathrm{CW}}\right\}$

$$\begin{bmatrix} \mathbb{I} & A_{\mathcal{C}} & A_{\mathcal{R}} & A_{\mathcal{S}} \\ \mathbb{O} & \mathbb{O} & \mathbb{O} & \mathbb{O} \\ \mathbb{O} & \mathbb{O} & \mathbb{O} & \mathbb{O} \\ \mathbb{O} & \mathbb{O} & \mathbb{O} & \mathbb{O} \end{bmatrix} \begin{pmatrix} -\frac{d}{dt} q \\ -\frac{d}{dt} q_{\mathcal{C}} \\ -i_{\mathcal{R}} \\ -i_{\mathcal{S}} \end{pmatrix} + \begin{bmatrix} \mathbb{O} & \mathbb{O} & \mathbb{O} & \mathbb{O} \\ -A_{\mathcal{R}}^{\top} & \mathbb{O} & \mathbb{I} & \mathbb{O} \\ -A_{\mathcal{C}}^{\top} & \mathbb{I} & \mathbb{O} & \mathbb{O} \\ -A_{\mathcal{S}}^{\top} & \mathbb{O} & \mathbb{O} & \mathbb{I} \end{bmatrix} \begin{pmatrix} \phi \\ u_{\mathcal{C}} \\ u_{\mathcal{R}} \\ u_{\mathcal{S}} \end{pmatrix} = \mathbb{O} \tag{6.25}$$

where $\mathbb{I}$ and $\mathbb{O}$ are appropriately sized identity and zero matrices, respectively and $q = 0$ and ϕ is the node potential. Expanding Equation 6.25

$$A_{\mathcal{C}} \frac{d}{dt} q_{\mathcal{C}} + A_{\mathcal{R}}(A_{\mathcal{R}}^{\top}\phi) + A_{\mathcal{S}} i_{\mathcal{S}} = 0 \tag{6.26}$$

$$-A_{\mathcal{C}}^{\top}\phi + u_{\mathcal{C}} = 0 \tag{6.27}$$

$$-A_{\mathcal{S}}^{\top}\phi + u_{\mathcal{S}} = 0 \tag{6.28}$$

The Dirac structure is given by the set where $(\mathcal{D}, \mathcal{L}, \mathcal{R})$

$$\left(-\tfrac{d}{dt}q, \quad -\tfrac{d}{dt}q_{\mathcal{C}}, \quad -i_{\mathcal{R}}, \quad -i_{\mathcal{S}}, \quad \phi, \quad u_{\mathcal{C}}, \quad u_{\mathcal{R}}, \quad u_{\mathcal{S}}\right) \in \mathcal{D} \tag{6.29a}$$

$$\left(q, \quad q_{\mathcal{C}}, \quad \phi, \quad u_{\mathcal{C}}\right) \in \mathcal{L} \tag{6.29b}$$

$$\left(-i_{\mathcal{R}}, \quad e_{\mathcal{R}}\right) \in \mathcal{R} \tag{6.29c}$$

6.6 MODEL NETWORK TOPOLOGY

(Directed graph) [106] A directed graph, $\mathcal{G}$ denotes the pair $(\mathcal{V}, \mathcal{A})$, where $\mathcal{V}(\mathcal{D})$ and $\mathcal{A}(\mathcal{D})$ denote the set of vertices and arcs respectively. An arc is a distinct ordered pair of vertices.

The directed graph of a mechanical ventilator model is composed of the disjoint union of the vertices associated with the patient, as well as the inspiratory and expiratory limbs of the ventilator given by $v_O, \mathcal{V}_I$ and $\mathcal{V}_E$ respectively. Similarly, the patient, inspiratory and expiratory arcs given by $a_O, \mathcal{A}_I$ and $\mathcal{A}_E$, respectively. Each arc and vertex can further be subdivided into those associated with blowers, valves, pipes and electric circuits present in the mechanical ventilator. Thus the totality of vertices and arcs are given by

$$\mathcal{V}(\mathcal{D}) = \{v_O\} \cup \mathcal{V}_I \cup \mathcal{V}_E = \{v_O\} \cup (\mathcal{V}_{I_b} \cup \mathcal{V}_{I_v} \cup \mathcal{V}_{I_p} \cup \mathcal{V}_{I_e}) \cup (\mathcal{V}_{E_b} \cup \mathcal{V}_{E_v} \cup \mathcal{V}_{E_p} \cup \mathcal{V}_{E_e})$$

and

$$\mathcal{A}(\mathcal{D}) = \{a_O\} \cup \mathcal{A}_I \cup \mathcal{A}_E = \{a_O\} \cup (\mathcal{A}_{I_b} \cup \mathcal{A}_{I_v} \cup \mathcal{A}_{I_p} \cup \mathcal{A}_{I_e}) \cup (\mathcal{A}_{E_b} \cup \mathcal{A}_{E_v} \cup \mathcal{A}_{E_p} \cup \mathcal{A}_{E_e})$$

respectively, where the subscripts $i \in \{O, p, b, v, p, e\}$ are used to indicate the patient, blowers, valves, pipes and electric circuits components, respectively.

Figure 6.8 shows a detailed graph of the mechanical ventilator given in Figure 6.1 indicating the patient vertex $\mathcal{V}_O$, the arcs and vertices along the inspiratory path given by

$$\mathcal{A}_I := \{\mathcal{A}_{I_{V12}}, \mathcal{A}_{I_{V23}}, \mathcal{A}_{I_{V3B}}, \mathcal{A}_{I_{V23}}, \mathcal{A}_{I_{BV4}}, \mathcal{A}_{I_{V4S1}}, \mathcal{A}_{I_{BV5}}, \mathcal{A}_{I_{V5S2}}\}$$

and

$$\mathcal{V}_I := \{\mathcal{V}_{I_{V1}}, \mathcal{V}_{I_{V2}}, \mathcal{V}_{I_{V3}}, \mathcal{V}_{I_B}, \mathcal{V}_{I_{V4}}, \mathcal{V}_{I_{S1}}, \mathcal{V}_{I_{V5}}, \mathcal{V}_{I_{S2}}\}$$

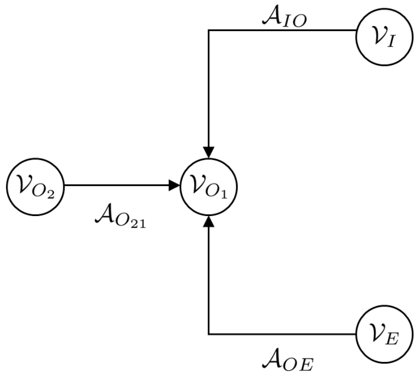

Figure 6.7: Simplified graph of the mechanical ventilator given in Figure 6.1 indicating the elements belonging to the patient, given by the arcs $\mathcal{A}_{O_{21}} \in \mathcal{A}_O$ and vertices $\{\mathcal{V}_{O_1}, \mathcal{V}_{O_2}\} \in \mathcal{V}_O$ as well as elements of the inspiratory and expiratory arcs and vertices given by and $\mathcal{V}_I, \mathcal{V}_E$ and $\mathcal{A}_{IO}, \mathcal{A}_{OE}$, respectively.

respectively, as well as the arcs and vertices along the expiratory path given by

$$\mathcal{A}_E := \{\mathcal{A}_{OE_{V1}}, \mathcal{A}_{E_{V12}}, \mathcal{A}_{E_{V23}}\} \qquad \text{and} \qquad \mathcal{V}_E := \{\mathcal{V}_{E_{V1}}, \mathcal{V}_{E_{V2}}, \mathcal{V}_{E_{V3}}\}$$

respectively.

6.7 MODEL INTERCONNECTION/COUPLING CONDITIONS

In this section, the coupling conditions of the port-Hamiltonian network model of the mechanical ventilator are given. The types of interconnections occurring in this model are given below:

1. Pump-to-pipe interconnection The pressure and flow rate of the fluid exiting the pump, P_b and Q_b respectively, are equal to the pressure and flow rate at the inlet of the pipe given by $p(0)$ and $m(0)$, respectively. Thus

$$P_b = p_0 \qquad \text{and} \qquad Q_b = m(0)$$

2. Pipe to valve interconnection The pressure and flow rate of the fluid entering/exiting a valve, P_v and Q_v respectively, are equal to the pressure and flow rate at the inlet/outlet of the pipe given by $p(0)$ and $m(0)$ for the inlet and $p(\ell)$ and $m(\ell)$. Thus

$$\begin{aligned} P_v &= p(0) \qquad \text{and} \qquad Q_v = m(0) \qquad \text{at the inlet} \\ P_v &= p(\ell) \qquad \text{and} \qquad Q_v = m(\ell) \qquad \text{at the outlet} \end{aligned}$$

3. Pipe to circuit interconnection The pressure and fluid flow-rate at the outlet of a pipe can act as inputs to a circuit model, thus

$$p(\ell) = v_{c_{\text{in}}} \qquad \text{and} \qquad m(\ell) = i_{c_{\text{in}}}$$

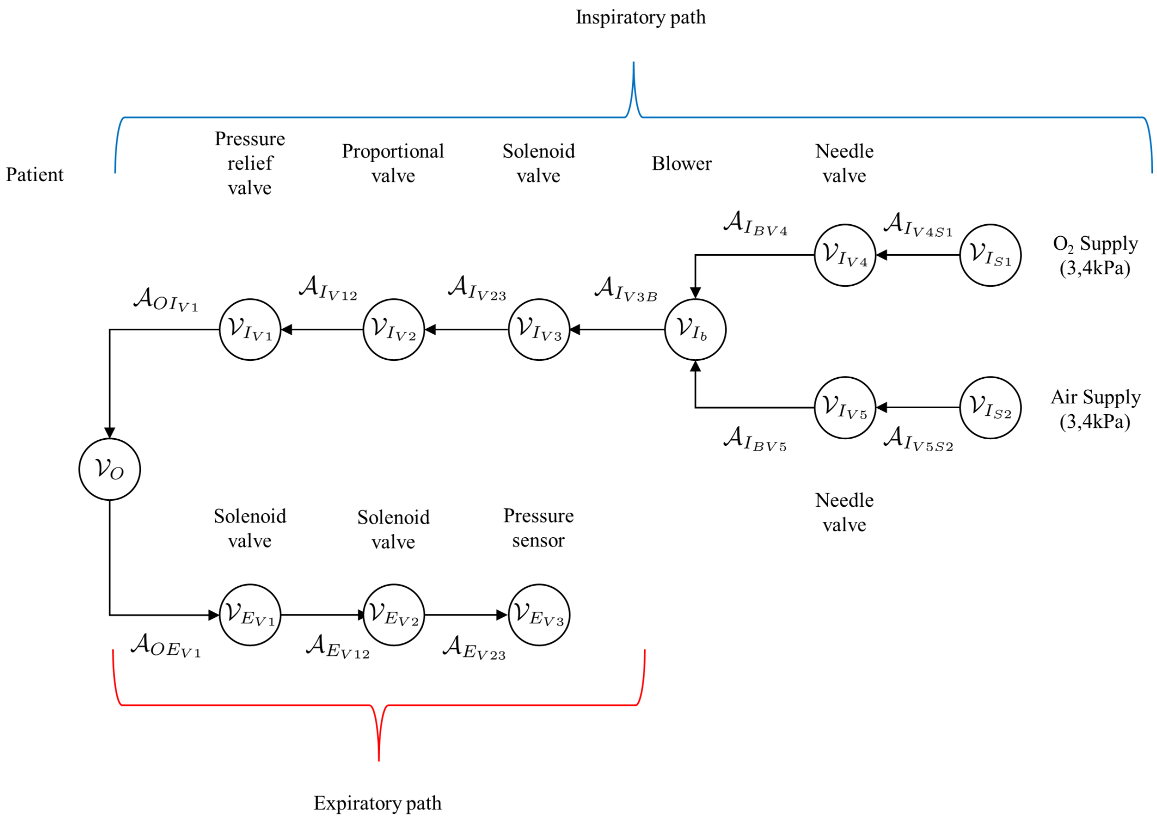

Figure 6.8: Detailed graph of the Mechanical Ventilator given in Figure 6.7 indicating the patient vertex $\mathcal{V}_O$, as well as the arcs and vertices along the inspiratory and expiratory paths.

On the other hand, the output voltage and current of a circuit can be interconnected to a fluid pipe at the inlet of the pipe. In this case, the output voltage and or current of the circuit should be equal to the inlet pressure and inlet flow rate respectively. This relation can expressed mathematically as:

$$v_{c_{out}} = p(0) \qquad \text{and} \qquad i_{c_{out}} = m(0) \qquad \text{at the inlet}$$

The Hamiltonian of the complete system is given by the sum of the Hamiltonian's of the individual systems

$$\mathcal{H} = \mathcal{H}_b + \mathcal{H}_s + \mathcal{H}_p + \mathcal{H}_\mathcal{C} \tag{6.30}$$

The rate of change of energy of the complete system is

$$\begin{aligned}\dot{\mathcal{H}} = \quad & \dot{P}_b(\partial_z p(0) + F_p) + \dot{Q}_b(\partial_z m(0) + M_p) \\ & +\dot{P}_{v_{in}}(\partial_z p(0) + F_{v_{in}}) + \dot{Q}_{v_{in}}(\partial_z m(0) + M_{v_{in}}) \\ & +\dot{P}_{v_{out}}(\partial_z p(\ell) + F_{v_{out}}) + \dot{Q}_{v_{out}}(\partial_z m(\ell) + M_{v_{out}}) \\ & +\dot{P}_{v_{out}}(\partial_z p(\ell) + F_{v_{out}}) + \dot{Q}_{v_{out}}(\partial_z m(\ell) + M_{v_{out}}) + \\ & \dot{\mathcal{H}}_b + \dot{\mathcal{H}}_s + \dot{\mathcal{H}}_c \end{aligned} \tag{6.31}$$

The terms $F_p, M_p, F_{v_{in}}, M_{v_{in}}, F_{v_{out}}$ and $M_{v_{out}}$ are the external pressure and flow rates acting on the system. They should be equal to zero to complete the interconnection.

6.8 STRUCTURE PRESERVING DISCRETIZATION

The port Hamiltonian model of the pipe is a partial differential equation, continuous in space. As such it is difficult to simulate the dynamics of a pipe section. In order to do this, it is necessary to approximate the model with a discrete model, in this case, a finite difference model which is an approximation of the original system. Within the context of port Hamiltonian systems, an additional requirement is the need to ensure that the discrete approximation maintains the structural properties of the original system e.g. skew symmetry etc. Each system state can be replaced with a discrete approximation consisting of a total on n elements as can be seen in Figure 6.9. As such, $\varrho \approx \varrho_d = \begin{bmatrix} \varrho_1, & \varrho_2, & \cdots, & \varrho_n \end{bmatrix} \in \mathbb{R}^{n\times 1}$ and $m \approx m_d = \begin{bmatrix} m_1, & m_2, & \cdots, & m_n \end{bmatrix} \in \mathbb{R}^{n\times 1}$. As such, state vector χ_p can be replaced by a discrete approximation $\chi_d = \begin{bmatrix} \varrho_1, & \cdots, & \varrho_n, & m_1, & \cdots, & m_n \end{bmatrix} \in \mathbb{R}^{2n\times 1}$. The i^{th} element of $\varrho_i, m_i \in \mathbb{R}^{1\times 1}$ is located at $z = \{\Delta(i-1), \Delta(i-1/2)\}$, where Δ is the fixed discrete step size between points and $i = 1, 2, \cdots, n$. In addition, the efforts at the boundaries are given by $\delta_{\chi_0}\mathcal{H}_0$ and $\delta_{\chi_n}\mathcal{H}_n$. Thus the Hamiltonian given in Equation 6.15 can be approximated by a discrete approximation such that $\mathcal{H}_p[\chi_p] \approx \Delta\mathcal{H}_d[\chi_d]$ so that the discrete system effort is now $\delta_{\chi_d}(\mathcal{H}_d)$. A finite difference approximation of the spatial derivatives at the i^{th} point is

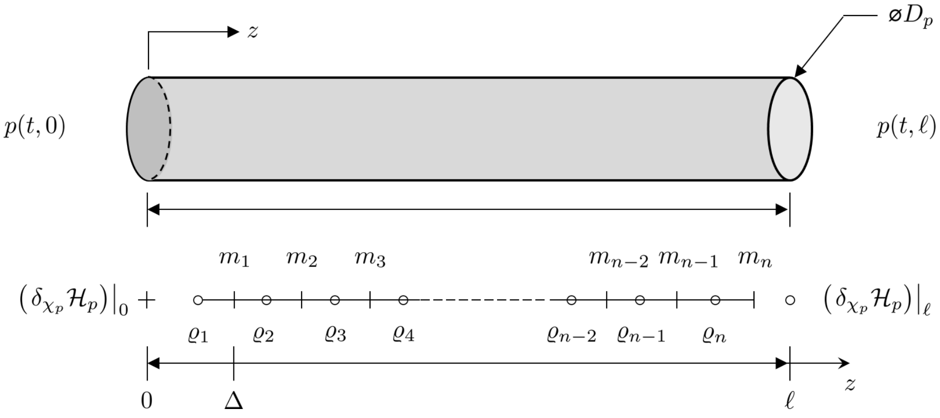

Figure 6.9: Staggered grid discretization of the one dimensional port Hamiltonian pipe dynamic model

$$\left.\frac{\partial}{\partial z}\varrho(t,z)\right|_i \approx \frac{1}{\Delta}(\varrho(t,z_{i+0.5}) - \varrho(t,z_{i-0.5})) \quad \text{and} \quad \left.\frac{\partial}{\partial z}m(t,z)\right|_i \approx \frac{1}{\Delta}(m(t,z_{i+1}) - m(t,z_i)) \tag{6.32}$$

The central difference approximation at the i^{th} point is

$$\partial_t \begin{bmatrix} \varrho_i \\ m_i \end{bmatrix} = \frac{1}{\Delta}\left(\begin{bmatrix} \delta_m\mathcal{H}[\chi_i] \\ \delta_\varrho\mathcal{H}[\chi_{i+1}] \end{bmatrix} - \begin{bmatrix} \delta_m\mathcal{H}[\chi_{i-1}] \\ \delta_\varrho\mathcal{H}[\chi_i] \end{bmatrix} \right) \tag{6.33}$$

In matrix form this is

$$
\begin{aligned}
\partial_t \varrho_d &= \frac{1}{\Delta} \begin{bmatrix} -1 & & & \\ 1 & -1 & & \\ & \ddots & \ddots & \\ & & 1 & -1 \end{bmatrix} \delta_m \mathcal{H}[\chi_d] + \frac{1}{\Delta} \begin{bmatrix} 1 \\ 0 \\ \vdots \\ 0 \end{bmatrix} \delta_m \mathcal{H}[\chi_d] \qquad (6.34) \\
\partial_t m_d &= \frac{1}{\Delta} \begin{bmatrix} 1 & -1 & & \\ & \ddots & \ddots & \\ & & 1 & -1 \\ & & & 1 \end{bmatrix} \delta_\varrho \mathcal{H}[\chi_d] + \frac{1}{\Delta} \begin{bmatrix} 0 \\ \vdots \\ 0 \\ -1 \end{bmatrix} \delta_\varrho \mathcal{H}[\chi_0] \qquad (6.35)
\end{aligned}
$$

which can be re-written as

$$
\begin{aligned}
\partial_t \varrho_d &= D \delta_m \mathcal{H}[\chi_d] + \mathcal{G}_\varrho \delta_m \mathcal{H}[\chi_0] \qquad (6.36a) \\
\partial_t m_d &= -D^\top \delta_\varrho \mathcal{H}[\chi_d] + \mathcal{G}_m \delta_\varrho \mathcal{H}[\chi_n] \qquad (6.36b)
\end{aligned}
$$

where

$$
D = \frac{1}{\Delta} \begin{bmatrix} -1 & & & \\ 1 & -1 & & \\ & \ddots & \ddots & \\ & & 1 & -1 \end{bmatrix}, \qquad \mathcal{G}_\varrho = \frac{1}{\Delta} \begin{bmatrix} 1 \\ 0 \\ \vdots \\ 0 \end{bmatrix} \qquad \text{and} \qquad \mathcal{G}_m = \frac{1}{\Delta} \begin{bmatrix} 0 \\ \vdots \\ 0 \\ -1 \end{bmatrix}
$$

The skew-symmetric operator is clear from Equation 6.36.

$$
\begin{bmatrix} \partial_t \varrho_d \\ \partial_t m_d \end{bmatrix} = \begin{bmatrix} & D \\ -D^\top & \end{bmatrix} \begin{bmatrix} \delta_\varrho \mathcal{H}[\chi_d] \\ \delta_m \mathcal{H}[\chi_d] \end{bmatrix} + \begin{bmatrix} & \mathcal{G}_m \\ \mathcal{G}_\varrho & \end{bmatrix} \begin{bmatrix} \delta_\varrho \mathcal{H}[\chi_0] \\ \delta_m \mathcal{H}[\chi_n] \end{bmatrix} \qquad (6.37)
$$

6.9 NUMERICAL SIMULATION RESULTS AND DISCUSSION

The pipe and solenoid valve model parameters used in this work are given in Tables 6.1 and 6.2, respectively.

Table 6.1: Pipe model parameters values.

Parameter	**Description**	**Value**	**Units**
A_p	Pipe cross-sectional area	3.8013×10^{-4}	m^2
D_p	Pipe diameter	2.2×10^{-3}	m
ℓ	Pipe length	1.5×10^{-1}	m

Table 6.2: Solenoid model parameters values [107].

Parameter	**Description**	**Value**	**Units**
A_e	Effective cross-sectional area	8×10^{-5}	m^2
A_{s_1}	Spool land area	2.657×10^{-3}	m^2
A_{s_2}	Spool land area	3.525×10^{-3}	m^2
A_{s_3}	Spool land area	5.586×10^{-3}	m^2
A_{s_4}	Spool land area	5.586×10^{-3}	m^2
b_s	Viscous damping factor	2×10^{-1}	$Ns \cdot m$
g	Acceleration due to gravity	9.81	$m \cdot s^{-2}$
k_s	Spring stiffness	1×10^{-4}	$N \cdot m^{-1}$
l_c	Length of the part of the magnetic circuit inside the core	1.15×10^{-2}	m
m_s	Mass of the spool	2.7×10^{-1}	kg
N	Number of turns in the coil	1250	turns
$q_{s_{\text{tot}}}$	Total air-gap	3.3×10^{-4}	m
q_{s_0}	Pre-tension in the spring	1.1×10^{-3}	m
R_s	Resistance of the coil	13	Ω
μ_0	Permeability of air	$4\pi \times 10^{-7}$	$N \cdot A^{-2}$
μ_c	Permeability of the magnetic core	$4.8\pi \times 10^{-5}$	$N \cdot A^{-2}$

Table 6.3: Lung circuit model parameters values [94].

Parameter	**Description**	**Value**	**Units**
R_{ML}	Resistance of the Mouth to Larynx	1.021	$\mathrm{cmH_2O} \cdot s \cdot \mathrm{l}^{-1}$
R_{LT}	Resistance of the Larynx to Trachea	3.369×10^{-1}	$\mathrm{cmH_2O} \cdot s \cdot \mathrm{l}^{-1}$
R_{TB}	Resistance of the Trachea to Bronchi	3.063×10^{-1}	$\mathrm{cmH_2O} \cdot s \cdot \mathrm{l}^{-1}$
R_{BA}	Resistance of the Bronchi to Alveoli	8.17×10^{-2}	$\mathrm{cmH_2O} \cdot s \cdot \mathrm{l}^{-1}$
C_{L}	Compliance of the Larynx	1.27×10^{-3}	$\mathrm{l/cmH_2O}$
C_{T}	Compliance of the Trachea	2.38×10^{-3}	$\mathrm{l/cmH_2O}$
C_{B}	Compliance of the Bronchi	1.31×10^{-2}	$\mathrm{l/cmH_2O}$
C_{A}	Compliance of the Alveoli	2×10^{-1}	$\mathrm{l/cmH_2O}$
C_{CW}	Compliance of the Chest wall	2.445×10^{-1}	$\mathrm{l/cmH_2O}$

6.9.1 *Model validation*

The model was validated using parameters obtained from the literature. The simulated results provided in the results and discussion section were found to be comparable to those in the existing literature.

6.9.2 *Simulation environment*

Simulations were conducted using MATLAB

6.9.3 *Results*

Three conditions were used to simulate the mechanical ventilator behaviour with the following lung conditions: compliance 50 mL/cmH2O and resistance 5cmH2O-s/L, compliance 20 mL/cmH2O and resistance 20cmH2O-s/L and compliance 10 mL/cmH2O and resistance 50cmH2O-s/L. For each condition, all the sizes were tested for 2 min per size and the ventilation curves air volume, The conditions were chosen in order to have a fair comparison with results that exist in literature that used similar lung compliance. pressure and flow over time were obtained. The simulation results are shown in Figures 6.10 and 6.11, where A, B, C, D, and E represent various cams sizes of the mechanical ventilator from extra small (A), small(B), Medium(C), Large (D) and extra-large(E)

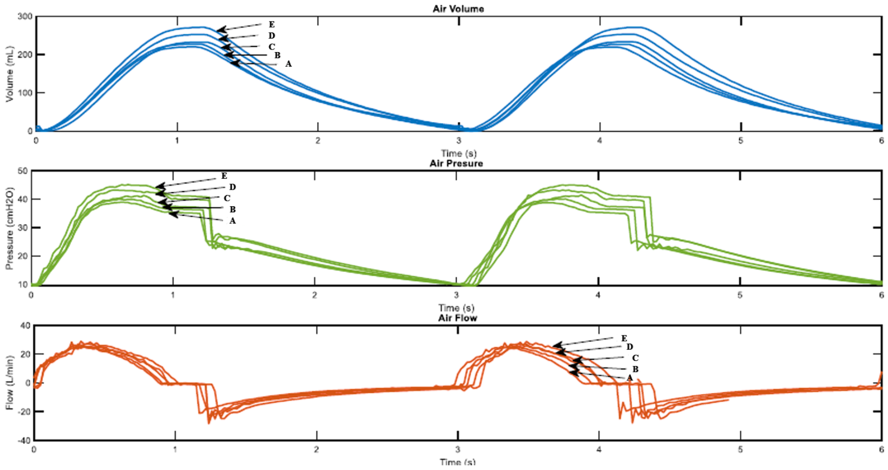

Figure 6.10: Air pressure, volume and flow versus time graph

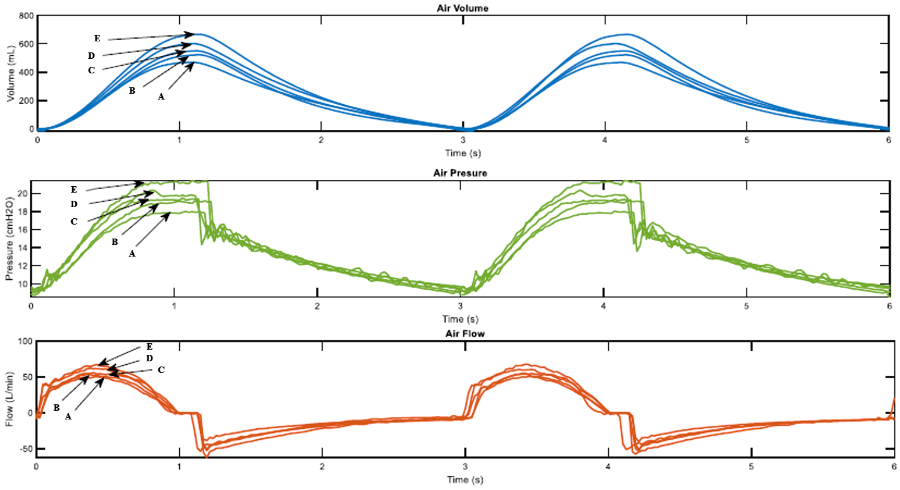

Figure 6.11: Mechanical Ventilator Simulation results

The figure show ventilation curves for a lung under two conditions, for a partially damaged lung whose compliance and resistance of 20 mL/cmH2O and 20cmH2O-s/L respectively. The lung with complete damage is represented by lung compliance and resistance of 10 mL/cmH2O and resistance 50cmH2O-s/L. As the cam size increases the ventilation curves maintain the same sinusoidal behavior. For a damaged lung case study, minimum ventilation values of flow over time and air volume are achieved. In a damaged lung, the compliance and resistance of the lung increases the pressure.

6.9.4 *Multi physics modelling of the respiratory system*

The model of the respiratory system presented in this section is a multi-physics and multi-scale model of the lung. The detailed model presented incorporates the action of the diaphragm, as well as the fluid flow.

6.9.5 *physical system*

Figure 6.9 provides the physical system diagram of the multi-physics model.

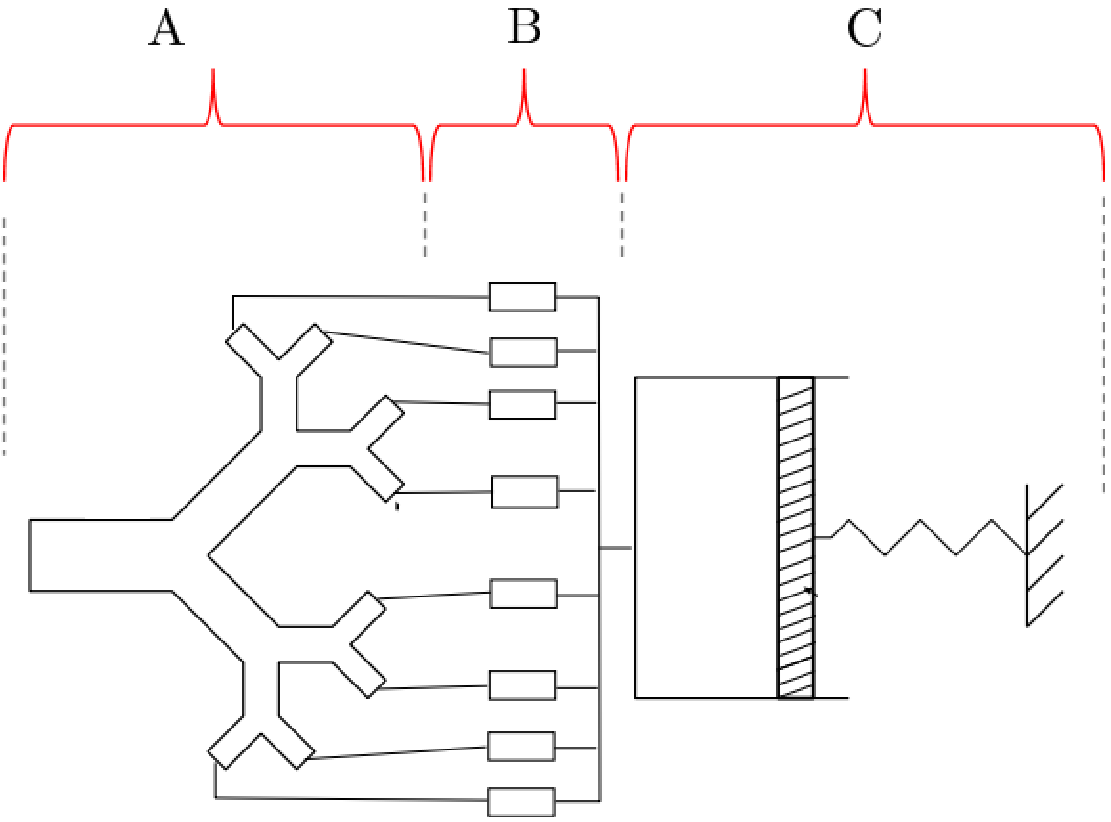

Figure 6.12: The Port Hamiltonian model of the Multiphysics respiratory system

6.9.6 *The Port Hamiltonian model of the Multiphysics respiratory system*

The description of the physical model is as follows:

- The upper part Labeled A represents up to the 6th generation and it is represented by incompressible Navier stoke equations. The trachea has a Mach number of less than 0.3 even during forced inspiration and expiration, therefore the flow incompressibility is valid.
- The distal part labelled B represents the 7th to the 17th generation. An assumption is made that Poiseuille's law or criterion is satisfied in each bronchiole.

- The last part of the model is labelled C, namely the Acini. This is where oxygen diffusion takes place and it is embedded in an elastic medium named the parenchyma.
- It is assumed that there is uniform pressure in the acini part and it is embedded in a box which is used to represent the parenchyma.
- A mass-spring model is used to describe the motion of the diaphragm and the parenchyma.

6.10 INTERGRATED MULTIPHYSICS PORT HAMILTONIAN MODEL OF THE MECHANICAL VENTILATOR RESPIRATORY SYSTEM

The formulation of fluid flow using the incompressible Navier stokes is presented in detail in Chapter 7. The final equations of the fluid flow is in the distal part are provided below.

Therefore the Stokes-Dirac structure $\mathcal{D}_{IF}$ of the incompressible fluid defined by the set

$$\begin{aligned}\mathcal{D}_{IF} := \Big\{ \quad & \left(f_{\tilde{v}},\ f_{\eta},\ f_p,\ f_{\partial p},\ e_{\tilde{v}},\ e_{\eta},\ e_p,\ e_{\partial p}\right) \in \mathcal{F} \times \mathcal{E} \Big| \\ & \begin{pmatrix} f_{\tilde{v}} \\ f_{\eta} \end{pmatrix} = \begin{pmatrix} \frac{1}{\star\eta}\iota_{\sharp\circ\star(\cdot)}d\tilde{v} & \mathrm{d} \\ \mathrm{d} & 0 \end{pmatrix} \begin{pmatrix} e_v \\ e_{\eta} \end{pmatrix} - \begin{pmatrix} \frac{1}{\star\eta} \\ 0 \end{pmatrix} e_p, \\ & f_p = \begin{pmatrix} \frac{1}{\star\eta} & 0 \end{pmatrix} \begin{pmatrix} e_{\tilde{v}} \\ e_{\eta} \end{pmatrix}, \\ & \begin{pmatrix} e_{\partial e} \\ f_{\partial e} \end{pmatrix} = \begin{pmatrix} 0 & 1 \\ -1 & 0 \end{pmatrix} \begin{pmatrix} i^{\star}(e_{\tilde{v}}) \\ i^{*}(e_{\eta}) \end{pmatrix} \Big\} \end{aligned} \tag{6.38}$$

The distal part is modeled using an electric circuit. The formulation is presented in detail in chapter 7 of this research work. The Dirac structure of the electric circuit can be represented as follows:

so that the associated Dirac structure of the electric circuit is $\mathcal{D}_e$ is

$$\begin{aligned}\mathcal{D}_e := \Big\{ \quad & (j,\ -u_{\mathcal{L}},\ -i_{\mathcal{C}},\ -i_{\mathcal{R}},\ -i_{\mathcal{S}},\ \phi, u_{\mathcal{L}},\ u_{\mathcal{R}},\ u_{\mathcal{S}}) \in \mathbb{R}^{n-|S|} \times \mathbb{R}^{m} \times \mathbb{R}^{n-|S|} \times \mathbb{R}^{m} \Big| \\ & \begin{bmatrix} I & 0 & A_{\mathcal{C}} & A_{\mathcal{R}} & A_{\mathcal{S}} \\ 0 & 0 & 0 & 0 & 0 \\ 0 & -I & 0 & 0 & 0 \\ 0 & 0 & 0 & 0 & 0 \\ 0 & 0 & 0 & 0 & 0 \end{bmatrix} \begin{pmatrix} j \\ -u_{\mathcal{L}} \\ -i_{\mathcal{C}} \\ -i_{\mathcal{R}} \\ -i_{\mathcal{S}} \end{pmatrix} + \begin{bmatrix} 0 & -A_{\mathcal{L}} & 0 & 0 & 0 \\ -A_{\mathcal{R}}^{\top} & 0 & 0 & 0 & 0 \\ -A_{\mathcal{L}}^{\top} & -I & 0 & 0 & 0 \\ -A_{\mathcal{C}}^{\top} & 0 & 0 & 0 & 0 \\ -A_{\mathcal{S}}^{\top} & 0 & 0 & 0 & I \end{bmatrix} \begin{pmatrix} \phi \\ i_{\mathcal{L}} \\ u_{\mathcal{C}} \\ u_{\mathcal{R}} \\ u_{\mathcal{S}} \end{pmatrix} = 0 \Big\} \end{aligned}$$

The acini part is presented as a model which is made up of a system of coupled masses, springs and dampers. The summed-up energy of the system is represented by the Hamiltonian function, H_3, which is made up of the sum of the kinetic energy T_3 and the potential energy U_3 described by

$$H_3(x_3) = T_3 + U_3 \tag{6.39}$$

where

$$\begin{aligned} T_3 &= \frac{1}{2}\left(\frac{\pi_{3_a}^2}{M_{3_a}} + \frac{\pi_{3_c}^2}{M_{3_c}} + \frac{\pi_{3_d}^2}{M_{3_d}}\right) \\ U_3 &= \frac{1}{2}\left(K_{3_a}\psi_{3_a}^2 + K_{3_b}(L\psi_{3_a} - \psi_{3_c})^2 + K_{3_c}\psi_{3_c}^2 + K_{3_d}\psi_{3_d}^2\right) \end{aligned}$$

where the subscripts 3_a, 3_b, 3_c and 3_d represent the various alveoli within the parenchyma. $M_{(\cdot)}$ is the mass, $\pi_{(\cdot)}$ is the translational momentum, $\psi_{(\cdot)}$ is the displacement, $K_{(\cdot)}$ is the parenchyma stiffness and G The Port Hamiltonian model of the parenchyma box is therefore represented as:

$$\begin{aligned} \partial_t x_3 &= (\mathcal{J}_3 - \mathcal{R}_3)\,\partial_{x_3} H_3 + \mathcal{G}_3 u_3 \\ y_3 &= \mathcal{G}_3^* \partial_{x_3} H_3 \end{aligned} \tag{6.40}$$

where y_3 is the output, the state vector is

$$x_3 = \begin{bmatrix} \pi_{3_a} & \psi_{3_a} & \pi_{3_c} & \psi_{3_c} & \pi_{3_d} & \psi_{3_d} \end{bmatrix}^T \tag{6.41}$$

the skew-symmetric matrix $\mathcal{J}_3 = -\mathcal{J}_3^T$ is

$$\mathcal{J}_3 = \begin{bmatrix} 0 & -1 & 0 & 0 & 0 & 0 \\ 1 & 0 & 0 & 0 & 0 & 0 \\ 0 & 0 & 0 & -1 & 0 & 0 \\ 0 & 0 & 1 & 0 & 0 & 0 \\ 0 & 0 & 0 & 0 & 0 & -1 \\ 0 & 0 & 0 & 0 & 1 & 0 \end{bmatrix} \tag{6.42}$$

the symmetric dissipation matrix, $\mathcal{R}_3 = \mathcal{R}_3^T$, is

$$\mathcal{R}_3 = \begin{bmatrix} B_{3_a} + L_3 B_{3_b} L_3 & 0 & -L_3 B_{3_b} & 0 & 0 & 0 \\ 0 & 0 & 0 & 0 & 0 & 0 \\ -L_3 B_{3_b} & 0 & B_{3_a} + B_{3_c} & 0 & 0 & 0 \\ 0 & 0 & 0 & 0 & 0 & 0 \\ 0 & 0 & 0 & 0 & B_{3_d} & 0 \\ 0 & 0 & 0 & 0 & 0 & 0 \end{bmatrix} \tag{6.43}$$

and the partial derivative of the Hamiltonian with respect to the states is

$$\partial_{x_3} H_3 = \begin{bmatrix} \pi_{3_a}/M_{3_a} \\ K_{3_a}\psi_{3_a} + L_3 K_{3_b}\left(L_3\psi_{3_a} - \psi_{3_c}\right) \\ \pi_{3_c}/M_{3_c} \\ K_{3_b}\psi_{3_c} - K_{3_b}\left(L_3\psi_{3_a} - \psi_{3_c}\right) \\ \pi_{3_d}/M_{3_d} \\ K_{3_d}\psi_{3_d} \end{bmatrix} \tag{6.44}$$

and the control input allocation and control input matrix

$$\mathcal{G}_3 = \begin{bmatrix} 0 & 0 & 0 \\ 1 & 0 & 0 \\ 0 & 0 & 0 \\ 0 & 1 & 0 \\ 0 & 0 & 0 \\ 0 & 0 & 1 \end{bmatrix}, \quad \mathcal{G}_3^* = \begin{bmatrix} 0 & 1 & 0 & 0 & 0 & 0 \\ 0 & 0 & 0 & 1 & 0 & 0 \\ 0 & 0 & 0 & 0 & 0 & 1 \end{bmatrix}, \quad u_3 = \begin{bmatrix} u_{3_a} \\ u_{3_c} \\ u_{3_d} \end{bmatrix} \tag{6.45}$$

The three parts are interconnected to form a multi scale, multi physics Port Hamiltonian model of the mechanical ventilator respiratory system.

6.10.1 *Reflection on the Contribution for the chapter*

The contribution in this chapter is the formulation of a detailed mechanical ventilator in the port Hamiltonian framework. This is followed by a Port Hamiltonian multi scale and multi physics model of the respiratory. These two systems are then integrated. There are currently no Port Hamiltonian models of the Mechanical ventilator system and no Port Hamiltonian models of the human respiratory system. This contribution introduces a paradigm shift in the modelling of the mechanical ventilator as well as the human respiratory system using the Port Hamiltonian framework. The work conducted in this research provides clear proof the Port Hamiltonian approach is a valid method in the modelling of such systems.

6.11 CONCLUSION

This chapter has presented a detailed port Hamiltonian formulation of the mechanical ventilator model. The presented model is made up of electromechanical and electromagnetic components. A multiscale and multiphysics model of the human respiratory system using the Hamiltonian approach has also been presented. In future, this work can be improved by relaxing some of the assumptions that were previously taken. Experimental results have also been presented for illustration purposes.

7

FORMULATION OF A GENERALIZED MULTIPHYSICS PORT HAMILTONIAN MODEL OF THE MECHANICAL VENTILATOR HUMAN RESPIRATORY SYSTEM

7.1 SUMMARY

Motivated by the work presented in the previous sections, in this chapter, we formulate a Port Hamiltonian generalisation of a mechanical ventilator lung system. This leads to a new class of algebraic constraints in the modelling of the mechanical ventilator lung physical system. The new class of constraint is due to the coupling of Partial Differential Equations (representing the fluid) with ordinary differential equations. In the context of Port Hamiltonian systems, this class of systems is called a mixed Port Hamiltonian system. This chapter presents a port Hamiltonian multi-physics generalized modelling approach for the mechanical ventilator lung system. The fluid flow is modelled using the Stokes-Dirac structure for an incompressible fluid. The main result presented is a novel interconnected Dirac structure of the fluid/electrically coupled system. The presented generalized model can be employed in the investigation of the influence of airway secretion on airflow dynamics in the mechanical ventilator lung system.

7.2 INTRODUCTION

Systematic modelling and analysis of a multidisciplinary complex system has been one of the dilemmas faced by scientists and engineers. For physical, chemical and biological systems, energy plays a significant role in building unified complex models of the system. These models are composed of interconnected systems defined in various domains for instance mechanical, electrical, thermodynamics and hydrodynamics systems. These systems are known as multiphysics systems in which energy and power are viewed as the "lingua franca" for the various physical domains. One of the key attributes of Port Hamiltonian formalism is that its outcome is a power-preserving interconnected system which results in another composite energy, dissipation and interconnected structure. Therefore, considering this principle, multi domain complex systems are modelled.

The evolution of Paynter's work which has been used for various decades has resulted in the formalization of the Port Hamiltonian systems. The Port Hamiltonian approach applies techniques from differential geometry and techniques from various methodologies in dynamical systems. The Dirac structure and Dirac manifold concepts are employed in the definition of Port Hamiltonian systems. The representation of the Dirac structure and connection of the Port Hamiltonian systems have been presented by various authors. [108] and [109] provide a detailed and precise description of fluids from a mathematical perspective. [110] Proposes a detailed focus on fluid mechanics models using differential geometry. [111] presented a one-dimensional Naiver Stokes formulation. [112] accounted for vorticity that naturally appears in higher space dimensions. dimensional

7.3 CONTRIBUTION

Contribution 7.3.1

The contribution in this chapter is the formulation of a multi-physics Port Hamiltonian generalized model of a Mechanical Ventilator-Human respiratory system with Navier stokes for the fluid flow in the mechanical ventilator lung system. A new class of algebraic constraints in the modelling of the mechanical ventilator lung physical system is formulated. The new class is due to the coupling of Partial Differential Equations (representing the fluid) with ordinary differential equations.

7.4 MULTI PHYSICS GENERALIZED MODELLING APPROACH FOR THE FLUID FLOW IN MECHANICAL VENTILATOR LUNG SYSTEM

The primary references for the content in this section are; [85], [92] and [110]. In this work, fluids in the trachea, bronchioles, alveoli as well as the air-tube of the MV are modelled as Eulerian fluids, evolving on manifolds $\mathcal{M}$ of dimension n with boundary $\partial\mathcal{M}$. Smooth functions are treated as elements of $C^\infty(\mathcal{M})$, smooth vector fields as elements of $\mathfrak{X}(\mathcal{M})$ and $^k(\mathcal{M})$ is used to denote the module of differential k-forms that are smooth. Each manifold M is compact with a Riemannian metric, $g : \mathfrak{X}(\mathcal{M}) \times \mathfrak{X}(\mathcal{M}) \rightarrow C^\infty(\mathcal{M})$, volume form $\eta_{\mathrm{vol}} \in^n (\mathcal{M})$ and the operator, $\star :^k (\mathcal{M}) \rightarrow^{n-k} (\mathcal{M})$, is the Hodge star.

The flat and sharp maps, denoted by $\flat$ and $\sharp$, respectively are defined as

$$\flat : \mathfrak{X}(\mathcal{M}) \rightarrow^1 (\mathcal{M}) \qquad \text{and} \qquad \sharp :^1 (\mathcal{M}) \rightarrow \mathfrak{X}(\mathcal{M})$$

so that for vector fields $u \in \mathfrak{X}(\mathcal{M})$ given by

$$u := u^i \frac{\partial}{\partial q^i} \tag{7.1}$$

and $k-$forms $\beta \in^1 (\mathcal{M})$, given by

$$\beta := \beta_{i_1 \cdots i_k} \mathrm{d}q^{i_1} \wedge \cdots \wedge \mathrm{d}q^{i_k} \tag{7.2}$$

they are given by

$$\flat(u) := g(u, \cdot) \qquad \text{and} \qquad g(\sharp(\beta), u) := \beta(u)$$

respectively, where

$$g := g_{ij} \mathrm{d}q^i \otimes \mathrm{d}q^i \tag{7.3}$$

is the Riemannian metric.

The state, x, of a fluid in the lung system or air-tube can be expressed in terms of the mass density $\varrho \in C^\infty(\mathcal{M})$ and the vector field $v \in \mathfrak{X}(\mathcal{M})$,

$$v := \nu^i \frac{\partial}{\partial q^i} \tag{7.4}$$

which is the fluid velocity. The first state of the fluid is the velocity state denoted by the one form

$$\tilde{v} \quad := \flat(v) \in^1 (\mathcal{M}) \tag{7.5}$$

$$\tilde{v} \qquad = g_{ij} \nu^i \mathrm{d}q^i \tag{7.6}$$

The second state of the fluid is the mass density,

$$\eta := \varrho \eta_{\mathrm{vol}} = \star \varrho \in^n (\mathcal{M}) \tag{7.7}$$

where $\eta_{\mathrm{vol}} = \sqrt{\det(g_{ij})} \mathrm{d}q^1 \wedge \cdots \wedge \mathrm{d}q^k$ is the volume form.

Thus the two dimensional fluid state

$$x \quad = \left(\tilde{v}, \eta\right) \in \mathfrak{X}(\mathcal{M}) \times^n (\mathcal{M}) \tag{7.8}$$

The kinetic energy of the fluid is therefore given by the Hamiltonian

$$H(\tilde{v}, \eta) \quad = \tfrac{1}{2} \int_M (\star \eta) \tilde{v} \wedge \star \tilde{v}$$

The effort associated with the fluid velocity is

$$\delta_{\tilde{v}} H(\tilde{v}, \eta) = \varrho \star \tilde{v} \in^{n-1} (\mathcal{M}) \tag{7.9}$$

where

$$\star v := \frac{1}{2} \sqrt{\det(g_{ij})} \epsilon_{ijk} \nu^i \mathrm{d}q^j \wedge \mathrm{d}q^k \tag{7.10}$$

is the $n - 1$ velocity form for a manifold of dimension $n = 3$. Take note that $\epsilon_{ijk} \in C^\infty(\mathcal{M})$ is the Levi Civita symbol.

The effort associated with the fluid density is given by the $0-$form

$$\delta_\eta H(\tilde{v}, \eta) = \frac{1}{2} \iota_v \tilde{v} \in^0 (\mathcal{M}) \tag{7.11}$$

where

$$\iota_v \quad :^k (\mathcal{M}) \to^{k-1} (\mathcal{M}) \tag{7.12}$$

$$\iota_v \quad \tilde{v} = g(v, v) = \tilde{v}(v) \tag{7.13}$$

is the inner product.

Thus one can define the rate of change of the Hamiltonian by the pairing between the flow variables $(\dot{\eta}, \dot{\tilde{v}})$ and the effort variables $(\delta_{\tilde{v}}, \delta_\eta H)$

$$\dot{H} \qquad = \textstyle\int_M \dot{\tilde{v}} \wedge \delta_{\tilde{v}} H + \dot{\eta} \wedge \delta_\eta H \tag{7.14}$$

$$= \textstyle\int_M \left(\varrho g_{ij} v^i \dot{v}^j + \frac{1}{2} g_{ij} v^i v^j \dot{\varrho} \right) \eta_{\text{vol}} \tag{7.15}$$

Since the fluid flow under consideration is incompressible, pressure acts as a Lagrange multiplier. Hence there is no power flow through the distributed pressure port given by the pairing

$$(p, \mathbf{0}) := (p, 0 \cdot \eta_{\text{vol}}) \in^0 (\mathcal{M}) \times^n (\mathcal{M}) \tag{7.16}$$

The power flow through the boundary due to the fluid pressure is

$$\int_{\partial \mathcal{M}} e_{\partial p} \wedge f_{\partial p} \tag{7.17}$$

where $e_{\partial p} \in C^\infty(\partial \mathcal{M})$ is the effort and $f_{\partial p} \in C^\infty(\partial \mathcal{M})$ the flow due to the pressure at the boundary.

The Stokes-Dirac structure of the incompressible fluid is given by the subspace for which

$$\underbrace{\int_M \dot{\tilde{v}} \wedge \delta_{\tilde{v}} H + \int_M \dot{\eta} \wedge \delta_\eta H}_{\int_M \dot{x} \wedge \delta_x H} = p \cdot \mathbf{0} + \int_M e_{\partial_p} \wedge f_{\partial p} \tag{7.18}$$

where $x = (\eta, \tilde{v})$. Since the term $\int_M \dot{x} \wedge \delta_x H$ is equal to the rate at which energy in the system changes, that is, $\dot{H}$, it is clear that pressure changes due to sources outside the boundary, resulting in the overall energy change given by

$$\dot{H} = \int_M e_{\partial_p} \wedge f_{\partial p} \tag{7.19}$$

The fluid dynamics take the following form

$$\begin{aligned}
\begin{pmatrix} \partial_t \tilde{v} \\ \partial_t \eta \end{pmatrix} &= -\mathcal{J} \begin{pmatrix} \delta_{\tilde{v}} H \\ \delta_\eta H \end{pmatrix} - \begin{pmatrix} \frac{1}{\star\eta} \mathrm{d}p \\ 0 \end{pmatrix} && (7.20) \\
0 &= \mathrm{d} \circ \tfrac{1}{\star\eta} (\delta_{\tilde{v}} H) && (7.21) \\
e_{\partial p} &= i^* \left(\tfrac{1}{2} (\star\eta) \iota_v \tilde{v} + p \right) && (7.22) \\
f_{\partial p} &= -i^* \left(\tfrac{1}{\star\eta} \delta_{\tilde{v}} H \right) && (7.23)
\end{aligned}$$

where $i^* : \partial\mathcal{M} \to M$ is the pull-back of the inclusion map and the operator $\mathcal{J} :^{n-1} (\mathcal{M}) \times^0 (\mathcal{M}) \to^1 (\mathcal{M}) \times^n (\mathcal{M})$ is skew-symmetric

$$\mathcal{J} := \begin{pmatrix} \frac{1}{\star\eta} \iota_{\sharp\circ\star(\cdot)} d\tilde{v} & \mathrm{d} \\ \mathrm{d} & 0 \end{pmatrix} \tag{7.24}$$

Therefore the Stokes-Dirac structure $\mathcal{D}_{IF}$ of the incompressible fluid defined by the set

$$\begin{aligned}
\mathcal{D}_{IF} := \Bigg\{ \quad & \left(f_{\tilde{v}},\ f_\eta,\ f_p,\ f_{\partial p},\ e_{\tilde{v}},\ e_\eta,\ e_p,\ e_{\partial p} \right) \in \mathcal{F} \times \mathcal{E} \Bigg| \\
& \begin{pmatrix} f_{\tilde{v}} \\ f_\eta \end{pmatrix} = \begin{pmatrix} \frac{1}{\star\eta} \iota_{\sharp\circ\star(\cdot)} d\tilde{v} & \mathrm{d} \\ \mathrm{d} & 0 \end{pmatrix} \begin{pmatrix} e_v \\ e_\eta \end{pmatrix} - \begin{pmatrix} \frac{1}{\star\eta} \\ 0 \end{pmatrix} e_p, \\
& f_p = \begin{pmatrix} \frac{1}{\star\eta} & 0 \end{pmatrix} \begin{pmatrix} e_{\tilde{v}} \\ e_\eta \end{pmatrix}, \\
& \begin{pmatrix} e_{\partial e} \\ f_{\partial e} \end{pmatrix} = \begin{pmatrix} 0 & 1 \\ -1 & 0 \end{pmatrix} \begin{pmatrix} i^\star (e_{\tilde{v}}) \\ i^* (e_\eta) \end{pmatrix} \Bigg\}
\end{aligned} \tag{7.25}$$

7.4.1 *Interconnection of the system*

Consider an electric circuit with current and voltage source vectors of dimension $m_\mathcal{S}$:

$$i_\mathcal{S} = \begin{pmatrix} i_{\mathcal{S}1} \\ \vdots \\ i_{\mathcal{S}m_\mathcal{S}} \end{pmatrix} \quad \text{and} \quad u_\mathcal{S} = \begin{pmatrix} u_{\mathcal{S}1} \\ \vdots \\ u_{\mathcal{S}m_\mathcal{S}} \end{pmatrix}$$

so that the associated Dirac structure of the electric circuit is $\mathcal{D}_e$ is

$$\mathcal{D}_e := \Bigg\{ \quad (j, -u_{\mathcal{L}}, -i_{\mathcal{C}}, -i_{\mathcal{R}}, -i_{\mathcal{S}}, \phi, u_{\mathcal{L}}, u_{\mathcal{R}}, u_{\mathcal{S}}) \in \mathbb{R}^{n-|S|} \times \mathbb{R}^{m} \times \mathbb{R}^{n-|S|} \times \mathbb{R}^{m} \Bigg| \\ \begin{bmatrix} I & 0 & A_{\mathcal{C}} & A_{\mathcal{R}} & A_{\mathcal{S}} \\ 0 & 0 & 0 & 0 & 0 \\ 0 & -I & 0 & 0 & 0 \\ 0 & 0 & 0 & 0 & 0 \\ 0 & 0 & 0 & 0 & 0 \end{bmatrix} \begin{pmatrix} j \\ -u_{\mathcal{L}} \\ -i_{\mathcal{C}} \\ -i_{\mathcal{R}} \\ -i_{\mathcal{S}} \end{pmatrix} + \begin{bmatrix} 0 & -A_{\mathcal{L}} & 0 & 0 & 0 \\ -A_{\mathcal{R}}^{\mathsf{T}} & 0 & 0 & 0 & 0 \\ -A_{\mathcal{L}}^{\mathsf{T}} & -I & 0 & 0 & 0 \\ -A_{\mathcal{C}}^{\mathsf{T}} & 0 & 0 & 0 & 0 \\ -A_{\mathcal{S}}^{\mathsf{T}} & 0 & 0 & 0 & I \end{bmatrix} \begin{pmatrix} \phi \\ i_{\mathcal{L}} \\ u_{\mathcal{C}} \\ u_{\mathcal{R}} \\ u_{\mathcal{S}} \end{pmatrix} = 0 \right\}$$

Assuming that the source voltages and currents is due to the union of two sets:

$$u_{\mathcal{S}} := u_{\mathcal{S}_e} \cup u_{\mathcal{S}_{(f/e)}} \qquad \text{and} \qquad i_{\mathcal{S}} := i_{\mathcal{S}_e} \cup i_{\mathcal{S}_{(f/e)}}$$

where there are

1. Purely electric sources:
   - Current sources $i_{\mathcal{S}_e} \in \mathbb{R}^{m_{\mathcal{S}_{(e)}}}$ and
   - Voltage sources $u_{\mathcal{S}_e} \in \mathbb{R}^{m_{\mathcal{S}_{(e)}}}$

   where $m_{\mathcal{S}_{(e)}}$ is the number of purely electric sources.
2. Sources due to the fluid/electric coupling:
   - Current sources $i_{\mathcal{S}_{(f/e)}} \in \mathbb{R}^{m_{\mathcal{S}} - m_{\mathcal{S}_{(e)}}}$ and
   - Voltage sources $u_{\mathcal{S}_{(f/e)}} \in \mathbb{R}^{m_{\mathcal{S}} - m_{\mathcal{S}_{(e)}}}$.

The Stokes-Dirac structure $\mathcal{D}_{IF}$ of the incompressible fluid defined by the set

$$\mathcal{D}_{IF} := \Bigg\{ \quad \Big(f_{\tilde{v}},\ f_{\eta},\ f_{p},\ f_{\partial p},\ e_{\tilde{v}},\ e_{\eta},\ e_{p},\ e_{\partial p}\Big) \in \mathcal{F} \times \mathcal{E} \Bigg| \\ \begin{pmatrix} f_{\tilde{v}} \\ f_{\eta} \end{pmatrix} = \begin{pmatrix} \frac{1}{\star\eta} \iota_{\sharp\circ\star(\cdot)} d\tilde{v} & \mathrm{d} \\ \mathrm{d} & 0 \end{pmatrix} \begin{pmatrix} e_{v} \\ e_{\eta} \end{pmatrix} - \begin{pmatrix} \frac{1}{\star\eta} \\ 0 \end{pmatrix} e_{p}, \\ f_p = \begin{pmatrix} \frac{1}{\star\eta} & 0 \end{pmatrix} \begin{pmatrix} e_{\tilde{v}} \\ e_{\eta} \end{pmatrix}, \\ \begin{pmatrix} e_{\partial e} \\ f_{\partial e} \end{pmatrix} = \begin{pmatrix} 0 & 1 \\ -1 & 0 \end{pmatrix} \begin{pmatrix} i^{\star}(e_{\tilde{v}}) \\ i^{*}(e_{\eta}) \end{pmatrix} \Bigg\}$$

Assuming that the fluid boundary, $\partial\mathcal{M}$ is the union of the purely fluid boundary and a boundary due to the fluid/electric coupling:

$$\partial\mathcal{M} := \partial\mathcal{M}_{(f)} \cup \partial\mathcal{M}_{(f/e)}$$

The fluid and electric circuit are coupled at $k = 1, \ldots, m_{\mathcal{S}_{(f/e)}}$ locations, where

$$m_{\mathcal{S}_{(f/e)}} = m_{\mathcal{S}} - m_{\mathcal{S}_{(e)}}$$

so that the fluid/electric coupling boundary is given by

$$\partial\mathcal{M}_{(f/e)} := \partial\mathcal{M}_{(f/e)_1} \cup \cdots \cup \partial\mathcal{M}_{(f/e)_{m_{\mathcal{S}_{(f/e)}}}}$$

The inclusion map due to the purely fluid boundary and the k^{th} fluid/electric coupling boundary are

$$i_{(f)} : \partial\mathcal{M}_f \to \mathcal{M}_f \qquad \text{and} \qquad i_{(f/e)_k} : \partial\mathcal{M}_{(f/e)_k} \to \mathcal{M}$$

for $k = 1, \ldots, m_{\mathcal{S}_{(f/e)}}$

7.5 DIRAC STRUCTURE AND THE INTERCONNECTION

The main result is now introduced:

Consider an electric circuit coupled to a fluid system to form a fluid/electrically coupled system.

1. The electric circuit has $m_{\mathcal{S}_{(e)}}$ purely electric current and voltage sources together with $m_{\mathcal{S}_{(f/e)}}$ sources due to the fluid/electric coupling.
2. The fluid has a purely fluid boundary

The Dirac structure of the fluid/electrically coupled system, $\mathcal{D}_{f/e}$ is given by the set

$$\mathcal{D}_{(f/e)} := \Bigg\{ \quad (j,\, -u_{\mathcal{L}},\, -i_{\mathcal{C}},\, -i_{\mathcal{R}},\, -i_{\mathcal{S}},\, \phi, u_{\mathcal{L}},\, u_{\mathcal{R}},\, u_{\mathcal{S}},$$

$$f_{\tilde{v}},\, f_{\eta},\, f_p,\, f_{\partial p_{(f)}},\, f_{\partial p_{(f/e)}},\, e_{\tilde{v}},\, e_{\eta},\, e_p,\, e_{\partial p_{(f)}}, e_{\partial p_{(f/e)}})$$

$$\in \mathbb{R}^{n-|S|} \times \mathbb{R}^{m} \times \mathbb{R}^{n-|S|} \times \mathbb{R}^{m} \times \mathcal{F} \times \mathcal{E} \Bigg| \tag{7.26a}$$

$$\begin{bmatrix} I & 0 & A_{\mathcal{C}} & A_{\mathcal{R}} & A_{\mathcal{S}} \\ 0 & 0 & 0 & 0 & 0 \\ 0 & -I & 0 & 0 & 0 \\ 0 & 0 & 0 & 0 & 0 \\ 0 & 0 & 0 & 0 & 0 \end{bmatrix} \begin{pmatrix} j \\ -u_{\mathcal{L}} \\ -i_{\mathcal{C}} \\ -i_{\mathcal{R}} \\ -i_{\mathcal{S}} \end{pmatrix} + \begin{bmatrix} 0 & -A_{\mathcal{L}} & 0 & 0 & 0 \\ -A_{\mathcal{R}}^{\mathsf{T}} & 0 & 0 & 0 & 0 \\ -A_{\mathcal{L}}^{\mathsf{T}} & -I & 0 & 0 & 0 \\ -A_{\mathcal{C}}^{\mathsf{T}} & 0 & 0 & 0 & 0 \\ -A_{\mathcal{S}}^{\mathsf{T}} & 0 & 0 & 0 & I \end{bmatrix} \begin{pmatrix} \phi \\ i_{\mathcal{L}} \\ u_{\mathcal{C}} \\ u_{\mathcal{R}} \\ u_{\mathcal{S}} \end{pmatrix} = 0, \tag{7.26b}$$

$$i_{\mathcal{S}} = \begin{pmatrix} i_{\mathcal{S}_{(e)}} \\ i_{\mathcal{S}_{(f/e)}} \end{pmatrix} \tag{7.26c}$$

$$u_{\mathcal{S}} = \begin{pmatrix} u_{\mathcal{S}_{(e)}} \\ u_{\mathcal{S}_{(f/e)}} \end{pmatrix} \tag{7.26d}$$

$$\begin{pmatrix} f_{\tilde{v}} \\ f_{\eta} \end{pmatrix} = \begin{pmatrix} \frac{1}{\star\eta}\iota_{\sharp\circ\star(\cdot)}d\tilde{v} & \mathrm{d} \\ \mathrm{d} & 0 \end{pmatrix} \begin{pmatrix} e_{\nu} \\ e_{\eta} \end{pmatrix} - \begin{pmatrix} \frac{1}{\star\eta} \\ 0 \end{pmatrix} e_p, \tag{7.26e}$$

$$f_p = \begin{pmatrix} \frac{1}{\star\eta} & 0 \end{pmatrix} \begin{pmatrix} e_{\tilde{v}} \\ e_{\eta} \end{pmatrix}, \tag{7.26f}$$

$$\begin{pmatrix} e_{\partial e_{(f)}} \\ f_{\partial e_{(f)}} \end{pmatrix} = \begin{pmatrix} 0 & 1 \\ -1 & 0 \end{pmatrix} \begin{pmatrix} i^{\star}_{(f)}(e_{\tilde{v}}) \\ i^{*}_{(f)}(e_{\eta}) \end{pmatrix} \tag{7.26g}$$

$$\begin{pmatrix} e_{\partial e_{(f/e)}} \\ f_{\partial e_{(f/e)}} \end{pmatrix} = \begin{pmatrix} 0 & 1 \\ -1 & 0 \end{pmatrix} \begin{pmatrix} i^{\star}_{(f/e)}(e_{\tilde{v}}) \\ i^{*}_{(f/e)}(e_{\eta}) \end{pmatrix} = \begin{pmatrix} i_{\mathcal{S}_{(f/e)}} \\ u_{\mathcal{S}_{(f/e)}} \end{pmatrix} \Bigg\} \tag{7.26h}$$

7.6 DISCUSSION OF THE RESULT

The presented main result has three key attributes that contribute to its novelty:

Firstly, the system is a combination of a lumped parameter system which represents electric ciruit components and a distributed parameter system representing the fluid. The lumped parameter system equations are Ordinary Differential Equations (ODE) while the distributed parameter are Partial Differential Equations (PDE). Both these systems are not operating in isolation, they are coupled by a bidirectional coupling. This implies, the electric circuit components can influence the dynamics of the fluid system and vice versa. The coordinates of the combined system are given by equation 7.26a, where one should pay attention in particular to the equations of the source current and source voltages given by equation 7.26c and 7.26d, which shows that the current and voltage are composed of two elements: The current and voltage sources that are purely electric (e) while (f/e) are due to the fluid electric coupling which means at the point of interconnection, the fluid acts as a source voltage or source current to the electric circuit.

In addition, equation 7.26a also distinguishes between the boundary efforts and flows that are due to the fluid alone, this are indicated by (f) whie those due to fluid/electric coupling are indicated by (f/e). Physically speaking, this indicates that the electric circuit is able to act as a source of effort of flow onto the fluid hence providing the bidirectional coupling between the fluid and the electric circuit.

$$\begin{aligned}&(j,\, -u_{\mathcal{L}},\, -i_{\mathcal{C}},\, -i_{\mathcal{R}},\, -i_{\mathcal{S}},\, \phi, u_{\mathcal{L}},\, u_{\mathcal{R}},\, u_{\mathcal{S}},\, f_{\tilde{v}},\, f_{\eta},\, f_{p},\, f_{\partial p_{(f)}},\, f_{\partial p_{(f/e)}},\, e_{\tilde{v}},\, e_{\eta},\, e_{p},\, e_{\partial p_{(f)}}, e_{\partial p_{(f/e)}})\\ &\in \mathbb{R}^{n-|S|} \times \mathbb{R}^{m} \times \mathbb{R}^{n-|S|} \times \mathbb{R}^{m} \times \mathfrak{F} \times \mathcal{E} \times \bar{\mathfrak{F}} \times \bar{\mathcal{E}} \qquad (7.26a)\end{aligned}$$

Secondly, equation 7.26b, although structurally it may look like the standard Port Hamiltonian Matrix, it is different due to the fact that the current and the voltage sources account for the fluid/electric coupling indicated by the subscript (f/e) as given in equations 7.26c and 7.26d. This tells us once again that at the fluid/electric boundary the fluid is capable of acting as a source voltage or current. Equations 7.26c and 7.26d have been repeated for reference purposes and to improve readability.

$$\begin{bmatrix} I & 0 & A_{\mathcal{C}} & A_{\mathcal{R}} & A_{\mathcal{S}} \\ 0 & 0 & 0 & 0 & 0 \\ 0 & -I & 0 & 0 & 0 \\ 0 & 0 & 0 & 0 & 0 \\ 0 & 0 & 0 & 0 & 0 \end{bmatrix} \begin{pmatrix} j \\ -u_{\mathcal{L}} \\ -i_{\mathcal{C}} \\ -i_{\mathcal{R}} \\ -i_{\mathcal{S}} \end{pmatrix} + \begin{bmatrix} 0 & -A_{\mathcal{L}} & 0 & 0 & 0 \\ -A_{\mathcal{R}}^{\mathsf{T}} & 0 & 0 & 0 & 0 \\ -A_{\mathcal{L}}^{\mathsf{T}} & -I & 0 & 0 & 0 \\ -A_{\mathcal{C}}^{\mathsf{T}} & 0 & 0 & 0 & 0 \\ -A_{\mathcal{S}}^{\mathsf{T}} & 0 & 0 & 0 & I \end{bmatrix} \begin{pmatrix} \phi \\ i_{\mathcal{L}} \\ u_{\mathcal{C}} \\ u_{\mathcal{R}} \\ u_{\mathcal{S}} \end{pmatrix} = 0 \qquad (7.26b)$$

$$i_{\mathcal{S}} = \begin{pmatrix} i_{\mathcal{S}_{(e)}} \\ i_{\mathcal{S}_{(f/e)}} \end{pmatrix} \qquad (7.26c)$$

$$u_{\mathcal{S}} = \begin{pmatrix} u_{\mathcal{S}_{(e)}} \\ u_{\mathcal{S}_{(f/e)}} \end{pmatrix} \qquad (7.26d)$$

Since the fluid is only coupled to the electric circuit at the boundary, equations 7.26e and 7.26f do not deviate significantly from the equations derived in the literature.

$$\begin{pmatrix} f_{\tilde{v}} \\ f_{\eta} \end{pmatrix} = \begin{pmatrix} \frac{1}{\star\eta}\iota_{\sharp\circ\star(\cdot)}d\tilde{v} & \mathrm{d} \\ \mathrm{d} & 0 \end{pmatrix} \begin{pmatrix} e_{v} \\ e_{\eta} \end{pmatrix} - \begin{pmatrix} \frac{1}{\star\eta} \\ 0 \end{pmatrix} e_{p}, \tag{7.26e}$$

$$f_p = \begin{pmatrix} \frac{1}{\star\eta} & 0 \end{pmatrix} \begin{pmatrix} e_{\tilde{v}} \\ e_{\eta} \end{pmatrix} \tag{7.26f}$$

Since the electric circuit and fluid are interconnected at discrete region in the lung, it means one can divide the fluid boundary into two distinct regions. The first region is the boundary in which there is no interconnection with the electric ciruit (f) and secondly the boundary in which the fluid and the electric circuit exists (f/e). This are given by equation 7.26g and 7.26h.

$$\begin{pmatrix} e_{\partial e_{(f)}} \\ f_{\partial e_{(f)}} \end{pmatrix} = \begin{pmatrix} 0 & 1 \\ -1 & 0 \end{pmatrix} \begin{pmatrix} i^{\star}_{(f)}(e_{\tilde{v}}) \\ i^{*}_{(f)}(e_{\eta}) \end{pmatrix} \tag{7.26g}$$

$$\begin{pmatrix} e_{\partial e_{(f/e)}} \\ f_{\partial e_{(f/e)}} \end{pmatrix} = \begin{pmatrix} 0 & 1 \\ -1 & 0 \end{pmatrix} \begin{pmatrix} i^{\star}_{(f/e)}(e_{\tilde{v}}) \\ i^{*}_{(f/e)}(e_{\eta}) \end{pmatrix} = \begin{pmatrix} i_{\mathcal{S}_{(f/e)}} \\ u_{\mathcal{S}_{(f/e)}} \end{pmatrix} \tag{7.26h}$$

7.6.1 *Remark*

Thirdly, in the absence of the fluid, the electric coupling in equations 7.26c and 7.26d vanish. As a result equation 7.26b reduces to a standard Port Hamiltonian formulation of electric circuits. Similarly in the absence of the fluid, equation 7.26h vanishes and the fluid dynamics in Port Hamiltonian formulation are given by 7.26e, 7.26f, and 7.26g which are Port Hamiltonian equations of fluid with any interaction with the electric circuit.

7.6.2 *Reflection on the Contribution for the chapter*

The contribution of this chapter is the formulation of a multi-physics Port Hamiltonian generalized model of a mechanical ventilator-Human respiratory system. This is viewed as a contribution since it leads to the development of a new class of algebraic constraints in the modeling of the Mechanical ventilator human respiratory system. The coupling of a fluid to an electric circuit forms a framework for applications in other fields for example fluid power systems.

7.7 CONCLUSION

This section has presented a generalized multi-physics port Hamiltonian model of the mechanical ventilator lung system. The system is modeled using the Stokes-Dirac structure coupled to an electric circuit. A new class of algebraic constraints in the modeling of the mechanical ventilator lung physical system has been presented. The new class of constraints is due to the coupling of Partial Differential Equations (representing the fluid) with ordinary differential equations. Future work includes an illustration of how this novel Dirac structure can be applied in real life. For example in the investigation of the influence of airway secretion on airflow dynamics in the mechanical ventilator lung system

8

APPLICATIONS OF THE DERIVED THEORY FOR PORT HAMILTONIAN MECHANICAL VENTILATOR HUMAN RESPIRATORY SYSTEM

8.1 SUMMARY

This section provides summarized applications of where the developed Port Hamiltonian theory can be applied. Firstly the application of the developed Port Hamiltonian lung model in a dual early warning health monitoring system for mine workers. This research work is the author's own work, published in [113]. The second application considers the theory of the integrated mechanical ventilator human respiratory system where the derived theory is applied in the investigation of the influence of the airway secretion on airflow dynamics for the mechanical ventilator human respiratory system

8.2 INTRODUCTION

Port Hamiltonian framework for modelling of the integrated mechanical ventilator human respiratory system is one of the main enabling tools and means by which the energy transfer between the mechanical ventilator and human respiratory systems and subsystems can be described. The Port Hamiltonian based model provides a compositional and structured framework for multi-physics system modelling from first principles whereby the fundamental underlying physical structure can be identified.

8.3 CONTRIBUTION

Contribution 8.3.1

The contribution of this chapter is a presentation of how the derived theory can be applied using real-life examples. The first illustration applies the unique formulation of a Dirac structure using nonlinear electric circuit elements to formulate a Port Hamiltonian lung model for investigation of the respiratory health of mine workers. The second application is a Port Hamiltonian model for investigation of the influence of airway secretion on airflow dynamics for mechanical ventilator Lung system by applying the theory derived on novel Dirac structure of a fluid coupled to an electrical system.

8.4 PORT HAMILTONIAN LUNG MODEL FOR INVESTIGATION OF THE RESPIRATORY HEALTH OF MINE WORKERS

The section summarizes the application of this model in monitoring the mine workers' respiratory state of health. The details have already been published by the author of this thesis in a paper titled" Smart dual occupational health monitoring system for mine workers" The publication provides the details of monitoring noise-induced hearing loss as well as a respiratory disease known as pneumoconiosis. The application presented in this section will provide a summarized application in the monitoring of respiratory health using a Port Hamiltonian model of the respiratory system.

8.4.1 *Motivation for the application*

Occupational diseases and injuries have a negative impact on an individual and society. Occupational diseases are currently increasing in South African mines due to the depletion of minerals on the surface and the use of sophisticated machines to go deeper to achieve the required outputs. One of these occupational diseases is pneumoconiosis which is caused by inhalation of respirable dust. The occupational disease impact has been documented to be approximately 1 to 3 percent of the Gross Domestic Production (GDP) in different countries. These costs may be direct; for instance compensation or indirect for example loss of income for dependents. Mining companies are also affected by losing workers to occupational disease, loss through their reputation being tarnished or loss of investors [114]. There is therefore a need in the development of integrated monitoring systems that can be used in conjunction with the existing system to aid in minimizing the risks associated with excessive respirable dust.

8.4.2 *Background*

Considering the environment mine workers are exposed to, they are at risk of being exposed to excessive dust particles from various sources. Miners are at risk of developing lung diseases for example pneumoconiosis because of their regular exposure to airborne respirable dust. Pneumoconiosis implying a dusty lung, can cause impairment disability and premature death (NIOSH). Lung diseases among mine workers can be caused by exposure to rock dust, coal dust, silica dust, diesel particulate matter, welding fume and other finely powdered materials that become airborne during mining [113].

8.4.3 *Methodology*

In this section the methodology followed in the investigation of the respiratory health of mine workers is provided.

8.4.4 *Contextualization of the case study*

Platinum and gold are mined using similar methods. In mining both minerals, the surrounding rock is blasted and drilled. This research, therefore, uses raw data from a platinum mine in South Africa. The developed model can be applied to any mining environment in the world. The contextualization in this research work is only used to give the model a context and validate the model.

8.4.5 *Data collection and testing protocol*

Prior to the commencement of the project, permission to conduct the research project was secured from the relevant stake holders. Data was collected through a retrospective document review of the mine in South Africa. All procedures contributing to this work complied with the relevant national institutional guidelines for research on human subjects and adhered to the Helsinki Declaration of 1975 revised in 2008. Permission to conduct the study at the mines was obtained from the mine management. Furthermore, approval was obtained from the University of the Witwatersrand University Research ethics committee and an ethical clearance certificate was obtained prior to the commencement of data collection.

8.4.6 *Description of the collected data*

Data sets consisting of 200 observations were collected from a platinum mine. The data was collected from particulate matter measurement sensor and in addition to that, information was extracted from the mine workers annual medical reports for the year submitted to the Department of Mineral resources. The medical health details provided information on whether the mine worker had been exposed to various risks which included chemicals, process emission for instance dust and gases which are associated with ill health effects for instance pneumoconiosis and any other respiratory diseases. The mining company also provided details of the tasks of the mine worker for instance whether they are a driller, Dump truck driver or winch operator. The shafts in which the mine worker performs their general duties, duration of exposure to particulate matter, type of respirator worn and the duration of exposure were also provided. The age, gender and previous exposure to dust history was also some of the information that was collected from the mine workers.

8.4.7 *Respiratory diseases monitoring system modeling*

The overall diagram for the respiratory health monitoring system is provided in figure 8.1 and the smart dual health monitoring system is provided in figure 8.2

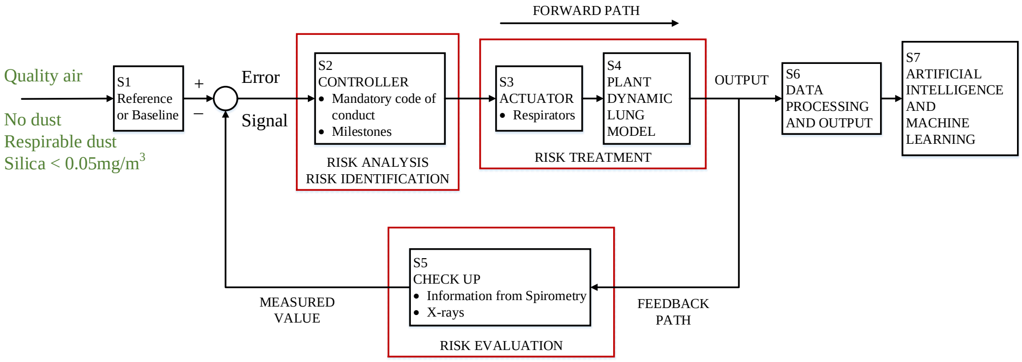

Figure 8.1: Monitoring respiratory diseases

8.4.7.1 *Reference or Baseline*

The S1 subsystem represents the baseline or the reference. The South African rules and regulations stipulate the following amounts as standard that should be followed by mines:

- Respirable dust should not exceed 1.5 mg per metre cubed
- Crystaline silica should not be greater than 0.05 milligram per metre cubed
- The coal dust should not be greater than 1.5 milligram per metre cubed.

This subsystem also has clean air (unpolluted air) in the following percentages:

- 78.09 Nitrogen
- 20.95 Oxygen
- 0.93 Argon
- 0.04 Carbon dioxide

- 0.4 Water vapour
- Other gases

8.4.7.2 *Controller*

S2 is a mandatory code of conduct imposed by the mine. The South African Mine Health and Safety Council (MHSC) has milestones for administrators to use as a target to ensure there is zero harm to the mine workers by the year 2024. This milestones act as a guideline on what the mine administrators should aim for. They are listed below for reference purposes.

- By December 2024: To Eliminate silicosis, the crystalline silica should be reduced to 0.05 milligrams per meter cubed.
- To eliminate pneumoconiosis in platinum mines the respirable dust particulate should be less than 1.5 milligrams per meter cubed.

These measures are an effort to eliminate silicosis, pneumoconiosis and any other respiratory disease.

8.4.7.3 *Actuators*

The actuator is represented by the respirator that mine workers wear in order to minimize the dust particles that they are inhaling.

8.4.7.4 *Dynamic lung model*

This subsystem is represented using the developed Port Hamiltonian model of the lung.

8.4.7.5 *Check up*

This subsystem represents both:

- Rapid check-ups to establish the respiratory health of a mine worker
- Elaborate annual check-ups that take place in the mine by thoroughly examining the mine workers and sometimes requesting a chest X-ray

8.4.7.6 *Data processing unit*

Data is processed in this Unit using the Internet of Things. The methods proposed by Madahana et al. (2019b) are applied in the data processing unit.

8.4.7.7 *Artificial Intelligence and Machine learning*

Artificial intelligence is implemented via machine learning. Deep learning techniques for instance Recurrent Neural Networks (RNN) are used.

8.4.8 *Smart dual Occupational health monitoring system for mine workers*

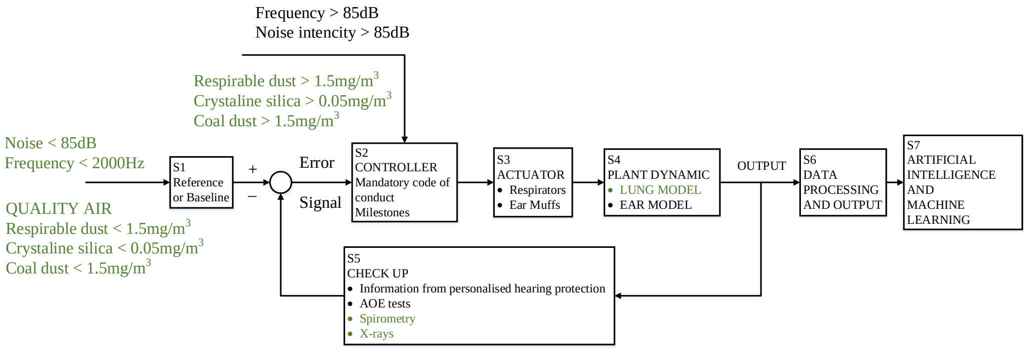

Figure 8.2: Smart dual health monitoring system

8.4.8.1 *Results and discussion*

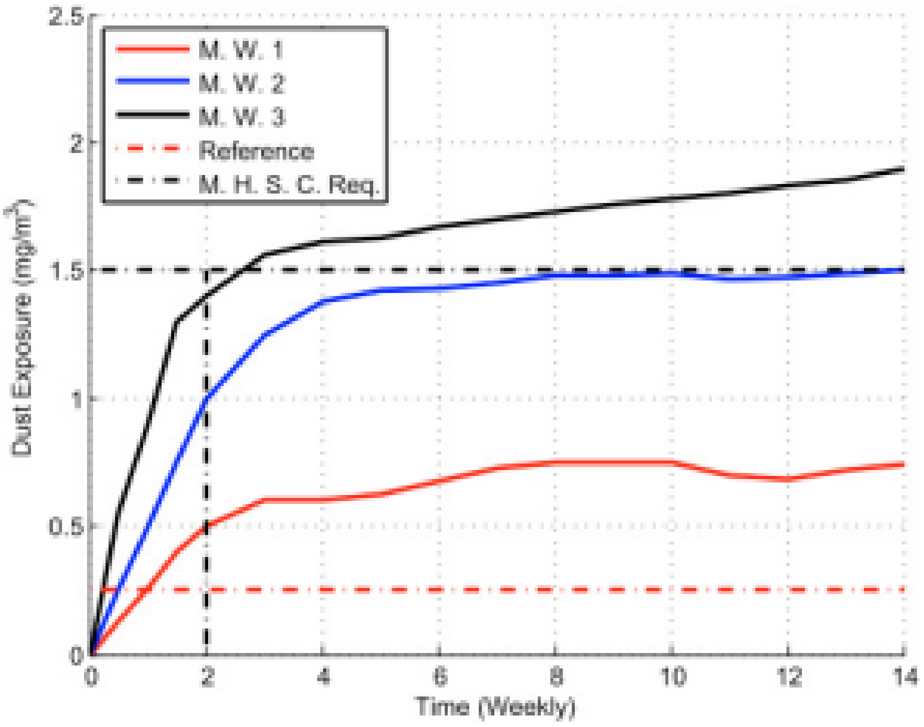

Figure 8.3: Respiratory Health monitoring system

From the results in the figure 8.3, the reference represents the minimum amount of dust accumulation a mine worker might already have prior to employment. The main goal of this system is to ensure the dust accumulation in the lung of the mine worker tracks the reference. This will be achieved by the application of the actuator (respirator) and closely monitoring the mine worker to ensure that there is no increase in dust accumulation in the lungs. M.W.1 represents the first mine worker whose respiratory health is fine and attempts to track the reference. M.W.2 is the second mine worker who has not violated the Mining Health and Safety Council (MHSC) requirements but still needs to be closely monitored to ensure that their wearable respirator is not faulty and that it is being worn correctly. There could be other reasons for an increase in the respirable dust. These should be provided and corrected so that the mine worker does not violate the MHSC requirements. M.W.3 represents a mine worker whose respiratory health has violated the MHSC requirements. This mine worker's case should be treated as an emergency and measures to prevent any further harm (to the mine worker), should be taken by the mine administrators.

8.5 PORT HAMILTONIAN MODEL FOR INVESTIGATION OF THE INFLUENCE OF AIRWAY SECRETION ON AIRFLOW DYNAMICS FOR MECHANICAL VENTILATOR LUNG SYSTEM

8.5.1 *Gas-Liquid Two-Phase Port Hamiltonian model*

The gas-liquid two-phase is modeled using the Navier Stokes equations formulated in chapter 7 of this research work. For reference purposes, the Stokes Dirac structure of the incompressible fluid is provided..

The Stokes-Dirac structure $\mathcal{D}_{IF}$ of the incompressible fluid defined by the set

$$
\begin{aligned}
\mathcal{D}_{IF} := \Big\{ \quad & \left(f_{\tilde{v}},\ f_{\eta},\ f_p,\ f_{\partial p},\ e_{\tilde{v}},\ e_{\eta},\ e_p,\ e_{\partial p}\right) \in \mathcal{F} \times \mathcal{E} \Big| \\
& \begin{pmatrix} f_{\tilde{v}} \\ f_{\eta} \end{pmatrix} = \begin{pmatrix} \frac{1}{\star\eta} \iota_{\sharp\circ\star(\cdot)} d\tilde{v} & \mathrm{d} \\ \mathrm{d} & 0 \end{pmatrix} \begin{pmatrix} e_{v} \\ e_{\eta} \end{pmatrix} - \begin{pmatrix} \frac{1}{\star\eta} \\ 0 \end{pmatrix} e_p, \\
& f_p = \begin{pmatrix} \frac{1}{\star\eta} & 0 \end{pmatrix} \begin{pmatrix} e_{\tilde{v}} \\ e_{\eta} \end{pmatrix}, \\
& \begin{pmatrix} e_{\partial e} \\ f_{\partial e} \end{pmatrix} = \begin{pmatrix} 0 & 1 \\ -1 & 0 \end{pmatrix} \begin{pmatrix} i^{\star}(e_{\tilde{v}}) \\ i^{*}(e_{\eta}) \end{pmatrix} \Big\}
\end{aligned}
$$

8.5.2 *Port Hamiltonian mechanical ventilator respiratory system Model*

The Port Hamiltonian respiratory system model can be represented using any of the models developed in chapters 4, 5, 6 or 7. The model presented in chapter 7 is used to illustrate the applications of the model.

If it assumed that the mechanical ventilator is a voltage source, In addition to that, assuming that the source voltages and currents are due to the union of two sets:

$$
u_S := u_{S_e} \cup u_{S_{(f/e)}} \qquad \text{and} \qquad i_S := i_{S_e} \cup i_{S_{(f/e)}}
$$

where there are

1. Purely electric sources:

  - Current sources $i_{\mathcal{S}_e} \in \mathbb{R}^{m_{\mathcal{S}_{(e)}}}$ and
  - Voltage sources $u_{\mathcal{S}_e} \in \mathbb{R}^{m_{\mathcal{S}_{(e)}}}$

  where $m_{\mathcal{S}_{(e)}}$ is the number of purely electric sources.

2. Sources due to the fluid/electric coupling:
   - Current sources $i_{\mathcal{S}_{(f/e)}} \in \mathbb{R}^{m_{\mathcal{S}} - m_{\mathcal{S}_{(e)}}}$ and
   - Voltage sources $u_{\mathcal{S}_{(f/e)}} \in \mathbb{R}^{m_{\mathcal{S}} - m_{\mathcal{S}_{(e)}}}$.

8.5.3 *Reflection on the Contribution for the chapter*

The applications of the derived Port Hamiltonian theory for the mechanical ventilator Human respiratory system has been presented as the contribution in this chapter. This chapter demonstrated the application of the developed theory.

8.6 CONCLUSION

This section provided examples of applications of the formulated Port Hamiltonian models. The first model is applied in a respiratory health monitoring system for mine workers and the second model is applied in the investigation of the influence of airway secretion on airflow dynamics for mechanical ventilator lung systems.

9

RECOMMENDATIONS AND CONCLUSIONS

9.1 SUMMARY AND CONTRIBUTIONS

This section provides a summary of the research work conducted, the contributions, and the direction for future work. The research work presented in the respective subsection has also presented the recommendations and conclusions

9.1.1 *Main Contributions*

The main contributions of this research work can be summarized as:

1. A compositional and geometric unifying approach for modeling the mechanical ventilator and the human respiratory system's complex physical network dynamics using open graphs in the Port Hamiltonian framework. The directed graph whose incidence matrix is associated with a Dirac structure, that relates the efforts and flow variables to the edges and vertices of the graph of a mechanical ventilator human respiratory system is formulated. In addition to that, the energy dissipating and storing relations between the effort and flow variables of the edges and the internal vertices are also presented. There is an association of state variables to the edges and a formalization of the interconnection of networks. The formulated Hamiltonian structure presents a systematic tool for the control and analysis of the resulting dynamics.
2. Formulation of a comprehensive integrated Port Hamiltonian model of the human respiratory system which includes the alveoli. This model can be applied in pressure analysis for patients with COPD. It can also be used in the design of robust controllers for the mechanical ventilation system
3. Presentation of a novel Port Hamiltonian model of the mechanical ventilator which is followed by the Port Hamiltonian formulation of a multiphysics and multiscale model of the respiratory system. The formulated Port Hamiltonian ventilator and the detailed respiratory system are interconnected to form a detailed integrated system that can be used for various applications; for instance investigation of the response to air pressure stimuli of the various segments of the respiratory system for a ventilated patient.
4. Formulation of a multi-physics Port Hamiltonian generalized model of a Mechanical Ventilator-Human respiratory system with Navier stokes for the fluid flow in the

mechanical ventilator lung system. A new class of algebraic constraints in the modelling of the mechanical ventilator lung physical system is formulated. The new class is due to the coupling of Partial Differential Equations (representing the fluid) with ordinary differential equations

5. The Contribution of this chapter is to present two examples of novel applications of the formulated models. The first example applies the novel Dirac structure of a fluid coupled to an electrical system. The second example uses the unique formulation of a Dirac structure using nonlinear electric circuit elements.

9.2 CONCLUSIONS AND RECOMMENDATIONS

The direction of future work is the following:

- To include the controller aspects of the system in the Port Hamiltonian framework.
- A test rig of the mechanical ventilator and the artificial respiratory system could be developed for testing to ensure the finding of the model can be applied in clinical studies

BIBLIOGRAPHY

[1] J. Reinders, B. G. B. Hunnekens, F. J. M. Heck, T. Oomen and N. van de Wouw, 'Adaptive control for mechanical ventilation for improved pressure support', *IEEE Transactions on Control Systems Technology*, vol. 29, pp. 180–193, 2021.

[2] P. Tamburrano, P. De Palma, A. Plummer, E. Distaso and R. Amirante, 'Simulink modelling for simulating intensive care mechanical ventilators', *E3S Web of Conferences*, vol. 197, 2020, ISSN: 2267-1242.

[3] M. Borrello, 'Modeling and control of systems for critical care ventilation', *Proceedings of the 2005, American Control Conference, 2005.*, vol. 3, pp. 2166–2180, 2005.

[4] S. Fox, *Human Physiology*. Newyork: Mcgraw hill international, 2018.

[5] H. Widmaier E.P.and Raff and K. strang, *Human Physiology*. Newyork: Mcgraw hill international, 2019.

[6] G. Bause, 'Emerson respiratory or iron lung,' *Anesthesiology.*, vol. 110, p. 812, 2009.

[7] S. Mesic, R. Babuska, H. Hoogsteden and A. Verbraak, 'Computer-controlled mechanical simulation of the artificially ventilated human respiratory system', *IEEE Transactions on Biomedical Engineering*, vol. 50, no. 6, pp. 731–743, 2003. DOI: `10.1109/TBME.2003.812166`.

[8] M. C. Madahana, J. E. Ekoru and O. O. Nyandoro, 'Energy based model of the human ear canal and tympanic membrane for sound transmission', *IFAC-PapersOnLine*, vol. 53, no. 2, pp. 16 406–16 411, 2020, 21st IFAC World Congress, ISSN: 2405-8963. DOI: `https://doi.org/10.1016/j.ifacol.2020.12.704`. [Online]. Available: `https://www.sciencedirect.com/science/article/pii/S2405896320310181`.

[9] M. C. I. Madahana, M. Ngwako, O. O. T. Nyandoro and J. E. D. Ekoru, 'Modelling of the human middle ear via the port hamiltonian approach', in *2021 International Automatic Control Conference (CACS)*, 2021, pp. 1–6. DOI: `10.1109/CACS52606.2021.9639063`.

[10] M. C. Madahana, O. T. Nyandoro and J. E. Ekoru, 'A human inner ear model for assessment of noise induced hearing loss via energy methods', *IFAC-PapersOnLine*, vol. 53, no. 2, pp. 16 424–16 429, 2020, 21st IFAC World Congress, ISSN: 2405-8963. DOI: `https://doi.org/10.1016/j.ifacol.2020.12.727`. [Online]. Available: `https://www.sciencedirect.com/science/article/pii/S2405896320310466`.

[11] M. Encina, J. Yuz, M. Zañartu and G. Galindo, 'Vocal fold modeling through the port-hamiltonian systems approach', in *2015 IEEE Conference on Control Applications (CCA)*, 2015, pp. 1558–1563. DOI: `10.1109/CCA.2015.7320832`.

[12] J. G. Fontanet, J. I. Yuz, J. A. Torres, M. A. Gordon and H. Ramírez, 'Port-hamiltonian modeling of the vocal folds using bond-graph representation', in *2021 IEEE International Conference on Automation/XXIV Congress of the Chilean Association of Automatic Control (ICA-ACCA)*, 2021, pp. 1–7. DOI: `10.1109/ICAACCA51523.2021.9465330`.

[13] L. A. Mora, J. I. Yuz, H. Ramirez and Y. L. Gorrec, 'A port-hamiltonian fluid-structure interaction model for the vocal folds⁎⁎this work was supported by conicyt-pfcha/2017-21170472, and ac3e conicyt-basal project fb-0008.', *IFAC-PapersOnLine*, vol. 51, no. 3, pp. 62–67, 2018, 6th IFAC Workshop on Lagrangian and Hamiltonian Methods for Nonlinear Control LHMNC 2018, ISSN: 2405-8963. DOI: https://doi.org/10.1016/j.ifacol.2018.06.016. [Online]. Available: https://www.sciencedirect.com/science/article/pii/S2405896318303069.

[14] A. Falaize and T. Hélie, 'Passive guaranteed simulation of analog audio circuits: A port-hamiltonian approach', *Applied Sciences*, vol. 6, no. 10, 2016, ISSN: 2076-3417. [Online]. Available: https://www.mdpi.com/2076-3417/6/10/273.

[15] A. Falaize, N. Lopes, T. Hélie, D. Matignon and B. Maschke, 'Energy-balanced models for acoustic and audio systems: a port-Hamiltonian approach', in *Unfold Mechanics for Sounds and Music*, cote interne IRCAM: Falaize14c, Paris, France, Sep. 2014, pp. 1–1. [Online]. Available: https://hal.science/hal-01156711.

[16] 'A port-hamiltonian approach to the control of interaction', in *Control of Interactive Robotic Interfaces: A Port-Hamiltonian Approach*. Berlin, Heidelberg: Springer Berlin Heidelberg, 2007, pp. 77–125, ISBN: 978-3-540-49715-8. DOI: 10.1007/978-3-540-49715-8_3. [Online]. Available: https://doi.org/10.1007/978-3-540-49715-8_3.

[17] M. Madahana, E. John and N. Otis, 'Compositional and geometric unifying approach for modeling the mechanical ventilator-human respiratory system', *Applied Sciences*, 2023. DOI: UnderReview.

[18] M. Madahana, E. John and N. Otis, 'Formulation of a comprehensive intergrated model of the human respiratory system via the porthamiltonian approach', *Applied Sciences*, 2023. DOI: UnderReview.

[19] M. Madahana, E. John and N. Otis, 'A mixed finite/infinite dimensional port-hamiltonian model of a mechanical ventilator', *Applied Sciences*, 2023. DOI: UnderReview.

[20] M. Madahana, E. John and N. Otis, 'Formulation of a generalized multiphysics port hamiltonian model of the mechanical ventilator human respiratory system', *Applied Sciences*, 2023. DOI: UnderReview.

[21] D Levac, H Colquhoun and K. K. O'Brien, 'Scoping studies: Advancing the methodology.', *Implementation science*, vol. 5, no. 69, 2010.

[22] H. Arksey and L. O'Malley, 'Scoping studies: Towards a methodological framework', *International Journal of Social Research Methodology*, vol. 8, no. 1, pp. 19–32, 2005. DOI: 10.1080/1364557032000119616.

[23] K. Ahookhosh, O. Pourmehran, H. Aminfar, M. Mohammadpourfard, M. M. Sarafraz and H. Hamishehkar, 'Development of human respiratory airway models: A review', *European Journal of Pharmaceutical Sciences*, vol. 145, p. 105 233, 2020, ISSN: 0928-0987. DOI: https://doi.org/10.1016/j.ejps.2020.105233. [Online]. Available: https://www.sciencedirect.com/science/article/pii/S0928098720300221.

[24] K. G. Hickling, 'The pressure-volume curve is greatly modified by recruitment. a mathematical model of ards lungs.', *American journal of respiratory and critical care medicine*, vol. 158 1, pp. 194–202, 1998.

[25] J. H. T. Bates, *Lung Mechanics: An Inverse Modeling Approach*. Cambridge, UK: Cambridge University Press, 2009.

[26] B. Maury, *The Respiratory System in Equations*. Jan. 2013, ISBN: 978-88-470-5213-0. DOI: 10.1007/978-88-470-5214-7.

[27] K. Burrowes, P. Hunter and M. Tawhai, 'Anatomically based finite element models of the human pulmonary arterial and venous trees including supernumerary vessels', *Journal of applied physiology (Bethesda, Md. : 1985)*, vol. 99, pp. 731–8, Sep. 2005. DOI: 10.1152/japplphysiol.01033.2004.

[28] M. Tawhai and J. Bates, 'Multi-scale lung modeling', *Journal of applied physiology (Bethesda, Md. : 1985)*, vol. 110, pp. 1466–72, Feb. 2011. DOI: 10.1152/japplphysiol.01289.2010.

[29] L. U. Berger, R. Bordas, K. Burrowes, C. E. Brightling, R. Hartley and D. Kay, 'Understanding the interdependence between parenchymal deformation and ventilation in obstructive lung disease', in *B30. DYNAMICS OF AIRWAY NARROWING IN ASTHMA: STILL MISUNDERSTOOD?*, American Thoracic Society, 2014, A2677–A2677.

[30] C. J. Roth, L. Yoshihara, M. Ismail and W. A. Wall, 'Computational modelling of the respiratory system: Discussion of coupled modelling approaches and two recent extensions', *Computer Methods in Applied Mechanics and Engineering*, vol. 314, pp. 473–493, 2017, Special Issue on Biological Systems Dedicated to William S. Klug, ISSN: 0045-7825. DOI: https://doi.org/10.1016/j.cma.2016.08.010.

[31] D. Doorly, D. Taylor and R. Schroter, 'Mechanics of airflow in the human nasal airways', *Respiratory Physiology Neurobiology*, vol. 163, no. 1, pp. 100–110, 2008.

[32] A. Bahammam, R. Tate, J. Manfreda and M. Kryger, 'Upper airway resistance syndrome: Effect of nasal dilation, sleep stage, and sleep position', *Sleep*, vol. 22, pp. 592–8, Sep. 1999. DOI: 10.1093/sleep/22.5.592.

[33] J. Sandeau, I. Katz, R. Fodil *et al.*, 'Cfd simulation of particle deposition in a reconstructed human oral extrathoracic airway for air and helium–oxygen mixtures', *Journal of Aerosol Science*, vol. 41, no. 3, pp. 281–294, 2010, ISSN: 0021-8502. DOI: https://doi.org/10.1016/j.jaerosci.2009.12.001.

[34] C. Ball, M. Uddin and A. Pollard, 'High resolution turbulence modelling of airflow in an idealised human extra-thoracic airway', *Computers Fluids*, vol. 37, no. 8, pp. 943–964, 2008, ISSN: 0045-7930. DOI: https://doi.org/10.1016/j.compfluid.2007.07.021.

[35] X. Xu, S. Ni, M. Fu, X. Zheng, N. Luo and W. Weng, 'Numerical investigation of airflow, heat transfer and particle deposition for oral breathing in a realistic human upper airway model', *Journal of Thermal Biology*, vol. 70, pp. 53–63, 2017, Assessing and modeling of the thermal impact of human-clothing environment, ISSN: 0306-4565. DOI: https://doi.org/10.1016/j.jtherbio.2017.05.003.

[36] R. Sarangapani, 'Modeling particle deposition in extrathoracic airways', *Aerosol Science and Technology*, vol. 32, no. 1, pp. 72–89, 2000. DOI: 10.1080/027868200303948.

[37] A. Heenan, W. Finlay, B Grgic, A Pollard and P. Burnell, 'An investigation of the relationship between the flow field and regional deposition in realistic extra-thoracic airways', *Journal of Aerosol Science*, vol. 35, no. 8, pp. 1013–1023, 2004, ISSN: 0021-8502. DOI: https://doi.org/10.1016/j.jaerosci.2004.03.004.

[38] A. Johnstone, M. Uddin, A. Pollard, A. Heenan and W. Finlay, 'The flow inside an idealised form of the human extra-thoracic airway', *Experiments in Fluids*, vol. 37, pp. 673–689, Nov. 2004. DOI: 10.1007/s00348-004-0857-4.

[39] D. Bartlett, J. Remmers and H. Gautier, 'Laryngeal regulation of respiratory airflow', *Respiration Physiology*, vol. 18, no. 2, pp. 194–204, 1973, ISSN: 0034-5687. DOI: https://doi.org/10.1016/0034-5687(73)90050-9. [Online]. Available: https://www.sciencedirect.com/science/article/pii/0034568773900509.

[40] T. Gemci, T. E. Corcoran and N. Chigier, 'A numerical and experimental study of spray dynamics in a simple throat model', *Aerosol Science and Technology*, vol. 36, no. 1, pp. 18–38, 2002. DOI: `10.1080/027868202753339050`.

[41] K. Stapleton, E Guentsch, M. Hoskinson and W. Finlay, 'On the suitability of k–turbulence modeling for aerosol deposition in the mouth and throat: A comparison with experiment', *Journal of Aerosol Science*, vol. 31, no. 6, pp. 739–749, 2000, ISSN: 0021-8502. DOI: `https://doi.org/10.1016/S0021-8502(99)00547-9`.

[42] S. Jayaraju, M. Brouns, C. Lacor, B. Belkassem and S. Verbanck, 'Large eddy and detached eddy simulations of fluid flow and particle deposition in a human mouth–throat', *Journal of Aerosol Science*, vol. 39, no. 10, pp. 862–875, 2008, ISSN: 0021-8502.

[43] G Allen, B Shortall, T. Gemci, T Corcoran and N. Chigier, 'Computational simulations of airflow in an in vitro model of the pediatric upper airways', *Journal of biomechanical engineering*, vol. 126, pp. 604–13, Nov. 2004. DOI: `10.1115/1.1800554`.

[44] T. Cheng, D. Carpenter, S. Cohen, D. Witsell and D. Frank-Ito, 'Investigating the effects of laryngotracheal stenosis on upper airway aerodynamics: Effects of lts on airflow dynamics', *The Laryngoscope*, vol. 128, Oct. 2017. DOI: `10.1002/lary.26954`.

[45] M. D. Goldman, H. Nazeran, C. D. Ramos *et al.*, 'Electrical circuit models of the human respiratory system reflect small airway impairment measured by impulse oscillation (ios)', *2010 Annual International Conference of the IEEE Engineering in Medicine and Biology*, pp. 2467–2472, 2010. [Online]. Available: `https://api.semanticscholar.org/CorpusID:10769618`.

[46] J. BROWN and D. CAMPBELL, 'The electrical analogue of a lung function', in *Biomechanics and Related Bio-Engineering Topics*, R. KENEDI, Ed., Pergamon, 1965, pp. 459–466, ISBN: 978-1-4831-6701-5. DOI: `https://doi.org/10.1016/B978-1-4831-6701-5.50047-4`. [Online]. Available: `https://www.sciencedirect.com/science/article/pii/B9781483167015500474`.

[47] D. M, N. V.S, R. S, R. R.P and S. S, 'Electrical modeling and analysis of human respiratory system', *Bulletin of Scientific Research*, vol. 2, pp. 43–48, May 2020. DOI: `10.34256/bsr2017`.

[48] S. Bagchi and M. Chattopadhyay, 'Electrical modeling of respiratory system and identification of two common copd diseases through stability analysis technique', in *2012 IEEE International Conference on Advanced Communication Control and Computing Technologies (ICACCCT)*, 2012, pp. 403–408. DOI: `10.1109/ICACCCT.2012.6320811`.

[49] A. Tran, H. Q. T. Ngo, K. Dong and V. Huy, 'Design, control, modeling, and simulation of mechanical ventilator for respiratory support', *Mathematical Problems in Engineering*, vol. 2021, pp. 1–15, Nov. 2021. DOI: `10.1155/2021/2499804`.

[50] A. El-Hadj, M. Kezrane, H. Ahmad *et al.*, 'Design and simulation of mechanical ventilators', *Chaos, Solitons & Fractals*, vol. 150, p. 111 169, 2021.

[51] J. Tharion, S. Kapil, N. Muthu, J. Tharion and K. Subramani, 'Rapid manufacturable ventilator for respiratory emergencies of covid-19 disease', *Transactions of the Indian National Academy of Engineering*, vol. 5, Jun. 2020. DOI: `10.1007/s41403-020-00118-6`.

[52] W. J. Pivik, G. M. Clayton, G. F. Jones and C. Nataraj, 'Dynamic modeling of a low-cost mechanical ventilator', *IFAC-PapersOnLine*, vol. 55, no. 37, pp. 81–85, 2022, ISSN: 2405-8963. DOI: `https://doi.org/10.1016/j.ifacol.2022.11.165`.

[53] N. Al Naggar, 'Modelling and simulation of pressure controlled mechanical ventilation system', *Journal of Biomedical Science and Engineering*, vol. 8, pp. 707 –716, Oct. 2015. DOI: `10.4236/jbise.2015.810068`.

[54] Y. Shi, S. Ren, M. Cai and W. Xu, 'Modelling and simulation of volume controlled mechanical ventilation system', *Mathematical Problems in Engineering*, vol. 2014, Jul. 2014. DOI: `10.1155/2014/271053`.

[55] N. Al Naggar, H. Al-Hetari and F. Alakwaa, 'Simulation of mathematical model for lung and mechanical ventilation', *Journal of Science and Technology*, vol. 21, pp. 1–11, Jun. 2016. DOI: `10.20428/JST.21.1.1`.

[56] J. Giri, N. Kshirsagar and A. Wanjari, 'Design and simulation of ai-based low-cost mechanical ventilator: An approach', *Materials Today: Proceedings*, vol. 47, pp. 5886–5891, 2021, SI: TIME-2021, ISSN: 2214-7853. DOI: `https://doi.org/10.1016/j.matpr.2021.04.369`.

[57] D. Hannon, S. Mistry, A. Das *et al.*, 'Modeling mechanical ventilation in silico—potential and pitfalls', *Seminars in Respiratory and Critical Care Medicine*, vol. 43, Apr. 2022. DOI: `10.1055/s-0042-1744446`.

[58] Y. Shi, S. Ren, M. Cai, W. Xu and Q. Deng, 'Pressure dynamic characteristics of pressure controlled ventilation system of a lung simulator', *Computational and mathematical methods in medicine*, vol. 2014, 2014.

[59] V. Chellaboina, W. M. Haddad, H. Li and J. M. Bailey, 'Limit cycle stability analysis and adaptive control of a multi-compartment model for a pressure-limited respirator and lung mechanics system', *International Journal of Control*, vol. 83, no. 5, pp. 940–955, 2010.

[60] M. Borrello, 'Modeling and simulation of pressure regulated control systems for ventilation of the lung', in *Proceedings of the Annual International Conference of the IEEE Engineering in Medicine and Biology Society Volume 13: 1991*, 1991, pp. 2178–2179. DOI: `10.1109/IEMBS.1991.684952`.

[61] M. A. Borrello, 'Adaptive inverse model control of pressure based ventilation', in *Proceedings of the 2001 American Control Conference. (Cat. No.01CH37148)*, vol. 2, 2001, 1286–1291 vol.2. DOI: `10.1109/ACC.2001.945900`.

[62] M. Scheel, A. Berndt and O. Simanski, 'Iterative learning control: An example for mechanical ventilated patients', *IFAC-PapersOnLine*, vol. 48, no. 20, pp. 523–527, 2015, 9th IFAC Symposium on Biological and Medical Systems BMS 2015, ISSN: 2405-8963. DOI: `https://doi.org/10.1016/j.ifacol.2015.10.194`.

[63] B. Lachmann, 'Open up the lung and keep the lung open', *Intensive Care Medicine*, vol. 18, pp. 319–321, 2005.

[64] B. H. B. Van De Wouw and S.Kamps, 'Switching control of medical ventilation systems', 532—538, 2018.

[65] T. Laubscher, W. Heinrichs, N Weiler, G. Hartmann and J. Brunner, 'An adaptive lung ventilation controller', *IEEE transactions on bio-medical engineering*, vol. 41, pp. 51–9, Feb. 1994. DOI: `10.1109/10.277271`.

[66] A. Pomprapa, S. Weyer, S. Leonhardt, M. Walter and B. Misgeld, 'Periodic funnel-based control for peak inspiratory pressure', in *2015 54th IEEE Conference on Decision and Control (CDC)*, 2015, pp. 5617–5622. DOI: `10.1109/CDC.2015.7403100`.

[67] M. Scheel, A. Berndt and O. Simanski, 'Iterative learning control: An example for mechanical ventilated patients', *IFAC-PapersOnLine*, vol. 48, no. 20, pp. 523–527, 2015, ISSN: 2405-8963. DOI: `https://doi.org/10.1016/j.ifacol.2015.10.194`.

[68] H. Li and W. M. Haddad, 'Model predictive control for a multi-compartment respiratory system', in *2012 American Control Conference (ACC)*, 2012, pp. 5574–5579. DOI: `10.1109/ACC.2012.6314968`.

[69] C. Sinderby, P. Navalesi, J. Beck *et al.*, 'Neural control of mechanical ventilation in respiratory failure', *Nature medicine*, vol. 5, pp. 1433–6, Jan. 2000. DOI: `10.1038/71012`.

[70] K. Volyanskyy, W. Haddad and J. Bailey, 'Pressure- and work-limited neuroadaptive control for mechanical ventilation of critical care patients', *Neural Networks, IEEE Transactions on*, vol. 22, pp. 614 –626, May 2011. DOI: `10.1109/TNN.2011.2109963`.

[71] I. Mehedi, M. H. Mohd Shah, U. Al-Saggaf, R. Mansouri and M. Bettayeb, 'Adaptive fuzzy sliding mode control of a pressure-controlled artificial ventilator', *Journal of Healthcare Engineering*, vol. 2021, pp. 1–10, Jun. 2021. DOI: `10.1155/2021/1926711`.

[72] A.-S. Mohammad and N. Ullah, 'Cascaded robust control of mechanical ventilator using fractional order sliding mode control', *AIMS Mathematics*, vol. 19, Nov. 2021. DOI: `10.3934/mbe.2022061`.

[73] D. I. R. Almeida, A. C. Cárdenas, I. O. H. Fuentes *et al.*, 'Modeling and control of an invasive mechanical ventilation system using the active disturbances rejection control structure', *ISA transactions*, 2021.

[74] J. Arcos-Legarda and A. Tovar, 'Mechatronic design and active disturbance rejection control of a bag valve-based mechanical ventilator', *Journal of Medical Devices-transactions of The Asme*, 2021.

[75] H. Guler and F. Ata, 'Estimation of inspiration and expiration time by using fuzzy control with respect to lung's dynamics', in *2009 Fifth International Conference on Soft Computing, Computing with Words and Perceptions in System Analysis, Decision and Control*, 2009, pp. 1–5. DOI: `10.1109/ICSCCW.2009.5379473`.

[76] Á. de Salem Martínez-Casaos, D. C. Lancón-Baños, J. A. Hernández-Mendoza *et al.*, 'Linear controller proposal applied to the virtual servomechanism from an open source mechanical ventilator system', in *2020 IEEE International Autumn Meeting on Power, Electronics and Computing (ROPEC)*, IEEE, vol. 4, 2020, pp. 1–7.

[77] H. Zhu and K. Moller, 'Ventilator control based on a fuzzy-neural network approach', in *2008 2nd International Conference on Bioinformatics and Biomedical Engineering*, IEEE, 2008, pp. 747–750.

[78] A. S. Gomes, W. Barra, A. da Silva Silveira, M. d. C. P. Fonseca and I. M. Miziara, 'Comparative performance of lqg versus pid optimized by swarm approaches: A case study on a biomedical ventilation system', in *2021 14th IEEE International Conference on Industry Applications (INDUSCON)*, IEEE, 2021, pp. 640–647.

[79] G. Männel, C. Hoffmann and P. Rostalski, 'A robust model predictive control approach to intelligent respiratory support', in *2018 IEEE Conference on Control Technology and Applications (CCTA)*, IEEE, 2018, pp. 12–17.

[80] I. M. Mehedi, H. S. Shah, U. M. Al-Saggaf, R. Mansouri and M. Bettayeb, 'Fuzzy pid control for respiratory systems', *Journal of Healthcare Engineering*, vol. 2021, 2021.

[81] A. Schaft and D. Jeltsema, 'Port-hamiltonian systems theory: An introductory overview', *Found. Trends Syst. Control*, vol. 1, pp. 173–378, Jan. 2014. DOI: `10.1561/2600000002`.

[82] G. Golo, S. van der Arjan, P. C. Breedveld, B. Maschke, R. Johansson and A. Rantzer, 'Hamiltonian formulation of bond graphs', 2003. [Online]. Available: `https://api.semanticscholar.org/CorpusID:119000758`.

[83] J. A. Villegas, 'A Port-Hamiltonian approach to distributed parameter systems', Ph.D. dissertation, Department of Applied Mathematics, Faculty EWI, Universiteit Twente, Enschede, Twente, Enschede, Netherlands, 2007.

[84] Y. Le Gorrec, H. Zwart and B. Maschke, 'Dirac structures and boundary control systems associated with skew-symmetric differential operators', *SIAM Journal on Control and Optimization*, vol. 44, no. 5, pp. 1864–1892, 2005. DOI: `10.1137/040611677`.

[85] A. J. van der Schaft and B. M. Maschke, 'Hamiltonian formulation of distributed-parameter systems with boundary energy flow', *Journal of Geometry and Physics*, vol. 42, no. 1, pp. 166–194, 2002, ISSN: 0393-0440. DOI: `10.1016/S0393-0440(01)00083-3`.

[86] M. madahana, *A study of example*, Available at `https://wiredspace.wits.ac.za/items/846400be-8e44-4b3a-aeb0-c5c290113ad4`, Johannesburg, South Africa, 2019.

[87] B. Hunnekens, S. Kamps and N. Van De Wouw, 'Variable-gain control for respiratory systems', *IEEE Transactions on Control Systems Technology*, vol. 28, no. 1, pp. 163–171, 2020. DOI: `10.1109/TCST.2018.2871002`.

[88] J. P. Desai and F. Moustarah, *Pulmonary Compliance* (StatPearls [Internet]). Treasure Island (FL): StatPearls Publishing, 2021, 2022 Jan. 2021 Sep 18.

[89] M. Tõnso, V. Kaparin and J. Belikov, 'Port-hamiltonian framework in power systems domain: A survey', *Energy Reports*, vol. 10, pp. 2918–2930, 2023, ISSN: 2352-4847.

[90] R. Ortega, A. Van Der Schaft, I. Mareels and B. Maschke, 'Putting energy back in control', *IEEE Control Systems Magazine*, vol. 21, no. 2, pp. 18–33, 2001. DOI: `10.1109/37.915398`.

[91] 'A port-hamiltonian approach to power network modeling and analysis', *European Journal of Control*, vol. 19, no. 6, pp. 477–485, 2013, Lagrangian and Hamiltonian Methods for Modelling and Control, ISSN: 0947-3580. DOI: `https://doi.org/10.1016/j.ejcon.2013.09.002`.

[92] H. Gernandt, F. E. Haller, T. Reis and A. J. van der Schaft, 'Port-Hamiltonian formulation of nonlinear electrical circuits', *Journal of Geometry and Physics*, vol. 159, p. 103 959, 2021, ISSN: 0393-0440. DOI: `10.1016/j.geomphys.2020.103959`.

[93] V. C. Rideout, *Mathematical and Computer Modeling of Physiological Systems*. USA: Prentice-Hall, Inc., 1991, ISBN: 0135633540.

[94] A. Albanese, L. Cheng, M. Ursino and N. W. Chbat, 'An integrated mathematical model of the human cardiopulmonary system: Model development.', *American journal of physiology. Heart and circulatory physiology*, vol. 310 7, H899–921, 2016. [Online]. Available: `https://api.semanticscholar.org/CorpusID:16326938`.

[95] L. Hao, Y. Shi, M. Cai *et al.*, 'Dynamic characteristics of a mechanical ventilation system with spontaneous breathing', *IEEE Access*, vol. 7, pp. 172 847–172 859, 2019. DOI: `10.1109/ACCESS.2019.2955075`.

[96] P. Barbini, C. Brighenti, G. Cevenini and G. Cevenini, 'A dynamic morphometric model of the normal lung for studying expiratory flow limitation in mechanical ventilation', *Annals of Biomedical Engineering*, vol. 33, pp. 518–530, DOI: `10.1007/s10439-005-2511-6`.

[97] F. C. Jandre, A. R. S. Carvalho, A. V. Pino and A. Giannella-Neto, 'Effects of filtering and delays on the estimates of a nonlinear respiratory mechanics model', *Respiratory Physiology Neurobiology*, vol. 148, no. 3, pp. 309–314, 2005, ISSN: 1569-9048. DOI: `https://doi.org/10.1016/j.resp.2005.02.009`. [Online]. Available: `https://www.sciencedirect.com/science/article/pii/S1569904805000558`.

[98] S. d. S. R. F. Rosa and M. L. Altoé, 'Bond graph modeling of the human esophagus and analysis considering the interference in the fullness of an individual by reducing mechanical esophageal flow', *Revista Brasileira de Engenharia Biomédica*, vol. 29, no. 3, 286–297, 2013, ISSN: 1517-3151. DOI: `10.4322/rbeb.2013.024`. [Online]. Available: `https://doi.org/10.4322/rbeb.2013.024`.

[99] D. L. Margolis and M. Tabrizi, 'Acoustic Modeling of Lung Dynamics Using Bond Graphs', *Journal of Biomechanical Engineering*, vol. 105, no. 1, pp. 84–91, Feb. 1983, ISSN: 0148-0731. DOI: `10.1115/1.3138390`. eprint: `https://asmedigitalcollection.asme.org/biomechanical/article-pdf/105/1/84/5481374/84\_1.pdf`. [Online]. Available: `https://doi.org/10.1115/1.3138390`.

[100] S. Mesic, R. Babuska, H. Hoogsteden and A. Verbraak, 'Computer-controlled mechanical simulation of the artificially ventilated human respiratory system', *IEEE Transactions on Biomedical Engineering*, vol. 50, no. 6, pp. 731–743, 2003. DOI: `10.1109/TBME.2003.812166`.

[101] M. Ochs, J. Nyengaard, A. Jung *et al.*, 'The number of alveoli in the human lung', *American journal of respiratory and critical care medicine*, vol. 169, pp. 120–4, Feb. 2004. DOI: `10.1164/rccm.200308-1107OC`.

[102] J. Rubio, C. Rojas, M. Sanchez *et al.*, 'Covox: Providing oxygen during the covid-19 health emergency', *HardwareX*, vol. 13, e00383, 2023, ISSN: 2468-0672. DOI: `https://doi.org/10.1016/j.ohx.2022.e00383`.

[103] A. El-Hadj, M. Kezrane, H. Ahmad *et al.*, 'Design and simulation of mechanical ventilators', *Chaos, Solitons Fractals*, vol. 150, p. 111 169, 2021, ISSN: 0960-0779. DOI: `https://doi.org/10.1016/j.chaos.2021.111169`.

[104] J. Anderson, *Computational Fluid Dynamics: The Basics with Applications* (McGraw-Hill International Editions: Mechanical Engineering). McGraw-Hill, 1995, ISBN: 9780071132107. [Online]. Available: `https://books.google.co.za/books?id=phG_QgAACAAJ`.

[105] Z. Kamiński, 'A simplified lumped parameter model for pneumatic tubes', *Mathematical and Computer Modelling of Dynamical Systems*, vol. 23, no. 5, pp. 523–535, 2017. DOI: `10.1080/13873954.2017.1280512`. eprint: `https://doi.org/10.1080/13873954.2017.1280512`. [Online]. Available: `https://doi.org/10.1080/13873954.2017.1280512`.

[106] J. A. Bondy and U. S. R. Murty, *Graph Theory with Applications*. MacMillan, 1976.

[107] M. Taghizadeh, A. Ghaffari and F. Najafi, 'Modeling and identification of a solenoid valve for pwm control applications', *Comptes Rendus Mécanique*, vol. 337, no. 3, pp. 131–140, 2009, ISSN: 1631-0721. DOI: `https://doi.org/10.1016/j.crme.2009.03.009`. [Online]. Available: `https://www.sciencedirect.com/science/article/pii/S1631072109000308`.

[108] P. J. Morrison, 'Hamiltonian description of the ideal fluid', vol. 70, no. 2, Apr. 1998.

[109] F. Boyer and P. Fabrie, *Mathematical tools for the study of the incompressible Navier-Stokes equations and related models* (Applied Mathematical Sciences). Springer New York, Nov. 2012, p. 538. DOI: `10.1007/978-1-4614-5975-0`. [Online]. Available: `https://hal.science/hal-00777731`.

[110] F. Califano, R. Rashad, F. P. Schuller and S. Stramigioli, 'Geometric and energy-aware decomposition of the Navier-Stokes equations: A port-Hamiltonian approach', *Physics of Fluids*, vol. 33, no. 4, p. 047 114, 2021. DOI: `10.1063/5.0048359`.

[111] R. Rashad, F. Califano, A. Brugnoli, F. P. Schuller and S. Stramigioli, ‘Exterior and vector calculus views of incompressible Navier-Stokes port-Hamiltonian models’, *IFAC-PapersOnLine*, vol. 54, no. 19, pp. 173–179, 2021, 7th IFAC Workshop on Lagrangian and Hamiltonian Methods for Nonlinear Control LHMNC 2021. DOI: `10.1016/j.ifacol.2021.11.074`.

[112] ‘About dissipative and pseudo port-hamiltonian formulations of irreversible newtonian compressible flows’, *IFAC-PapersOnLine*, vol. 53, no. 2, pp. 11 521–11 526, 2020, 21st IFAC World Congress, ISSN: 2405-8963.

[113] M. C. Madahana, O. T. Nyandoro and J. E. Ekoru, ‘Intelligent comprehensive occupational health monitoring system for mine workers’, *IFAC-PapersOnLine*, vol. 53, no. 2, pp. 16 494–16 499, 2020, 21st IFAC World Congress, ISSN: 2405-8963. DOI: `https://doi.org/10.1016/j.ifacol.2020.12.751`. [Online]. Available: `https://www.sciencedirect.com/science/article/pii/S2405896320310739`.

[114] M. Hermanus, ‘‘occupational health and safety in mining—status, new developments, and concerns’. journal of the southern african institute of mining and metallurgy 107, 531–538.’, Jan. 2007.